Technical Note BN-626 November 1969

LAMINAR SHOCKS AND OTHER NONLINEAR WAVES IN WARM PLASMAS*

by

William F. Crevier
University of Maryland
College Park, Maryland

*This research was supported by the NASA through grants NGL 21-002-005/7 and NGL 21-002-033.

UNIVERSITY OF MARYLAND

Technical Note BN-626 November 1969

LAMINAR SHOCKS AND OTHER NONLINEAR WAVES IN WARM PLASMAS*

by

William F. Crevier
University of Maryland
College Park, Maryland

THE INSTITUTE FOR FLUID DYNAMICS *and* APPLIED MATHEMATICS

ABSTRACT

Title of Thesis: Laminar Shocks and Other Nonlinear Waves in Warm Plasmas

William Francis Crevier, Doctor of Philisophy, 1970

Thesis directed by: Professor Derek A. Tidman

A two fluid model for collisionless shock waves in warm plasmas is presented. Dissipation is included by assuming an effective collision frequency. The model is capable of describing waves over a wide range of Mach numbers and angles of propagation.

The wave behavior is compared to the motion of a particle moving in a somewhat complicated force field[11]. A part of this force can be written as the gradient of a potential. By studying the shape of the potential for various initial conditions we are able to make quite general conclusions about the wave behavior. The potential well analogy is complicated by the fact that friction heats the plasma and alters the shape of the potential well.

The response of the plasma to a small perturbation is analyzed by linearizing the equations of motion about their equilibrium values. Comparing the shape of the potential well near the origin with the results of the linearized equations of motion provides considerable physical insight into the initial wave behavior.

The Rankine-Hugoniot relations for a shock transition in a

warm plasma are derived and used to study the possible downstream equilibrium states. Again the potential well analogy proves useful by providing information on the stability of the final equilibrium states.

The usual two fluid model is expanded to include high Mach number shock waves. By including a thin region of intense electrostatic turbulence in an otherwise laminar shock[21] we are able to produce shock waves with Alfvén Mach numbers up to 40 or more.

A digital computer is used to provide examples of the various kinds of wave behavior we predict analytically. Examples of waves with and without dissipation are given.

ACKNOWLEDGMENTS

I would like to take this opportunity to express my deep gratitude to Professor Derek A. Tidman for suggesting this topic and for the continuous help and guidance he provided during the course of my research. I would also like to thank the members of the Physics Department and the Institute for Fluid Dynamics and Applied Mathematics for many stimulating discussions, particularly Dr. K. Papadopoulos.

The help of the staff of the Institute in preparing this work is greatly appreciated.

This research was supported by the NASA through grants NGL 21-002-005/7 and NGL 21-002-033. This support is gratefully acknowledged.

TABLE OF CONTENTS

Chapter		Page
Acknowledgements		ii
I.	INTRODUCTION	1
II.	THE EQUATIONS OF MOTION FOR NONLINEAR WAVES	8
	A. Presentation of the Equations	8
	B. Introduction of Dimensionless Variables	15
	C. Preliminary Analysis of the Equations	18
	D. Introduction of the Particle Analogy	21
	E. Example of Wave Motion	27
III.	INITIAL CONDITIONS	31
	A. The Linearized Equations of Motion	31
	B. The Shape of the Potential Well Near the Origin	39
	C. Examples of Initial Behavior	48
IV.	THE FINAL STATES OF THE PLASMA	53
	A. The Rankine-Hugoniot Relations	55
	B. The Initial Shape of the Potential Well	62
	C. Waves in the Absence of Friction	71
	a. Wave Trains in Region II_c	73
	b. Solitary Waves in Regions II_r and II_c	76
	c. Solitary Waves in Region I_r	80

Chapter		Page
	D. Laminar Shock Waves	83
	a. Shock Waves in Regions 2_{ms} and 1_m.	84
	b. Wave Trains in Regions 1_s and 0...	85
	c. Shock Waves in Region 1_s	87
V.	DOUBLE SHOCK WAVES	91
	A. Model for High Mach Number Shock Waves	91
	B. A Possible Instability Mechanism	95
	C. Relationship Between Double Shock Waves and Two Fluid Theory	98
IV.	CONCLUDING REMARKS	107
APPENDIX 1.		109
APPENDIX 2.		113
APPENDIX 3.		119
APPENDIX 4.		124
References		127

LIST OF TABLES

Table	Page
1	33
2	95

LIST OF FIGURES

Chapter	Page
1.1	3
2.1	9
2.2	24
2.3	28
2.4	30
3.1	37
3.2	43
3.3	50
3.4	51
4.1	54
4.2	59
4.3	61
4.4	64
4.5	66
4.6	70
4.7	74
4.8	75
4.9	78
4.10	79
4.11	86
4.12	88
4.13	90
5.1	92
5.2	94
5.3	97
5.4	100
5.5	104
5.6	105

CHAPTER I

INTRODUCTION

The existence of shock waves in hot tenuous plasmas had been predicted theoretically by several authors (see for example references 1-3). These so called "collisionless" shocks have since been observed in the earth's bow shock[4,5] and in laboratory theta pinch experiments[6,7]. The fact that these shocks have a thickness much less than the Coulomb collision mean free path has led to an extensive search for a theoretical explanation.

The basic problem has been to find physical mechanisms that can produce a shock wave on such a short length scale. It is generally agreed today that it is the interaction between the plasma and its self-consistent electric and magnetic fields that is responsible for the shock structure. Turbulence in these fields can often provide a dissipation mechanism with a length scale much less than the length scale for the usual particle-particle collisions[8].

In general, the fields in a plasma can be thought of as consisting of a smooth, slowly varying component and a rapidly fluctuating component. If the energy density of the smooth component is very large compared to that of the fluctuations, we can use a laminar theory to describe the plasma. If, on the other hand, a large fraction of the field energy density inside the shock resides in fluctuations, a turbulent theory is needed. When the fields are primarily laminar but the turbulence is not negligible, it is sometimes possible to include the effects of turbulence within a laminar theory as an effective dissipation. To see how this can be done, we first consider the geometry of the problem and then examine the relevant length scales.

We assume an infinite plane shock front. The reference frame is chosen such that the shock front appears stationary and the incident streaming velocity is normal to the shock front (see Figure 1.1). In this frame, the upstream plasma flows in from the left, is deflected and slowed down in the shock front, and flows out to the right.

The magnetic field is constant in time but varies in space along the x-axis. The length scale, L_B, for variation of the magnetic field through the shock, changes from c/ω_i to c/ω_e as the angle the magnetic field makes with the incident streaming velocity changes from zero to $\pi/2$ (ω_i and ω_e are the ion and electron plasma frequencies).

If there are electrostatic fluctuations present, they will have length scales, L_E, on the order of a few Debye lengths. A Debye length is equal to the electron thermal velocity divided by ω_e. As long as the electron thermal velocity is much less than the speed of light, L_E will be much less than L_B.

The large difference between these two length scales enables us to use a two fluid theory to describe the laminar variations of the magnetic field, and indirectly include the electrostatic microturbulence in the form of macroscopic transport coefficients such as an effective collision frequency.

The emphasis in this thesis is on the solution of the two fluid equations and not on the sources of the microturbulence or the details of the relationship between the microturbulence and the macroscopic

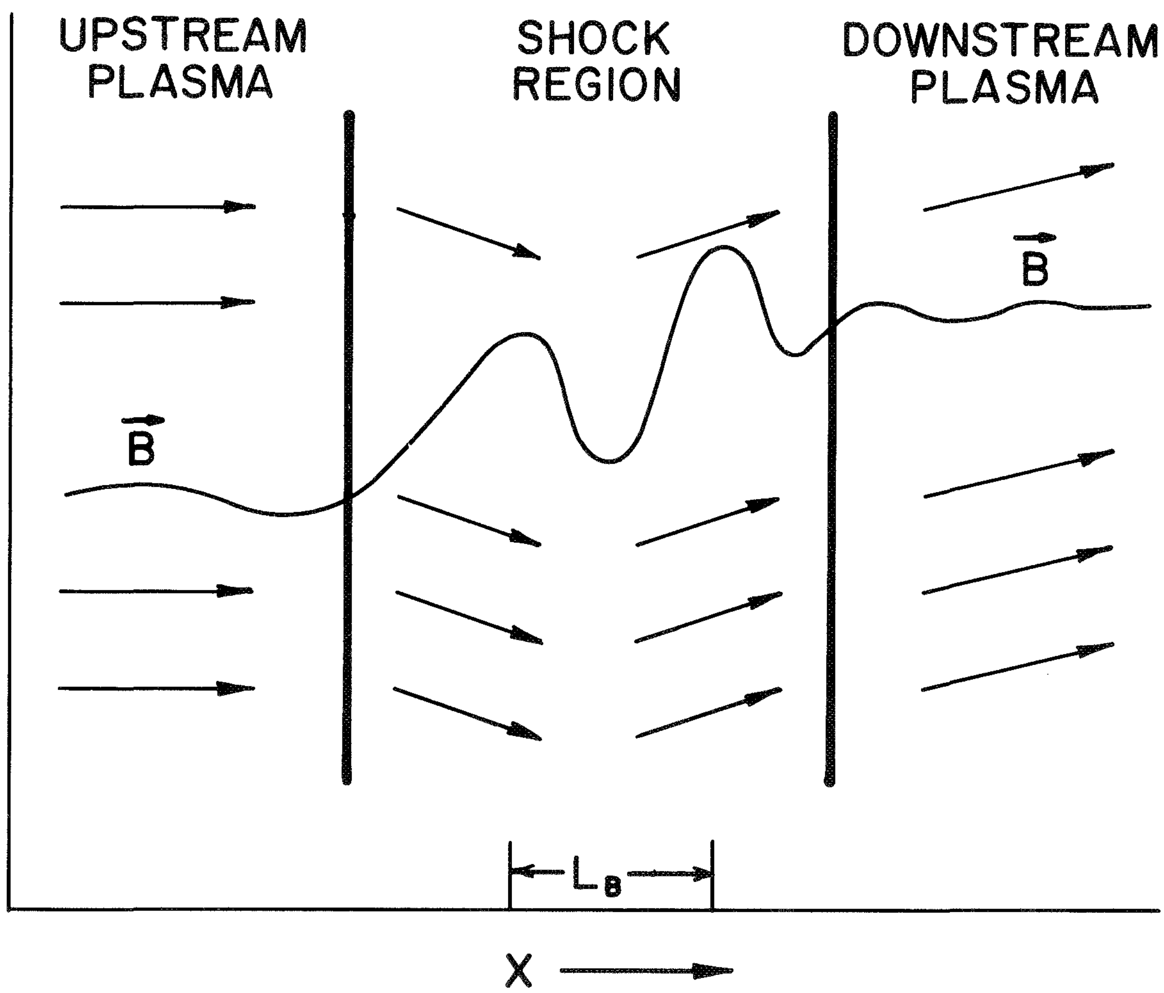

Figure 1.1 The plasma is uniform in the plane perpendicular to the x-axis. It flows in normal to the shock front and is deflected. The magnetic field is constant in time but varies along the x-axis with a length scale L_B.

transport coefficients. However the laminar and turbulent waves are so closely interrelated that we have occasion to discuss the turbulent nature of the waves several times during the thesis.

Like many problems in physics, the solution of the two fluid equations has seen a gradual evolution from the simplest case to the more complicated. There have been three main areas of approximation. These have involved assumptions about the geometry of the problem, assumptions about the equation of state of the plasma, and assumptions about the form of dissipation if any.

Initially it was assumed that the plasma was cold and that there was no dissipation. The simplest geometric configuration was treated by Adlam and Allen[9] who required the direction of plasma flow to be exactly perpendicular to the magnetic field. Saffman[10] did the parallel propagation problem and later[11] he set up the differential equations for propagation at arbitrary angles. This latter case was found to be too complicated to be solved explicitly. He also pointed out the similarity between the behavior of magnetic waves and the motion of a particle in a rotating potential well. We will make extensive use of a more general form of this analogy. Further work on the propagation of cold plasmas at arbitrary angles was done by Cordey[12], Kellogg[13], and others. Kellogg introduced a convenient way of classifying the initial motion of the waves at various Mach numbers and angles of propagation which we use with some slight modifications.

Other authors[14,15,16] examined the effects of temperature on the structure of the waves. Most of them assumed some form of adiabatic pressure law. Kakutani _et al_[17] disputed the validity of using an adiabatic law and assumed instead that the electrons remained at a constant temperature and that the ions were cold. However, all the authors found the same qualitative behavior regardless of which equation of state they picked. It is only the quantitative details of the motion that depend upon the choice of an equation of state. These authors generally restricted their investigations of warm plasmas to the two simplest geometries (i.e. perpendicular and parallel propagation) although some work at arbitrary angles has been done.

All the above cases assumed there was no dissipation. Even without dissipation, Saffman[11] and Cordey[12] found what they call quasi-shocks in which the average downstream state was different from the upstream state. However all their equations are time reversible and there is no change in the entropy of the plasma. We will assume that there is frictional dissipation, acting through wave-particle interactions, so that the equations are irreversible and true laminar shock waves can be found. Sagdeev[8] considered such a frictional force for the cold magnetosonic (perpendicular propagation) case and found laminar shock solutions. As a simplification, he did not allow the friction to heat the plasma and so the energy of the system was not conserved. Cavaliere and Engelmann[13] expanded Sagdeev's analysis to arbitrary angles of propagation. Morton[19] also treated the problem with friction at arbitrary angles of propagation but, in addition, he included some limited finite temperature effects.

In this thesis we present the theory of laminar shock waves in a way which is simple enough to permit an intuitive feeling for how waves with various initial conditions will behave. At the same time we avoid making approximations which limit the range of validity of our results. When explicit analytic solutions are not possible, we use a digital computer to solve the equations rather than generate unwieldy asymptotic solutions or make restrictive approximations. However, a great deal of analytic work is done without resorting to the computer. The computer is used mainly to generate concrete examples of the analytic conclusions we reach.

To keep the results as general as possible, we treat cases of propagation at any angle with respect to the magnetic field and allow any value for the temperature. However only low temperature plasmas are considered in detail (i.e. sound speed less than the Alfvén speed). The pressure is assumed to be isotropic and to obey an adiabatic pressure law in the absence of friction. Friction is included and heats the plasma, altering the adiabatic pressure law. The collision frequency is held constant once it is turned on. Since we do not assume that the ratio of electron to ion masses is small, our results are accurate to all orders of m/M .

In the next chapter we present the equations used to describe the shock structure and discuss some of their general characteristics. In the third chapter the initial effects of a small perturbation in the upstream state of the plasma are investigated. In the fourth chapter the Rankine-Hugoniot relations are used to analyze the possible final states of the plasma. Our model, which only includes frictional dissipation, is not capable of producing high Mach number shock waves so in the fifth chapter the model is modified and the range of Mach numbers is extended. In the last chapter we summarize the principle conclusions of the thesis. Length calculations are presented in the appendices to preserve the continuity of the main text.

CHAPTER II

THE EQUATIONS OF MOTION FOR NONLINEAR WAVES

The purpose of this chapter is to present the basic equations used in this thesis and to develop an analogy between the equations of motion for nonlinear waves and the equations of motion of a particle moving in a rotating potential well[11].

A. Presentation of the Equations

The equations used to describe the motion of nonlinear waves in a plasma are the steady state form of Maxwell's equations and the first three moments of the time independent Boltzmann equation. An additional equation of state is used to determine the partition of thermal energy between electrons and ions.

The geometry of the problem is shown in Figure 2.1. As we stated in Chapter I, the reference frame is chosen such that the shock front is stationary. In this frame all the variables are independent of time. The variables are assumed to vary spatially only in the x-direction. The usual assumption of quasi-neutrality is made so n_i is set equal to n_e in all the equations. The validity of this assumption is discussed in a later section of this chapter. The temperature is assumed to be isotropic and the moment equations are terminated by assuming there is no heat conduction. We also include a frictional force which is proportional to the current times a collision frequency, ν .

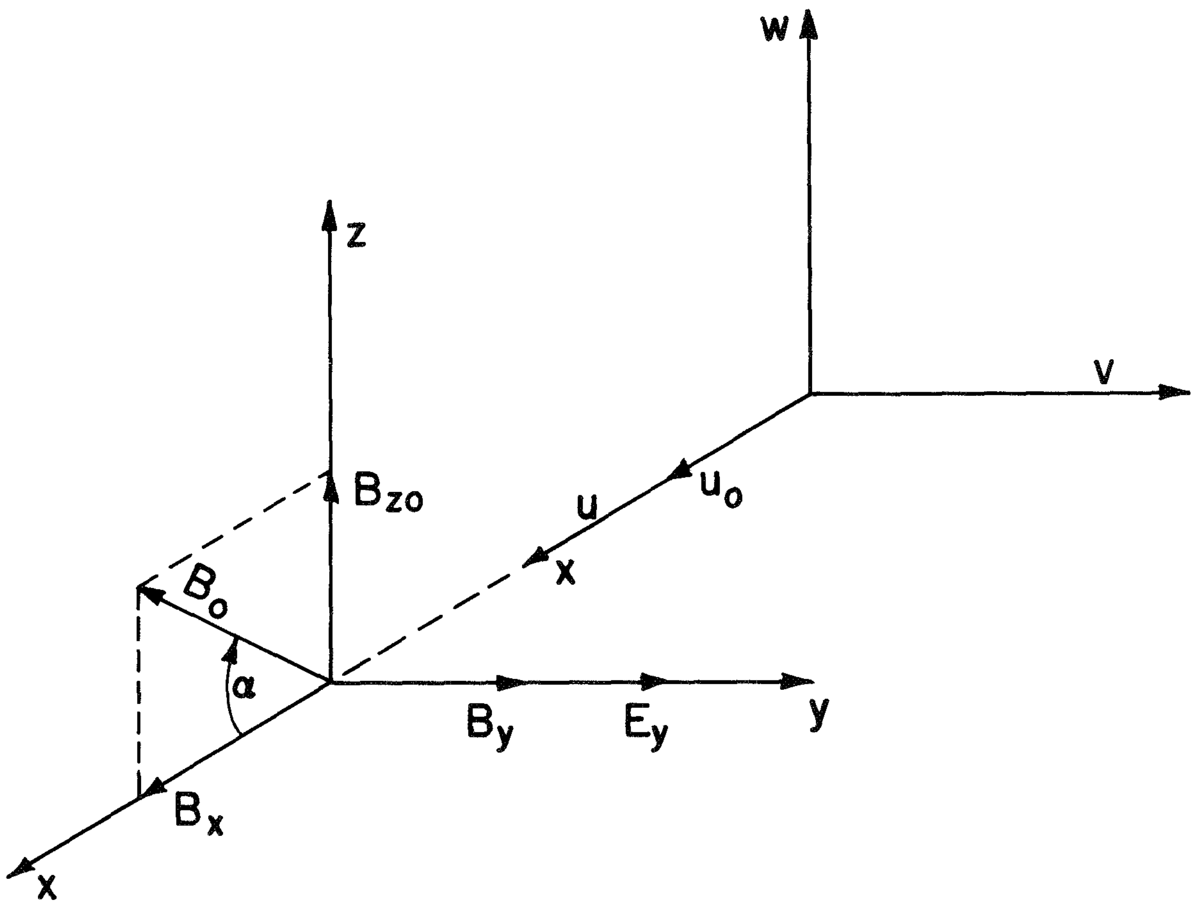

Figure 2.1 The plasma flows into the shock front with a velocity u_o. The magnetic field is initially in the x,z-plane and makes an angle α with the x-axis. The initial electric field is in the y-direction. In the shock front, y and z-components of velocity and a y-component of magnetic field appear.

At $x = -\infty$ the boundary conditions are chosen to be:

$$
\begin{aligned}
\vec{v}_e &= \vec{v}_i = \hat{i}\, u_o \\
\vec{B} &= \vec{B}_o = \hat{i}\, B_x + \hat{k}\, B_{zo} \\
\vec{E} &= \hat{j}\, E_y \\
T_e + T_i &= T_o
\end{aligned}
\tag{2.1}
$$

The first moment equations (one for the electrons and one for the ions) give particle flux conservation relationships:

$$
\begin{aligned}
n_i\, u_i &= j_i = \text{constant} \\
n_e\, u_e &= j_e = \text{constant}
\end{aligned}
\tag{2.2}
$$

Since $u_i = u_e$ at $x = -\infty$ and $n_i = n_e$ we conclude

$$j_i = j_e = j \tag{2.3}$$

and

$$u_i = u_e = u \tag{2.4}$$

for all x .

Next consider the x-component of the second moment equations:

$$\frac{d}{dx}\left(mnu^2 + n\ T_e\right) = -\ ne\left[E_x + \left(v_e\ B_z - w_e\ B_y\right)/c\right] \tag{2.5}$$

and

$$\frac{d}{dx}\left(Mnu^2 + n\ T_i\right) = ne\left[E_x + \left(v_i\ B_z - w_i\ B_y\right)/c\right] \quad . \tag{2.6}$$

Adding (2.5) and (2.6) to eliminate E_x gives

$$\frac{d}{dx}\left(m_t\ nu^2 + nT\right) = \frac{ne}{c}\left[B_z(v_i - v_e) - B_y(w_i - w_e)\right] \tag{2.7}$$

where $T = T_i + T_e$, the sum of the ion and electron thermal energies; and $m_t = M + m$, the sum of the ion and electron masses.

From Maxwell's curl $\vec{B}$ equation we get

$$\frac{d\ B_z}{dx} = -\ \frac{4\pi ne}{c}\ (v_i - v_e) \tag{2.8}$$

and

$$\frac{d\ B_y}{dx} = \frac{4\pi ne}{c}\ (w_i - w_e) \tag{2.9}$$

Using (2.8) and (2.9) in (2.7) gives

$$\frac{d}{dx}\left[u + \frac{T}{m_t u} + \frac{B_z^2 + B_y^2}{8\pi m_t j}\right] = 0 \quad . \tag{2.10}$$

Using the known values at $x = -\infty$, (2.10) becomes

$$u + T/m_t u + \left(B_z^2 + B_y^2\right)\Big/ 8\pi m_t j =$$

$$u_o + T_o/m_t u_o + B_{zo}^2 \Big/ 8\pi m_t j \tag{2.11}$$

This equation is an expression of the conservation of momentum flux in the x-direction. We can also use (2.5) and (2.6) to derive an expression for E_x . This is done in Appendix 1.

The ion and electron equations for the other two components can similarly be combined and, with the use of the curl $\vec{B}$ equations, yield two additional momentum flux conservation relations as well as two equations of motion for the electrons. In the y-direction we find:

$$mu \frac{d\, v_e}{dx} = -\, e\left[E_y - \left(u\, B_z - w_e B_x\right) \Big/ c\right] - \nu_e m(v_e - v_i) \tag{2.12}$$

and

$$v_i = B_x B_y \Big/ 4\pi j M - v_e\, m/M \tag{2.13}$$

In the z-direction:

$$mu \frac{d\, w_e}{dx} = -\, e\left[E_z + \left(u\, B_y - v_e B_x\right) \Big/ c\right] - \nu_e m(w_e - w_i) \tag{2.14}$$

and

$$w_i = B_x\left(B_z - B_{zo}\right)\Big/4\pi jM - w_e m/M \tag{2.15}$$

The ion velocities can be eliminated from the curl $\vec{B}$ equations using (2.13) and (2.15), and the curl $\vec{B}$ equations can be used to eliminate the relative velocity factor in the friction term of (2.12) and (2.14).

The curl $\vec{E}$ equation and the divergence of $\vec{B}$ equation establish that E_y , E_z , and B_x are constant. Since we assume E_z is initially zero, it is zero for all x . We can express E_y in terms of B_{zo} and u_o by observing that the right hand side of (2.12) must be zero at $x = -\infty$. Thus we find

$$E_y = u_o B_{zo}/c \tag{2.16}$$

Poisson's equation is not useful because the quasi-neutrality assumption is being made. The fact that n_i is set equal to n_e does not imply E_x is a constant however. In this approximation, E_x appears in the equations as a field with just the correct magnitude to keep $n_i = n_e$. Physically we attribute the source of E_x to a very small charge separation which creates an electric field tending to keep $n_i \approx n_e$. We have neglected all the derivatives of E_x by making the quasi-neutrality assumption, and thus the electric field energy density does not appear in momentum conservation equations as a self-consistent field would.*

---

* To see this add the electron and ion moment equations before assuming $n_i = n_e$. The resulting equation can be integrated as before and contains the electric field energy density.

Obviously the quasi-neutrality condition loses its validity if the derivative of E_x becomes large.

We still need two additional equations to determine T_e and T_i. For our first equation of state we use the third moment equations. In the absence of friction and heat conduction and with the added assumption of isotropic pressure the two equations can be added together, in a manner similar to that used for the second moment equations, to yield a conservation of energy flux equation:

$$\tfrac{1}{2}\left[m_t u^2 + m\left(v_e^2 + w_e^2\right) + M\left(v_i^2 + w_i^2\right) + 5T\right] + E_y B_z c/4\pi j$$

$$= \tfrac{1}{2}\left(m_t u_o^2 + 5T_o\right) + E_y B_{zo} c/4\pi j \tag{2.17}$$

For an equation of state we assume the validity of (2.17) throughout the shock, even when there is friction heating the plasma. Since only the sum $T_e + T_i = T$ appears in these equations, we need not specify how the thermal energy is partitioned between the electrons and ions to obtain wave profiles.* However in a later chapter we discuss the instability mechanisms that develop within the waves and the ratio of T_e to T_i plays a critical role in these instabilities. As a second equation of state we assume that the ion temperature is constant.

---

* The determination of E_x depends upon T_e and T_i separately, but E_x has been eliminated from the problem. See Appendix 1.

B. Introduction of Dimensionless Variables

The above equations can be simplified by introducing dimensionless variables. We normalize all velocities with respect to u_o, the streaming velocity at $x = -\infty$. Thus u is replaced by uu_o and

$$v_e \rightarrow vu_o \ , \quad w_e \rightarrow wu_o \ , \quad \text{etc.} \tag{2.18}$$

The fields are normalized in terms of their energy density as compared to the streaming kinetic energy density at $x = -\infty$:

$$B_o^2/8\pi \rightarrow B_o^2\left(\tfrac{1}{2}\, m_t n u_o^2\right) \ , \quad B_z^2/8\pi \rightarrow B_z^2\left(\tfrac{1}{2}\, m_t n u_o^2\right) \ , \ \text{etc.} \tag{2.19}$$

The thermal energy can be expressed either in terms of the field energy density or the streaming kinetic energy. Expressed in terms of the field energy density, it is commonly referred to as the plasma's beta:

$$\beta \equiv \frac{n\,T}{B^2/8\pi} \tag{2.20}$$

We will often express it in terms of the streaming kinetic energy rather than the field energy density:

$$T \rightarrow T(m_t u_o^2) \tag{2.21}$$

Note that the two are related by

$$T/\beta \;=\; \frac{B^2/8\pi}{m_t n u_o^2} \;\rightarrow\; B^2/2 \tag{2.22}$$

where we have used (2.19) to write B^2 in dimensionless form. The initial ratio of streaming kinetic energy density to field kinetic energy density defines the Alfvén Mach number

$$M_A^2 \equiv \frac{\frac{1}{2} m_t n u_o^2}{B_o^2/8\pi} \;\rightarrow\; \frac{1}{B_o^2} \tag{2.23}$$

in our dimensionless notation. The two measures of temperature are initially related by

$$T_o = \tfrac{1}{2}\,\beta_o B_o^2 = \tfrac{1}{2}\,\beta_o/M_A^2 \tag{2.24}$$

The angle of propagation of the wave is taken to be the angle between u_o and B_o and is called α . (See Figure 2.1.) Our unit of length is c/ω_p where

$$\omega_p^2 \;=\; 4\pi n e^2 \left(\frac{1}{m} + \frac{1}{M}\right) \tag{2.25}$$

In dimensionless form the collision frequency becomes

$$\nu_e \;\rightarrow\; \nu(\omega_p u_o/c) \tag{2.26}$$

We also define

$$\gamma^2 = m/M \tag{2.27}$$

and replace

$$u\,\frac{du}{dx} \text{ by } \frac{d}{dt} = (\dot{\ }) \tag{2.28}$$

Finally in dimensionless form the equations of motion are:*

$$\dot{B}_z = \gamma(v - B_x B_y) \quad , \tag{2.29}$$

$$\dot{B}_y = -\gamma\Big(w - B_x(B_z - B_{zo})\Big) \quad , \tag{2.30}$$

$$\dot{v} = (uB_z - B_{zo} - wB_x - \nu\dot{B}_z)/\gamma \quad , \tag{2.31}$$

$$\dot{w} = (vB_x - uB_y + \nu\dot{B}_y)/\gamma \quad , \tag{2.32}$$

$$u + T/u + \tfrac{1}{2}(B_z^2 + B_y^2) = 1 + T_o + \tfrac{1}{2}B_{zo}^2 \quad , \tag{2.33}$$

$$u^2 + \gamma^2(v^2 + w^2) - 2\gamma^2 B_x\Big(B_y v + (B_z - B_{zo})w\Big)$$

$$+ B_x^2(1 + \gamma^2)\Big(B_y^2 + (B_z - B_{zo})^2\Big) + 5T + 2B_{zo}B_z$$

$$= 1 + 5T_o + 2B_{zo}^2 \tag{2.34}$$

---

* See Appendix 1 for an example of the procedure used to make an equation dimensionless.

These six equations in six unknowns along with their boundary conditions (2.1) form a closed set of equations and it is their solution that this thesis is concerned with.

C. Preliminary Analysis of the Equations

Except for a few well known special cases[9,10], these six equations can not be solved exactly. We have written a computer program to solve them for various starting conditions and several solutions are presented below. Before turning to the computer we want to analyze the equations further to gain some insight into the nature of the solutions.

We can reduce the number of equations from six to four by eliminating v and w. They can be eliminated from (2.34) by using (2.29) and (2.30):

$$\left(\dot{B}_z^2 + \dot{B}_y^2\right) - \left[1 - u^2 + 5(T_o - T) - B_x^2\left((B_z - B_{zo})^2 + B_y^2\right) - 2B_{zo}(B_z - B_{zo})\right] = 0 \tag{2.35}$$

The electron velocities can also be eliminated from (2.31) and (2.32) by differentiating (2.29) and (2.30):

$$\ddot{B}_z = \left[(u - B_x^2)(B_z - B_{zo}) - (1 - u)B_{zo}\right] + \dot{B}_y B_x\left(\frac{1}{\gamma} - \gamma\right) - \nu\dot{B}_z \quad , \tag{2.36}$$

$$\ddot{B}_y = \left[(u - B_x^2)B_y\right] - \dot{B}_z B_x\left(\frac{1}{\gamma} - \gamma\right) - \nu\dot{B}_y \tag{2.37}$$

By differentiating (2.33) and (2.35) and using (2.36) and (2.37) we find after some straight forward algebra that

$$\dot{u} = -\frac{\left[\dot{B}_z B_z + \dot{B}_y B_y + 2\nu\left(\dot{B}_z^2 + \dot{B}_y^2\right)/3u\right]}{\left[1 - (5/3)\ T/u^2\right]} \tag{2.38}$$

and

$$\dot{T} = -\ (2/3)\left[(T/u)\,\dot{u} - \nu\,(\dot{B}_z^2 + \dot{B}_y^2)\right] \tag{2.39}$$

Note that in the absence of friction

$$T = T_o\ u^{-2/3} \tag{2.40}$$

This is the adiabatic pressure law for an ideal gas and is a direct result of our choosing (2.17) as an equation of state.

In the cold plasma case, $T = 0$, u can be any positive number. But if u reaches zero the two fluid model breaks down and the wave is said to break. In the warm plasma case, $T \neq 0$, the velocity, as we can see from (2.38), is limited to a value*

$$u^2 > (5/3)\ T \tag{2.41}$$

In analogy with the cold plasma case we say the wave breaks when (2.41)

---

* We shall assume that initially $u_o^2 > 5/3\ T_o$.

is an equality. It is easy to see that the two fluid equations are not valid when u is zero (or negative) because the conservation of particle flux equations require the density to be infinite (or negative) in such a case. To better understand the warm plasma case we solve for E_x which appears in (2.5) and (2.6) but was eliminated in (2.7). In Appendix 1 an expression for E_x is derived and noted here:

$$E_x = -\frac{B_x B_y B_{zo}}{c} - \frac{1}{c\gamma\left[1 - (5/3)T/u^2\right]} \times$$

$$\left\{ \left(B_z \dot{B}_z + B_y \dot{B}_y\right) \left[1 - \gamma^2 + \frac{5\gamma^2 \; T_e - T_i\left(3 - 2\gamma^2\right)}{3\;u^2}\right] + \frac{2\nu(\dot{B}_z^2 + \dot{B}_y^2)}{3u} \left[1 - T_i(1 + \gamma^2)/u^2\right] \right\}$$

We see from (2.42) that E_x becomes infinite when T/u^2 is equal to 3/5. This violates the assumption of quasi-neutrality because for E_x to become infinite in a finite time requires that its derivative be infinite. This is inconsistent with our assumption that the charge separation is very small. In the zero temperature case E_x also becomes infinite when the wave breaks $(u = 0)$. In both cases the validity of the two fluid equations ceases sometime before the singularity is reached. To see this, note that if we had set $n_i = n_e$ <u>after</u> adding the two second moment equations we would have had an extra term in (2.11) for the electric field energy density. In writing (2.11) we have implicitly assumed that

$$\left(B_z^2 + B_y^2 - B_{zo}^2\right) \gg E_x^2 \qquad (2.43)$$

Obviously (2.43) will be violated before E_x becomes infinite.

The particular value of T/u^2 at which the wave breaks depends upon the equation of state being used. If the temperature can be written as

$$T = T_o u^{(1 - c_p/c_v)} , \qquad (2.44)$$

then the singularity will appear at*

$$T/u^2 = (c_p/c_v)^{-1} \qquad (2.45)$$

In general the wave will break when the streaming velocity approaches the local speed of sound. Several authors[15,17] have noted that it is possible for the numerator and denominator of (2.38) to go to zero simultaneously so that u stays finite. They even have a separate classification for such waves. But since they only occur at certain discrete Mach numbers, they seem to have little physical relevance and will therefore not be considered in this thesis.

D. Introduction of the Particle Analogy

Consider (2.36) and (2.37). If we were to substitute position variables y and z for B_y and $(B_z - B_{zo})$, then the equations would be very similar to the equations of motion for a particle moving in a

---

* See for example Kakutani et al[17] who assume an isothermal temperature ($c_p/c_v = 1$). c_v and c_p are the specific heats at constant volume and constant pressure.

somewhat complicated force field. There are three distinct forces. The first is very much like the force exerted by a gravitational or an electrostatic force field and depends primarily on the particles position. The second force is proportional to the perpendicular component of the particle velocity and thus can be compared to a coriolis force or to an interaction with a perpendicular magnetic field[12] of magnitude $B_x(1/\gamma - \gamma)$. Finally there is a force proportional to the parallel component of the particle velocity which is equivalent to a frictional force with a coefficient of friction, ν .

For the first force to really be analogous to a gravitational force field, u must be a function of position (B_y and $B_z - B_{zo}$) only. However when there is frictional dissipation u , which is a function of T , also depends upon the particle's past history. To show this dependence explicitly we express T as

$$T = (T_o + \delta)u^{-2/3} \tag{2.46}$$

Inserting this into (2.39) gives

$$\delta(t) = 2/3\ \nu \int_o^t u^{2/3} \left(\dot{B}_z^2 + \dot{B}_y^2\right) dt \quad . \tag{2.47}$$

Note that δ depends upon the particle velocity ($\dot{B}_z$ and $\dot{B}_y$) at previous times. Using (2.33) and (2.47) we can write an equation for u with no explicit T dependence:

$$(1 - u) - \tfrac{1}{2}\left(B_z^2 + B_y^2 - B_{zo}^2\right) + T_o\left(1 - u^{-5/3}\right) = \delta u^{-5/3} . \qquad (2.48)$$

Figure 2.2 shows a plot of $(B_z - B_{zo})$ vs. u with $B_y = 0$, $B_{zo} = .5$, $T_o = 0.1$, and δ having the values zero and 0.1. Note the infinite derivative of u with respect to B_z at $T/u^2 = 3/5$.

As long as there is dissipation δ will be increasing and u will not be a function of B_z and B_y alone. In this case the analogy between the wave motion and a particle moving in a potential well is no longer exact. This does not mean the analogy is not useful however. In the case of solitons and wave motion without friction the analogy is exact with the relationship between u and B given by (2.48) with $\delta = 0$.

By examining the shape of the potential well we can make general statements about the wave motion without finding exact solutions to the equations of motion. For instance if we find our imaginary particle is confined to a region that does not include any points where the wave will break, $(T/u^2 > 3/5)$, then we can be sure that the wave is stable.

Even when there is friction the potential well analogy is useful. With friction present the particle must either come to rest somewhere where the potential well is level or reach a point where $T/u^2 = 3/5$ and break. The possible final states can be found from the Rankine-Hugoniot relations. These are derived in Appendix 2 and discussed more fully in Chapter IV. The important thing in this context is that they enable us to calculate the values of δ where the particle may come to rest:

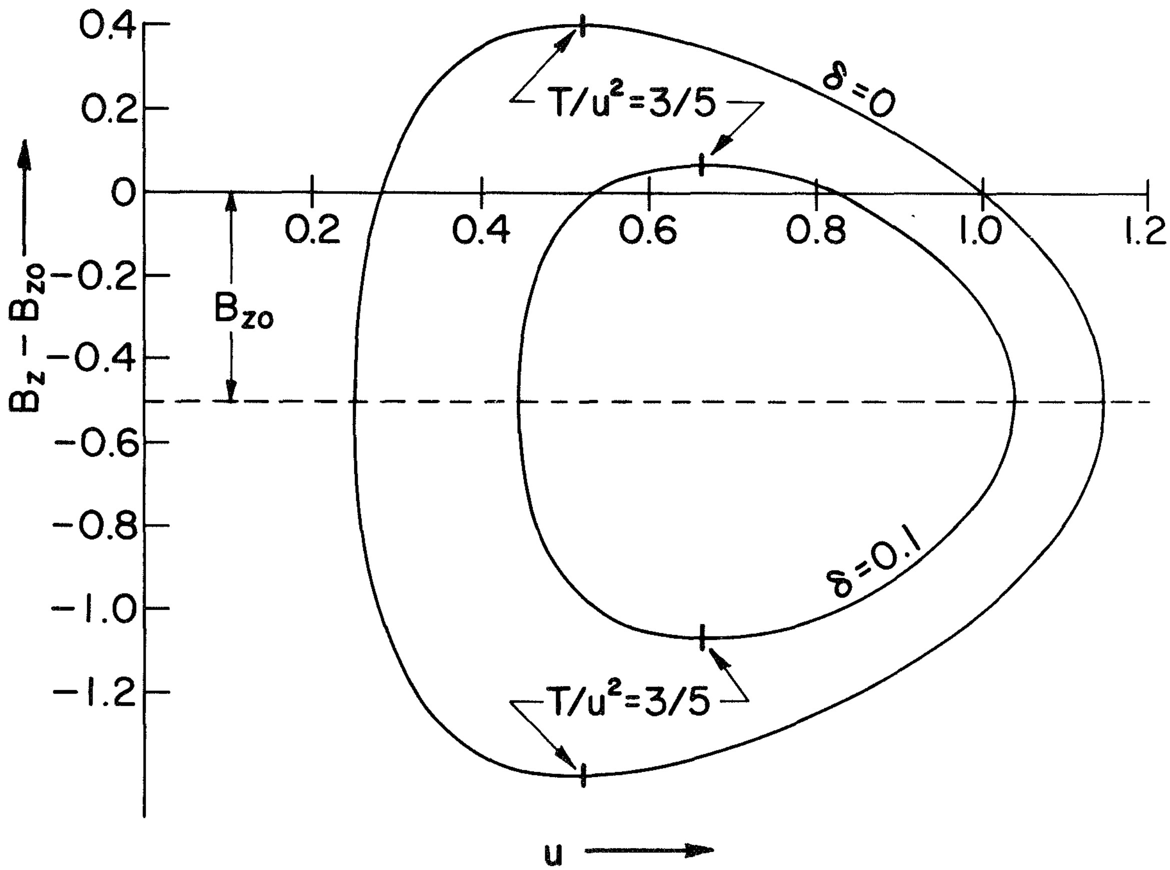

Figure 2.2 A plot of (2.48) with $B_{zo}=0.5$, $B_y=0$, and $T_o=0.1$. Note that the curves are symmetric about B_{zo}.

$$\delta_f = T_f u_f^{2/3} - T_o \quad , \tag{2.49}$$

where the f subscript refers to final values. From δ_f we can find the final shape of the potential and examine the stability of the final state. Before going further we must derive an expression for the potential.

The usual procedure for finding an energy integral when studying a mechanical system is to take the dot product of the force equation and the velocity:

$$m \ddot{\vec{x}} \cdot \dot{\vec{x}} = \vec{F} \cdot \dot{\vec{x}} \quad , \tag{2.50}$$

and integrate both sides. This yields a result of the form

$$\tfrac{1}{2} m \dot{\vec{x}}^2 + V_1(\vec{x}) = E(t) \quad . \tag{2.51}$$

$E(t)$ represents the loss in energy due to friction:

$$E(t) = -\nu \int_0 \dot{\vec{x}}^2 \, dt \tag{2.52}$$

We could also write (2.51) as

$$\tfrac{1}{2} m \dot{\vec{x}}^2 + V_2(\vec{x},t) = 0 \quad , \tag{2.53}$$

where

$$V_2(\vec{x},t) = V_1(\vec{x}) - E(t) \quad . \tag{2.54}$$

This can be looked at as the energy equation for a particle moving without friction in a potential well where the shape is fixed but the whole well is rising upwards in time. The particle can never rise above line where $V_2(\vec{x},t)$ is equal to zero but this line changes as the well moves upwards. The rate of movement upwards is determined by the frictional dissipation.

The reason for choosing (2.53) rather than (2.51) is that we already have an equation similar to (2.53) namely (2.35). The part corresponding to $V_2(\vec{x},t)$ is evidently

$$V(\vec{B},t) = -\tfrac{1}{2}\left[(1-u^2) + 5(T_o - T) - B_x^2\left((B_z - B_{zo})^2 + B_y^2\right) - 2B_{zo}(B_z - B_{zo})\right] \tag{2.55}$$

The difference between (2.53) and (2.55) is that, as long as there is dissipation, the potential well given by (2.55) not only rises as a whole but changes shape. If the shape of V changed drastically during the course of the wave's motion, the analogy would not be very useful. Fortunately the changes in the shape of the potential are quite minor. The essential topological features such as maxima, minima, and saddle points generally remain fixed in number and relative location although their exact positions vary. This makes it possible to determine the general behavior of the waves even with friction present. For example if the T/u^2 breaking line is outside the range of the particle's motion for all δ's from zero to δ_f, we can be sure the wave will not break before δ_f is reached.

For certain ranges of initial conditions the important features of the potential may change enough as δ goes from zero to δ_f to affect the stability of the wave. This only happens if an equilibrium point is near the breaking line. Several examples will be considered in the following three chapters to show more fully the close relationship between the wave behavior and the particle analogy developed in this section. We will consider a particularly simple example here.

E. Example of Wave Motion

The simplest type of nonlinear wave motion is the well-known magnetosonic wave[9]. Since $B_x = 0$ for a magnetosonic wave we do not have a perpendicular magnetic field acting on our hypothetical particle (recall that the analogy included a magnetic field of magnitude $B_x(1/\gamma-\gamma)$). Also note that if B_y is zero initially it will stay zero so we only have to examine the potential along the B_z axis.

The lowest curve in Figure 2.3 shows the initial shape of the potential well $(\delta = 0)$. Since the origin $(B_z = B_{zo})$ is level we must perturb the particle from this unstable equilibrium. If we perturb it either to the right or the left and there is no friction, the wave will surely break because the T/u^2 breaking line (really points in this one-dimensional potential) is below the $V = 0$ line.

Figure 2.3 also shows the potential with $\delta = .35\ \delta_f$. Now the right hand side is stable because the breaking line has moved above the $V = 0$ line and is out of the range of the particle's motion. If

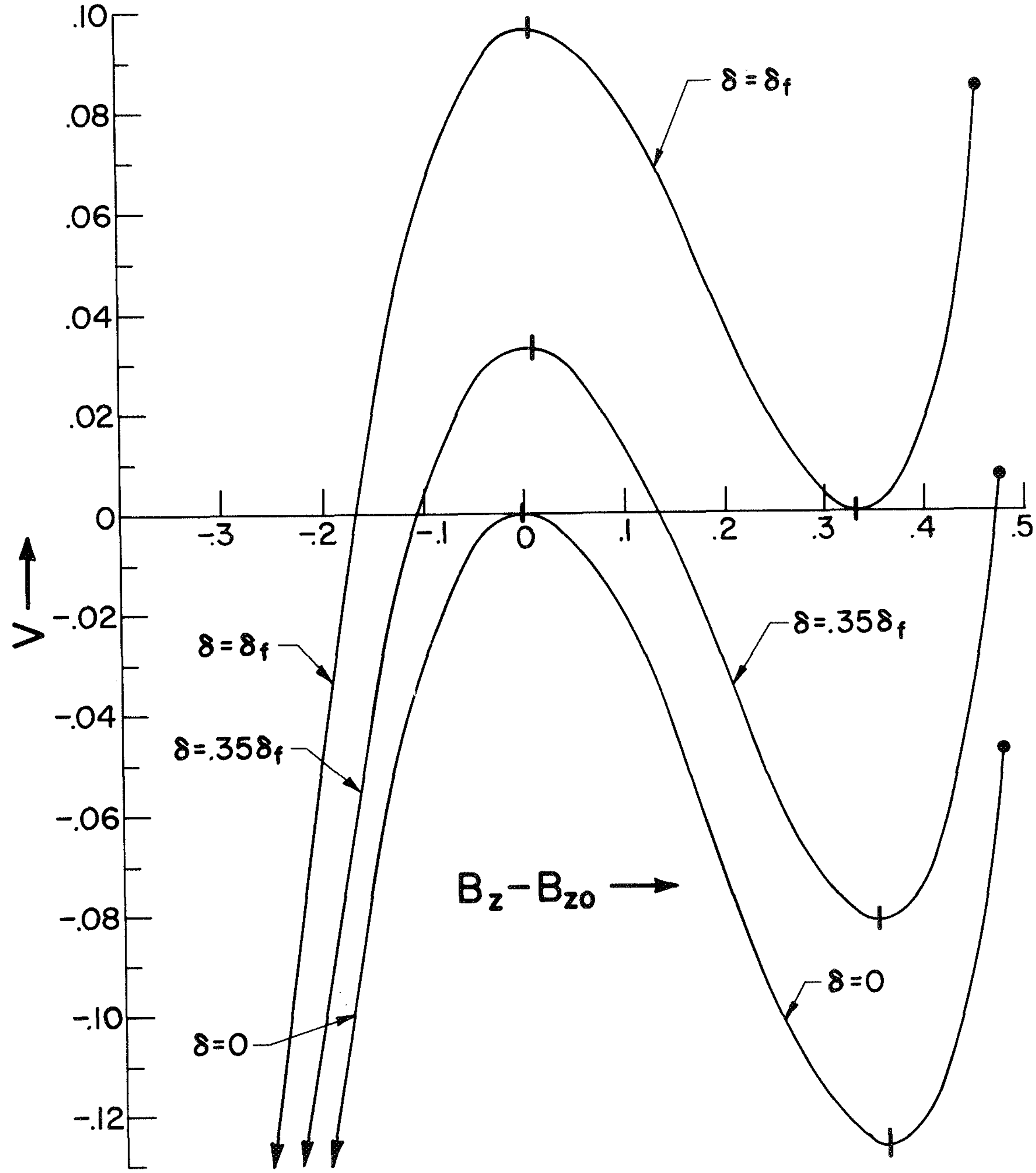

Figure 2.3 The potential well for a magnetosonic soliton with M_A=1.5 and β_o=0.2. As friction heats the plasma, δ increases from zero to δ_f. As it increases, the potential well rises and changes shape.

the particle was perturbed to the left it would still break, even with friction. If it was perturbed to the right with enough dissipation that δ increased to $.35\delta_f$ before the particle reached the breaking line, it would appear that a stable state has been reached.

The upper curve in Figure 2.3 labelled $\delta = \delta_f$, shows the final shape of the potential well. Since there is only one point on the positive axis of the upper curve that is not above the $V = 0$ line, the particle must come to rest there. Since the particle's velocity is zero, δ remains constant and the system is static.

From the potential picture we have been able to predict when the wave will break, when it might break, and what the final state will be if it does not break.

Figure 2.4 shows a computer calculation of the same wave. The initial perturbation was to the right, and the friction was chosen by trial and error to be just large enough to keep the wave from breaking. Notice that T/u^2 always stays below 3/5. The arrows at $t = 14$ indicate the values of the various parameters when $\delta = .35\delta_f$.

In the next two chapters we will investigate in detail the allowed initial perturbations and the possible final states of the plasma. The particle analogy developed in this chapter will be developed further and will prove to be very helpful in giving an intuitive feel to the results we derive in the following chapters.

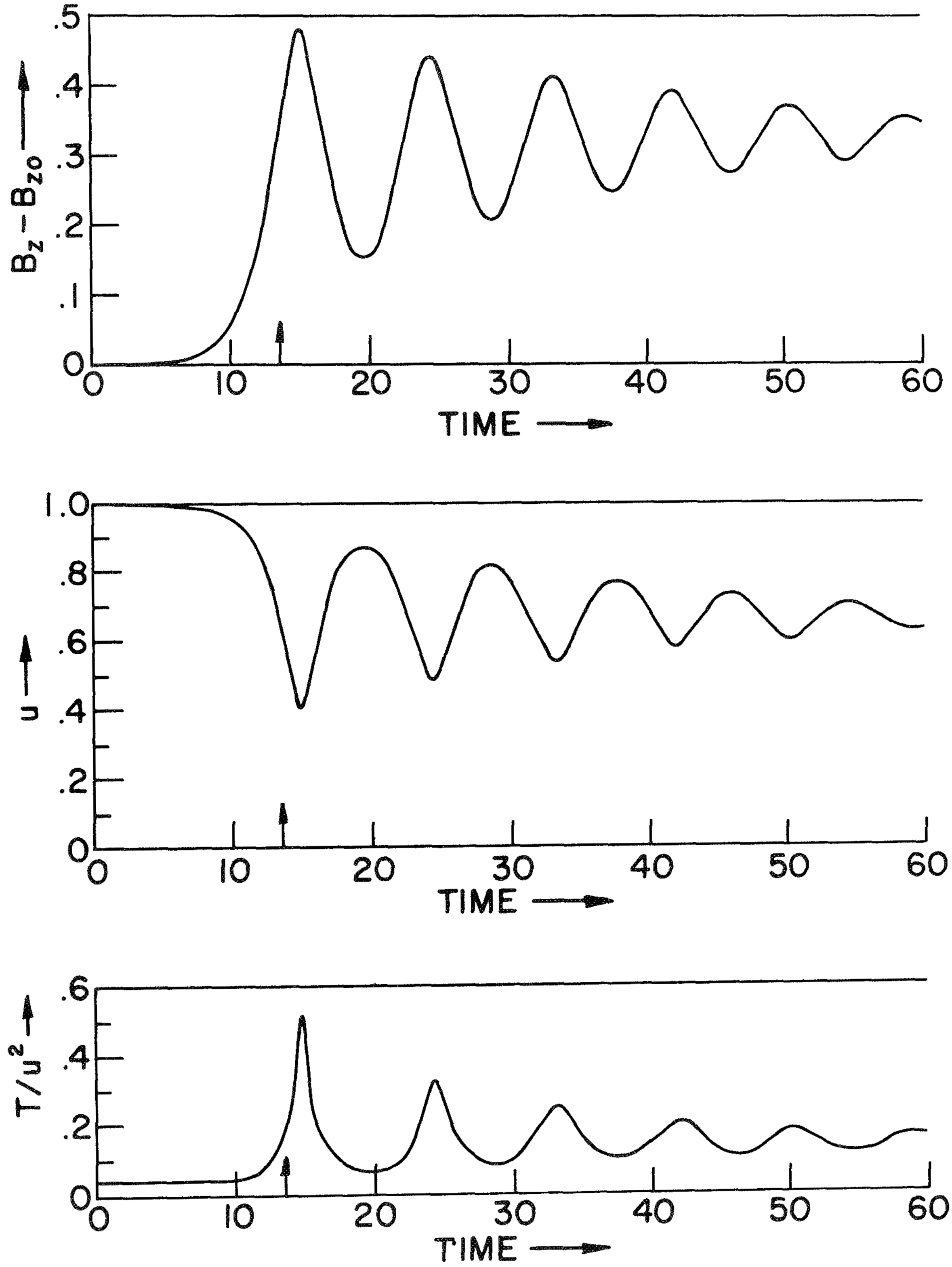

Figure 2.4 The time behavior of a magnetosonic wave with M_A=1.5, β_o=0.2, and ν=0.1.

CHAPTER III

INITIAL CONDITIONS

At $x = -\infty$ the plasma is assumed to be in a state of equilibrium. There are no currents and all the fields and velocities are constant. Unless the plasma is perturbed from this equilibrium, it will just stay in a static state much like a marble resting on top of a mountain. To create a wave we must perturb the plasma.

A. The Linearized Equations of Motion

For small departures from equilibrium the equations of motion ((2.29) to (2.34)) are linear and have solutions of the form

$$A = A_o + A_1 e^{\lambda t} \tag{3.1}$$

A_o is the value at $x = -\infty$ and A_1 is a small perturbation. Assuming this form for all the variables and dropping second order terms, the equations of motion become

$$\lambda B_{z1} = \gamma(v_1 - B_x B_{y1}) \tag{3.2}$$

$$\lambda B_{y1} = -\gamma(w_1 - B_x B_{z1}) \tag{3.3}$$

$$\lambda v_1 = \left[B_{z1}\left(1 - B_{zo}^2/(1 - 5/3\ T_o)\right) - w_1 B_x\right]/\gamma \tag{3.4}$$

$$\lambda w_1 = (v_1 B_x - B_{y1})/\gamma \tag{3.5}$$

Making the same approximations we also find

$$u_1 = - B_{z1} B_{zo} \Big/ \Big[1 - (5/3)\ T_o\Big] \tag{3.6}$$

and

$$T_1 = \frac{2\ T_o\ B_{z1}\ B_{zo}}{3[1 - (5/3)T_o]} = - \frac{2}{3} T_o\ u_1 \tag{3.7}$$

In deriving these relationships we have assumed that $\nu = 0$. This is reasonable because ν is an anomalous resistivity and is associated with certain instability mechanisms. For small deviations from equilibrium we do not expect instabilities. The dissipation will be switched on deeper in the shock wave where the gradients are large.

The linearized equations of motion form a homogeneous set of four linear equations. For there to exist a nontrivial solution it is necessary that the determinant of the coefficients be zero. Thus we find:

$$\lambda^4 + \lambda^2 \Big\{B_x^2(1/\gamma^2 + \gamma^2) + B_{zo}^2 \Big/ \Big[1 - (5/3)T_o\Big] - 2\Big\}$$

$$+ \Big(1 - B_x^2\Big)\Big[1 - B_x^2 - B_{zo}^2 / \Big(1 - (5/3)T_o\Big)\Big] = 0 \tag{3.8}$$

With $T_o = 0$ (3.8) reduces to Kellogg's[13] equation 23 except for some differences in notation. Following Kellogg, but allowing for thermal effects, we write (3.8) as

$$\lambda^4 + \lambda^2 b + c = 0 \tag{3.9}$$

which has solutions

$$\lambda = \pm\left[\tfrac{1}{2}\left(-b + \sqrt{b^2 - 4c}\right)\right]^{\frac{1}{2}}$$

and

$$\lambda = \pm\left[\tfrac{1}{2}\left(-b - \sqrt{b^2 - 4c}\right)\right]^{\frac{1}{2}} \tag{3.10}$$

If the roots are not real they must occur in complex conjugate pairs since b and c are real. Roots that have negative real parts do not give the correct behavior at $x = -\infty$ so they are not considered. All other roots are listed in Table 1 along with their dependence on b and c.

c	b^2-4c	b	Type of Roots	Region
neg	–	–	λ_r ; $\pm\lambda_i$	I_r
pos	neg	–	$\lambda_r \pm \lambda_i$	II_c
pos	pos	neg	λ_{r1} ; λ_{r2}	II_r
pos	pos	pos	$\pm\lambda_{i1}$; $\pm\lambda_{i2}$	IV_i

<u>Table 1</u>

The coefficients b and c are functions of the initial state of the plasma. We would like to exhibit this dependence in a two-dimensional graph. Then the boundaries between the various regions listed in Table 1 will be the lines across which c or $b^2 - 4c$ change sign. If $b = c = 0$, all four regions can share a common point.

The state of the plasma at $x = -\infty$ is determined by four parameters -- its streaming velocity, its thermal energy, the magnitude of the magnetic field, and the angle between the magnetic field and the streaming velocity. If we express three of the parameters as a ratio to the fourth, we still have to fix one of the ratios to make a two-dimensional plot of the various regions of Table 1. The conventional procedure is to fix the ratio of the thermal energy density to the magnetic field energy density. This ratio was defined in (2.20) and is commonly known as the plasma's beta. The relationship between β_o and T_o is given in (2.24). We will follow this convention and so our plots will be constant β_o plots rather than constant T_o plots. For independent variables we will follow Kellogg[13] and use B_{zo} and B_x. Replacing T_o with β_o in (3.8), we now solve for the lines which form the boundaries of the regions defined in Table 1.

The boundaries in region I_r are found where c changes sign. This occurs where $c = 0$:

$$\left(1 - B_x^2\right)\left[1 - B_x^2 - B_{zo}^2\Big/\left(1 - 5\beta_o B_o^2/6\right)\right] = 0 \qquad (3.11)$$

But these are not the only boundaries because c can also change sign by going through infinity when $T_o = 3/5$. Thus we find an additional boundary for region I_r at

$$B_o = \left(5\beta_o/6\right)^{-\frac{1}{2}} \tag{3.12}$$

The boundaries for region II_c occur where $b^2 - 4c$ is equal to zero:

$$\frac{B_{zo}^4}{[1 - 5\beta_o B_o^2/6]^2} + \frac{2B_x^2 B_{zo}^2 (1 - \gamma^2)^2/\gamma^2}{[1 - 5\beta_o B_o^2/6]}$$

$$+ \; B_x^2\left[B_x^2\left(1 + \gamma^2\right)^2/\gamma^2 - 4\right]\left[1 - \gamma^2\right]^2/\gamma^2 \tag{3.13}$$

In this case there is no change in sign when (3.13) goes through infinity because the singularity is of second order.

The $c = 0$ and $b^2 - 4c$ curves may intersect at as many as three points. One of these corresponds to the one found by Kellogg[13] in the zero temperature case and occurs at

$$B_x \approx \gamma \; ; \quad B_{zo} \approx \left(1 + 5\beta_o/6\right)^{-\frac{1}{2}} \tag{3.14}$$

The approximations in (3.14) make use of the smallness of γ. A second common point is located at

$$B_x = 1 \; ; \quad B_{zo} \approx \left[\left(1 - 5\beta_o/6\right)/\left(5\beta_o/6 - \gamma^2\right)\right]^{\frac{1}{2}} \quad , \tag{3.15}$$

and a third at

$$B_x = \left(5\beta_o/6\right)^{-\frac{1}{2}} \; ; \quad B_{zo} = 0 \tag{3.16}$$

If β_o is zero, only the first of these ponts occurs in the finite B_x, B_{zo}-plane. If β_o is less than $6\gamma^2/5$ or greater than $6/5$ the second point does not occur in the real B_x, B_{zo}-plane.

These curves are shown in Figure 3.1 and the various regions are labelled according to the scheme of Table 1. The value of β_o was taken to be 0.2. The figure was plotted with $\gamma^2 = 1/25$ to expand regions II_r and II_c. Note that the boundary of II_c intersects the B_x-axis at $B_x \approx 2\gamma$ and is thus not amenable to graphing if the proper value of γ^2 is used. All the curves upon which c changes sign are independent of γ and are therefore not affected.

In this thesis we will only consider plasmas which are initially "warm" and exclude those which are initially "hot". The dividing line between a warm and a hot plasma is taken to be the line defined by (3.12) on which $T_o = 3/5$. An equivalent definition is to define a warm plasma as one where the plasma flow is supersonic and a hot plasma as one where the streaming velocity is less than the speed of sound. This limits the thermal energy density with respect to the streaming kinetic energy density. We will also limit the thermal energy density with respect to the field energy density by considering only plasmas with β_o less than 6/5. This is equivalent to requiring that the Alfvén speed be greater than the sound speed and ensures that the rightmost $c = 0$ line in Figure 3.1 is always to the right of the $B_x = 1$ line.

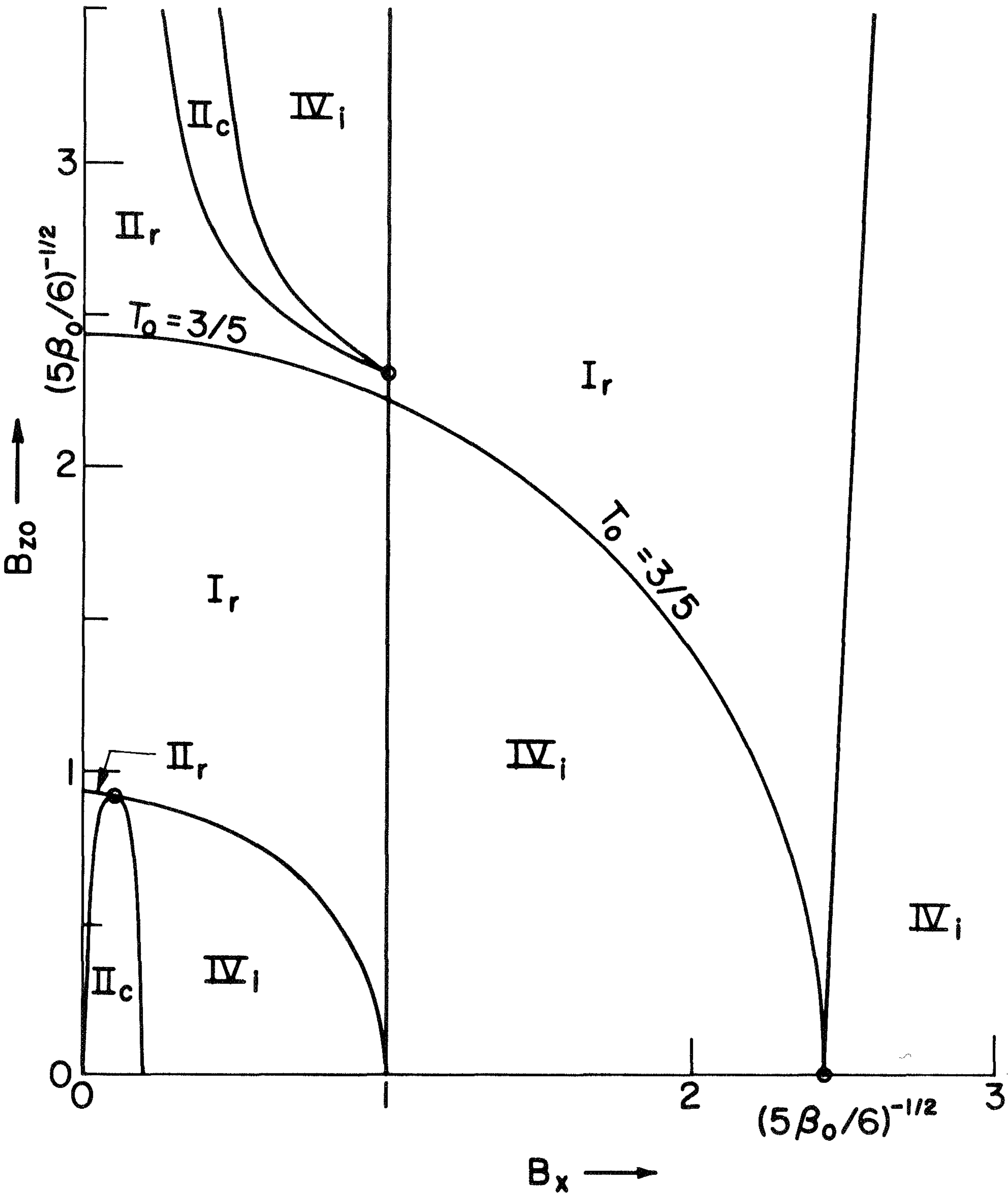

Figure 3.1 A plot of the regions defined in Table 1 with β_o=0.2 and γ^2=1/25.

In regions IV_i and I_r there are pure imaginary roots to (3.9). Waves with these roots do not grow in amplitude from one oscillation to the next since λ does not have a real part. Also these waves do not approach the assumed equilibrium values at $x = -\infty$. Since we are interested in nonlinear waves we could exclude pure imaginary roots from considearation as several authors[12] have. This is of no real consequence in region I_r because there is also a real root to (3.9) in I_r with which to produce nonlinear waves. However in region IV_i all the roots are imaginary, and to exclude all of region IV_i is to exclude many oblique waves of laboratory and astrophysical interest. We will therefore modify our assumptions about the state of the plasma at $x = -\infty$, in region IV_i, to include small linear oscillations about the equilibrium values given in (2.1).

The waves in region IV_i will still be of no interest unless a way is found to make them grow into nonlinear waves. This can be done quite simply by allowing for a small amount of dissipation at $x = -\infty$. The linearized equations are modified to include friction in Appendix 3. It is shown there that only the low frequency roots in the part of IV_i where B_x is less than one will grow in amplitude with the addition of friction. The high frequency roots always damp out as do the low frequency roots in the regions where B_x is greater than one. Thus we will only be concerned with the lower of the two frequencies in region IV_i where B_x is less than one.

The significance of these various regions and the effect of friction on the initial wave behavior will become clearer when we examine the shape of the potential well the analogous particle moves in near the origin.

The potential well analogy provides a convenient bridge between the nonlinear and the linear theory as we shall see below.

B. The Shape of the Potential Near the Origin

Recall from Chapter II that, in the absence of friction, the equations of motion for the wave are the same as those for a particle moving in a gravitational or electrostatic potential with a uniform magnetic field perpendicular to the plane of motion. In this section we are interested in the shape of the potential near the origin and how it changes from one region of Figure 3.1 to the next. The shape of the potential near the origin is found by solving for the first and second derivatives of the potential and evaluating them at the origin.

The origin is assumed to be an equilibrium point so the first derivatives of the potential should be zero there. The sign of the second derivatives indicates whether the origin is a maximum, a minimum, or a saddle point. If it is a maximum the second derivatives must be negative, and if it is a minimum they must be positive. A necessary and sufficient condition for the existence of a maximum or a minimum rather than a saddle point is

$$(V_{yz})^2 < V_{zz} V_{yy} \qquad , \tag{3.17}$$

where

$$V_{ij} = \frac{d^2V}{dB_j \, dB_i} \tag{3.18}$$

Recall that

$$V = -\tfrac{1}{2}\left[(1 - u^2) + 5(T_o - T) - B_x^2\left[(B_z - B_{zo})^2 + B_y^2\right]\right.$$

$$\left. - 2B_{zo}(B_z - B_{zo})\right] \tag{3.19}$$

Differentiating (3.19) with respect to B_z gives

$$V_z = u\,u_z + (5/2)T_z + B_x^2(B_z - B_{zo}) + B_{zo} \tag{3.20}$$

The subscripts on u and T imply partial differentiation with respect to B_z. We can write

$$T_z = \frac{\partial T}{\partial u}\,u_z = -\frac{2Tu_z}{3u} \tag{3.21}$$

from (2.39). Using this result in (3.20) gives

$$V_z = u_z\left[u - (5/3)T/u\right] + B_x^2(B_z - B_{zo}) + B_{zo} \tag{3.22}$$

From (2.38) we have

$$u_z = -B_z\Big/\left[1 - (5/3)T/u^2\right] \tag{3.23}$$

Finally we find

$$V_z = \left[(B_z - B_{zo})\ (B_x^2 - u) + B_{zo}(1 - u)\right] \tag{3.24}$$

Similarly we find

$$V_y = B_y(B_x^2 - u) \tag{3.25}$$

These are just the negative of the quantities in the brackets on the right-hand sides of (2.36) and (2.37), which is to be expected since the force should be the negative gradient of the potential. At the origin $B_z = B_{zo}$, $B_y = 0$, and $u = 1$ so both V_z and V_y are zero as expected.

The second derivatives are calculated in the same manner and we find:

$$V_{zz} = \left\{(B_x^2 - u) + B_z^2\Big/\left[1 - (5/3)T/u^2\right]\right\} \quad , \tag{3.26}$$

$$V_{yy} = \left\{(B_x^2 - u) + B_y^2\Big/\left[1 - (5/3)T/u^2\right]\right\} \quad , \tag{3.27}$$

and

$$V_{yz} = B_z B_y / \left(1 - (5/3)T/u^2\right) \tag{3.28}$$

Substituting in the values these variables have at the origin and using (2.24) to replace T_i by β_o, we find:

$$V_{zz}\Big|_o = \left[(B_x^2 - 1) + B_{zo}^2\Big/(1-5\beta_o B_o^2/6)\right] \tag{3.29}$$

$$V_{yy}\Big|_o = (B_x^2 - 1) \tag{3.30}$$

and

$$V_{yz}\Big|_o = 0 \tag{3.31}$$

Since V_{yz} is equal to zero, (3.17) is always satisfied if V_{zz} and V_{yy} have the same sign.

Comparing (3.29) and (3.30) with (3.11) and (3.12) we can see that when c changes sign one (or both) of the second derivatives changes sign also. The lines across which c changes sign are lines across which the potential at the origin changes from a maximum or a minimum to a saddle point. Like the c lines, the derivatives are independent of the electron to ion mass ratio.

Using Figure 3.1 and (3.29) and (3.30) we can distinguish three distinct regions below the $T_o = 3/5$ line. In the lower left-hand corner of Figure 3.1, below the curved c line, both V_{zz} and V_{yy} are negative at the origin and thus we conclude that the origin is a maximum* in this region. Above the c line but to the left of the $B_x = 1$ line the origin is a saddle point. For B_x greater than one, the origin is a local minimum since V_{yy} and V_{zz} are both positive. This analysis can easily be carried out in the regions above the $T_o = 3/5$ line. In Figure 3.2 each of the three regions is labelled according to

---

* When referring to a maximum or a minimum we always mean a local maximum or a local minimum.

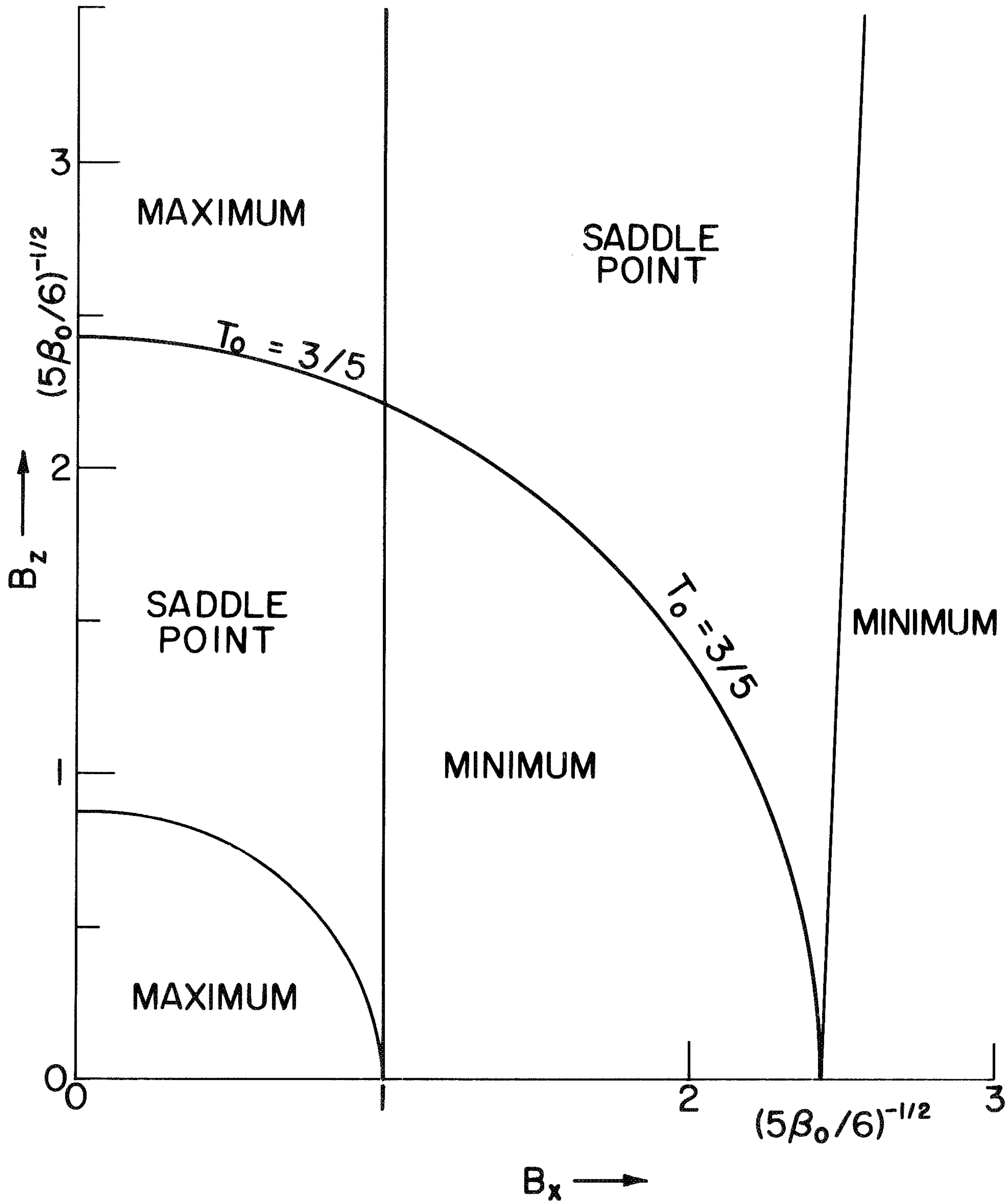

Figure 3.2 The initial shape of the potential well at the origin.

whether the origin is a maximum, a minimum, or a saddle point there. The results above the $T_o = 3/5$ line are also shown for comparison.

In the region where the origin is a maximum there are three types of initial behavior predicted (see Figure 3.1) corresponding to the three regions II_r , II_c , and IV_i . The waves in each of these regions have quite different initial behaviors. Here we will present a heuristic argument to explain the initial wave motion in each of these three regions as well as in the other regions of Figure 3.2.

In the regions where the origin is a maximum the analogous particle can move in a closed orbit about the origin (region IV_i), it can spiral down the potential peak (region II_c), or it can roll straight down the potential peak without spiralling (region II_r). The key to which of these three modes the particle will move in is the perpendicular magnetic field which acts on the particle. Recall that it has a magnitude of $B_x(1/\gamma - \gamma)$. The influence of this perpendicular field is best seen by noting that both the magnitude of the field and the boundaries of the three regions depend upon γ while the shape of the potential well is independent of γ .

In region IV_i , B_x is much larger than γ so the magnetic forces will predominate over the gradients in the potential as soon as the particle moves away from the origin. It is of course necessary for the particle to move a small distance from the origin and acquire a velocity on the order of γ because the magnetic force is proportional to the particle's velocity.

In region II_c , where $B_x \approx \gamma$, the magnetic force no longer can overcome the gradients in the potential well without the velocity becoming on the order of unity. As a result, the particle spirals down the potential peak.

In region II_r the magnetic field is even weaker than in region II_c . Since the field is so weak, the shape of the potential peak becomes more important. To show the shape explicitly we can replace $(B_z - B_{zo})$ and B_y with polar coordinates B_r and θ in (3.19):

$$V = -\tfrac{1}{2}\left[(1-u^2) + 5(T_o - T) - B_x^2 B_r^2 - 2B_{zo}B_r \cos\theta\right] . \qquad (3.32)$$

Using the same procedure as above we find

$$\left.\frac{d^2V}{dB_r^2}\right|_o = (B_x^2 - 1) + \frac{B_{zo}^2 \cos\theta}{(1 - 5\beta_o B_o^2/6)} \qquad (3.33)$$

which is in agreement with (3.29) and (3.30) when θ is equal to 0 and $\pi/2$.

Notice in Figure 3.1 that the part of region II_r with the largest value of B_x occurs where the coefficient of $\cos\theta$ in the last term in (3.33) is the largest. It is this term that determines the asymmetry of the potential peak. As B_{zo} gets smaller, we have to go to smaller and smaller B_x before the particle can roll straight down the potential peak. It is clear that it is the asymmetry in the potential peak that determines the dividing line between regions II_c and II_r (along with the perpendicular magnetic field of course). In region II_r , the normal to the potential surface has a large enough tangential component to overcome the tendency of the weak magnetic field to curve the particle's path.

In the region where B_x is greater than one, the potential is a minimum and non-growing waves are predicted from the linearized equations. At first it might seem that no motion is possible in this region because all the points near the origin are above the $V = 0$ plane except for the origin itself. The reason the linearized equations can predict waves which violate the energy relationship is that the changes in energy are of second order and the linearized equations only consider first order effects. It is clear from the shape of the potential well that although linear waves may be allowed, nonlinear waves certainly are not.

We found in Appendix 3 that the addition of friction would cause linear waves in this region to damp out. This is consistent with one's intuitive feeling for what effects friction would have in a region where the origin is a minimum. In the region of IV_i where the origin is a maximum the situation is more complicated. In the absence of a potential force, we would expect the friction to cause the particle's orbit to decay since the radius of the orbit of a particle in a magnetic field is proportional to its velocity. If, however, there were no perpendicular magnetic field and the potential at the origin were a maximum, we would expect the particle to move away from the origin. Friction would only slow the rate at which the particle moved away. In the low frequency mode in region IV_i, there is a balance between the magnetic forces and the potential forces. Friction, by reducing the velocity of the particle, reduces the effectiveness of the magnetic field and the particle moves away from the origin. In the high frequency mode the potential gradients only play a secondary role. The particle acts essentially as if there were no gradients and spirals into the origin when friction is added.

In region I_r the origin is a saddle point. Since part of the potential near the origin is above the $V = 0$ plane, we do not expect to find nonlinear waves oscillating about the origin. Oscillatory linear waves are possible, and predicted, since the energy differences near the origin are second-order effects. However since there is also an exponentially growing root to the linear equations, we will not consider the oscillatory linear waves in this region.

After the discussion about region II_r , one might be surprised that an exponentially growing root is possible with B_x so large. The reason it is possible is that the origin is a saddle point. That means that the particle can move away from the origin and still keep the potential (and hence the particle velocity) small. To do this the particle must move away from the origin close to the line where the potential well intersects the $V = 0$ plane. We can obtain an equation for the $V = 0$ line by setting (3.33) equal to zero:

$$\cos\theta = \frac{(1 - B_x^2)(1 - 5\beta_o B_o^2/6)}{B_{zo}^2} \tag{3.34}$$

If $\pm\theta$ is a solution, then of course $\pi \pm \theta$ is also a solution. Of these four directions only two are such that the magnetic forces and the forces due to the potential gradients are in opposite directions and can balance one another. For the two forces to balance, the particle must move off in the $-B_y$ direction.

As B_x gets weaker the particle must move further away from the $V = 0$ lines to acquire enough velocity for the two forces to balance. Finally, when B_x equals zero, the particle rolls straight down the B_y-axis.

Since we are using only one root in region I_r the solutions will be unique except for an arbitrariness in which of the two $V = 0$ line the particle follows. In all the other regions there are an infinity of solutions because any linear combination of the allowed roots satisfies the linearized equations of motion.

C. Examples of Initial Behavior

As an example of the various starting conditions discussed above we will consider waves propagating at an angle of $\pi/4$ $(B_x = B_{zo})$ and with a β_o of 0.2. By varying the Mach number $(M_A = 1/B_o = \sin(\pi/4)/B_x)$ we will include waves from regions II_c, IV_i, and I_r.

Since we are fixing β_o and setting $B_x = B_{zo}$ (3.8) can be considered a function of a single variable -- say B_x. We could plot λ as a function of B_x for this specific β_o and angle of propagation. The plot will seem more familiar though if we recognize that (3.8) was obtained just as one obtains the equation for a linear dispersion curve. The usual variables for a dispersion curve are ω and k and they are related to our variables by

$$\omega = M_A(-i\lambda) \quad ; \quad k = (-i\lambda) \tag{3.35}$$

Notice that the phase velocity, ω/k, is just equal to the Alfvén Mach number in our dimensionless units. Figure 3.3 was generated from (3.8) using (3.32) and (2.24). Lines corresponding to Mach numbers equal to the Alfvén and sonic speeds are drawn in. A γ^2 of 1/10 was used to reduce the difference between Ω_e and Ω_i.

High Mach number lines do not intersect any of the dispersion curves indicating that there are no pure imaginary roots for such Mach numbers. This obviously corresponds to region II_c. As the slope of the Mach line decreases, it will eventually intersect the dispersion curve. The first point of contact occurs where ω is approximately equal to one. At the first point of contact the Mach line will be tangent to the dispersion curve, indicating that the phase and group velocities are equal. This Mach number divides region II_c from IV_i.

At lower Mach numbers, the Mach line will intersect the dispersion curve at two points corresponding to the high and low frequencies of region IV_i. As the Mach number approaches one, the lower frequency goes to zero. The Mach number at which the lower frequency goes to zero is the boundary between regions IV_i and I_r. The Mach line only intersects the dispersion curve at one point in region I_r.

This analysis can be continued with the aid of Figure 3.1. As the Mach number decreases regions IV_i, I_r, and finally IV_i appear. At very low Mach numbers the upper and lower frequencies of region IV_i approach $\Omega_e \cos\alpha$ and $\Omega_i \cos\alpha$.

In Figure 3.4 four examples of initial wave behavior are shown along with the potential contours near the origin.

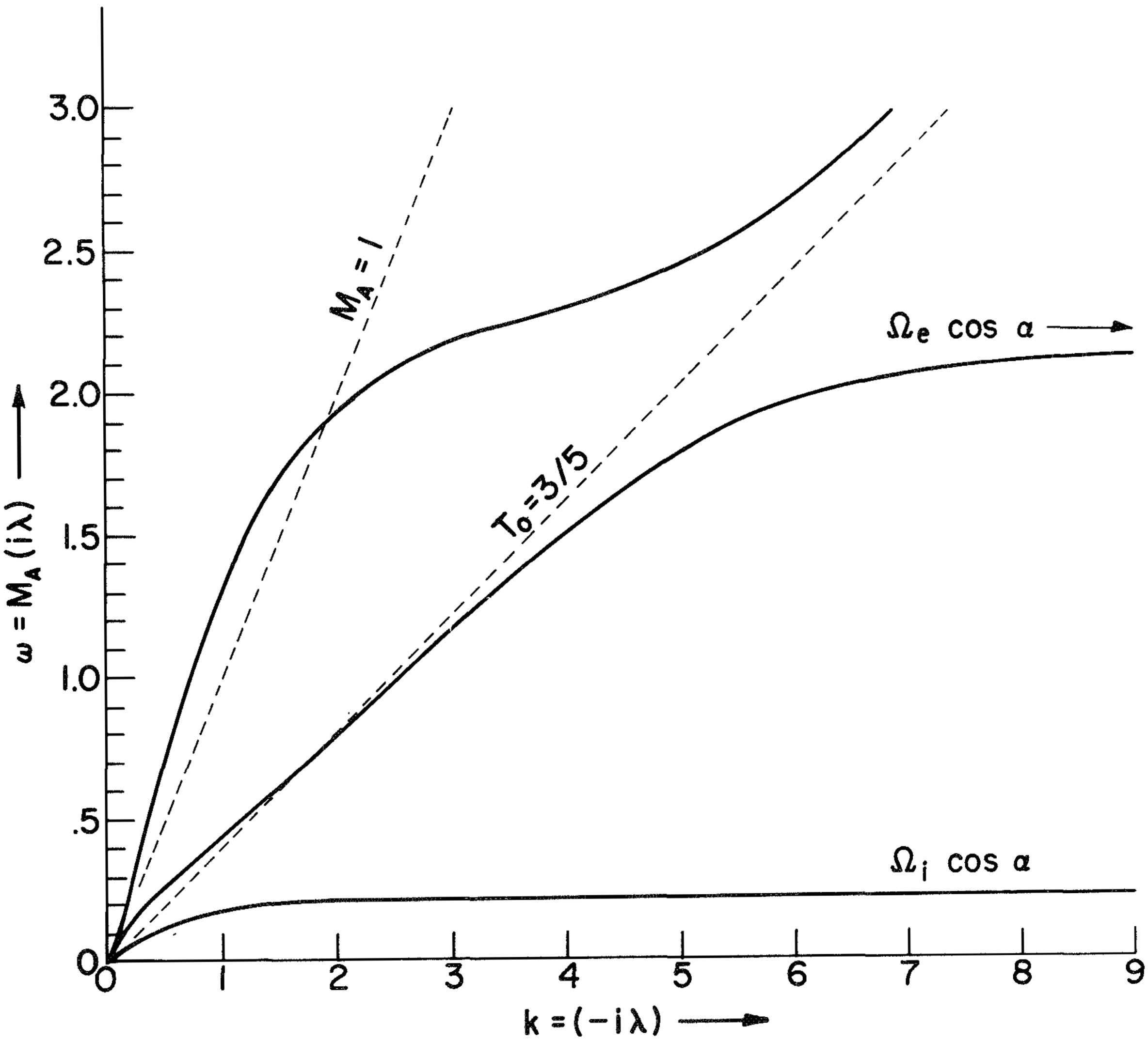

Figure 3.3 A dispersion diagram for $\alpha = \pi/4$ and $\beta_0 = 0.2$. A value for γ^2 of 0.1 is assumed to reduce the difference between the electron and ion gyro-frequencies.

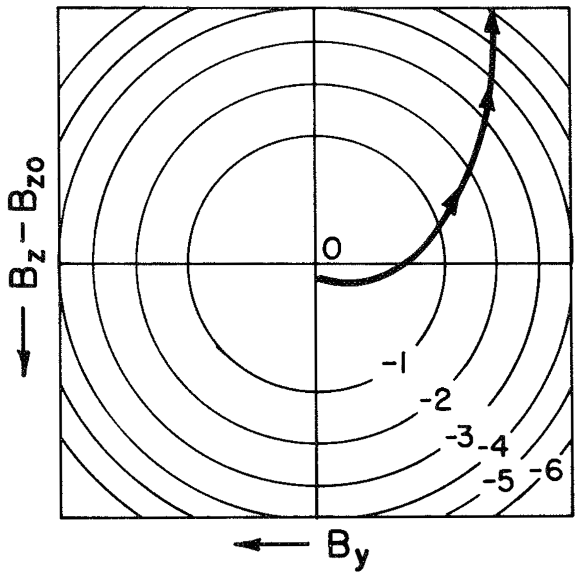

(a) Region II_c, M_A=25

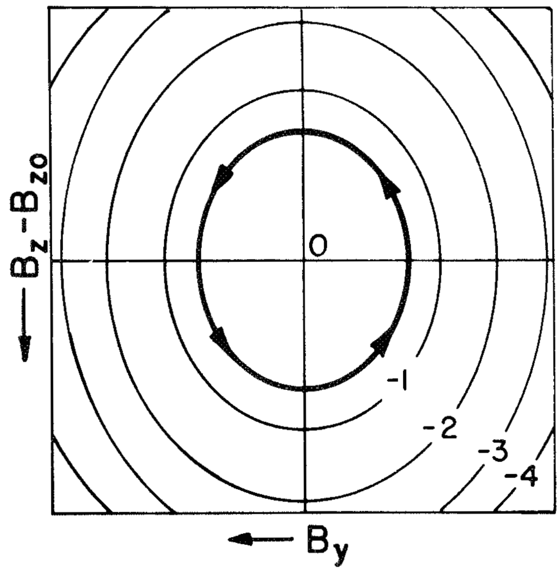

(b) Region IV_i, M_A=1.5

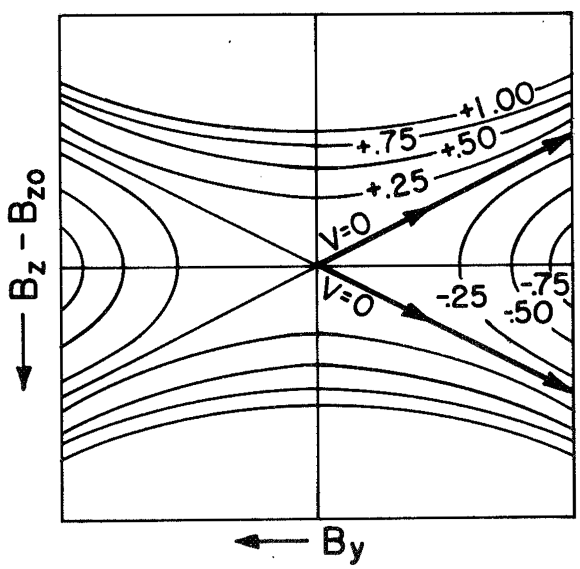

(c) Region I_r, M_A=0.8

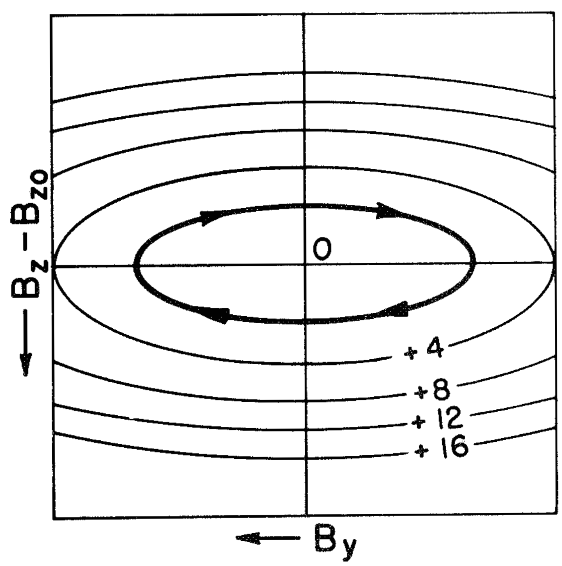

(d) Region IV_i, M_A=0.5

Figure 3.4 Particle motion near the origin. In all four examples, $\alpha = \pi/4$ and $\beta_o = 0.2$. Each figure is drawn to the same scale for ease of comparison.

CHAPTER IV

THE FINAL STATES OF THE PLASMA

In the previous chapter we analyzed the initial response of the plasma to small perturbations. We found that the potential well analogy was very useful in understanding the behavior of these linear waves. In this chapter we expand our analysis beyond the linear leading edge of the shock wave into the nonlinear regions. We are interested in the behavior of the plasma as it moves through the shock front and on towards infinity.

To help orient our analysis, the profile of a typical potential well is shown in Figure 4.1. The potential is a double valued function of $\vec{B}$. On the upper surface T/u^2 is greater than 3/5, and on the lower one it is less than 3/5. The upper surface resembles a sombrero resting on an inclined plane. The peak of the sombrero is at the origin, and there are two equilibrium points on the rim. The upper one is a saddle point and therefore not stable. The lower equilibrium point is a minimum* and is stable. On the lower surface, which resembles a somewhat distorted bowl, there is also an equilibrium point which is a minimum. On the dotted line where the two surfaces intersect T/u^2 equals 3/5 and the wave breaks. Notice in the figure that part of the breaking line lies above the $V = 0$ plane and is therefore out of the range of the particle's motion.

---

* When referring to a point as a maximum or a minimum, we always mean a local maximum or a local minimum.

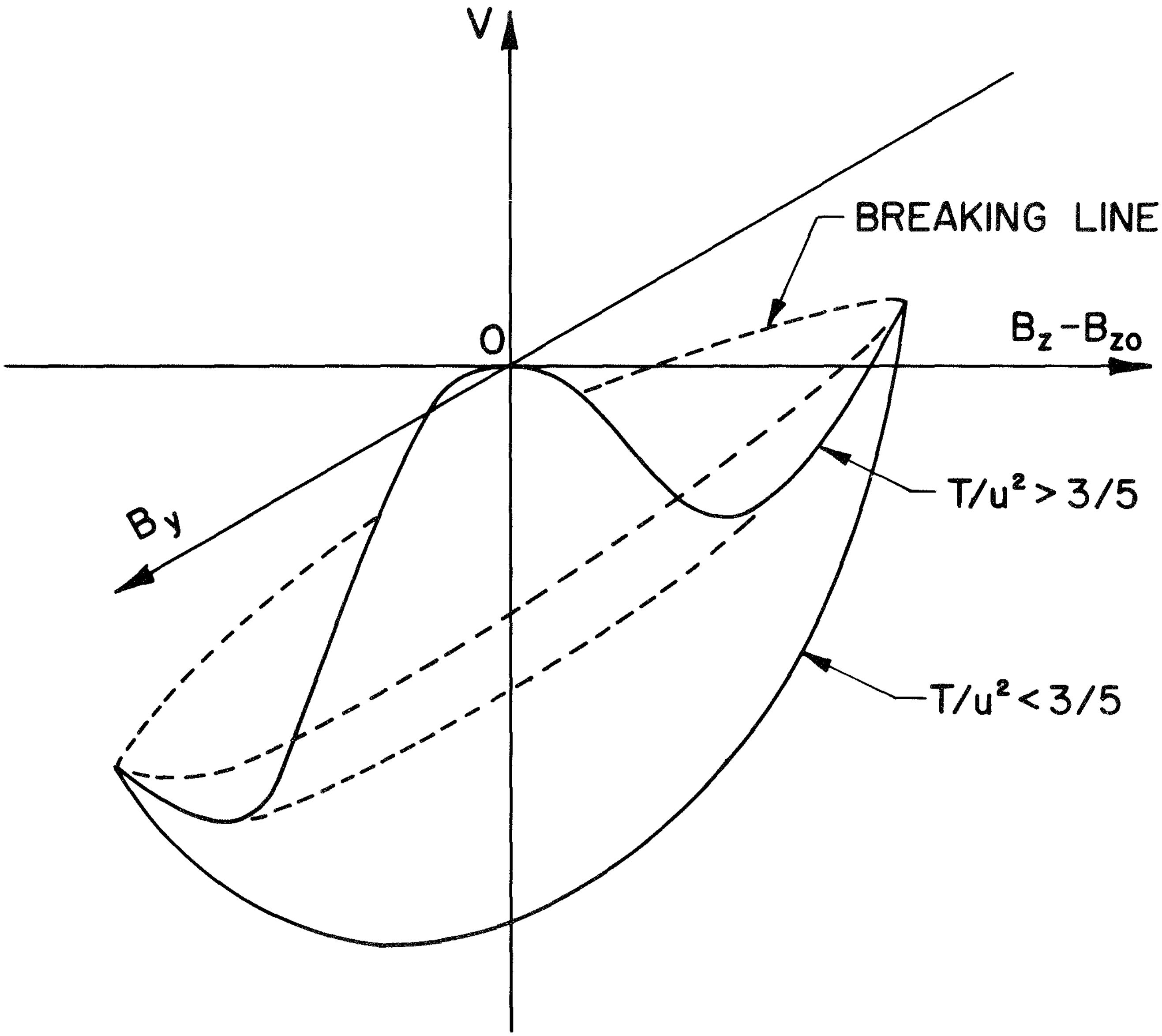

Figure 4.1 The potential well for a typical low Mach number plasma. The solid lines show the potential profile along the B_z-axis. The upper dashed line is the intersection of the upper and lower surfaces of the potential well. The lower one is the line of steepest descent connecting the two equilibrium points on the upper surface.

In this chapter we are particularly interested in the number, location, and stability of the equilibrium points and whether all or part of the breaking line lies above the $V = 0$ plane. The problem is complicated by the fact that the potential well changes shape as friction heats the plasma. We therefore examine both the initial and final shapes of the potential surfaces. Once the various shapes of the potential well have been categorized, we examine the relationship between the potential well configurations and the possible types of wave motion.

A. The Rankine-Hugoniot Relations

As we saw in Figure 4.1, there may be several equilibrium points in the potential well. As friction heats the plasma, these points move upwards towards the $V = 0$ plane. If our analogous particle is at one of these equilibrium points when it crosses the $V = 0$ plane, it will come to rest there. We saw an example of this type of motion for a magnetosonic wave at the end of Chapter II. The Rankine-Hugoniot relations enable us to calculate the position of the equilibrium points as they cross the $V = 0$ plane. The positions of these equilibrium points determine the possible downstream states of the plasma if the downstream state is in equilibrium.

The Rankine-Hugoniot relations assume the validity of the equations of motion ((.29) to (2.34)) at $x = +\infty$ but do not necessarily assume that the equations are valid throughout the whole shock transition. The downstream states are found by setting all the derivatives in the equations of motion equal to zero. The six algebraic equations that result from this can be solved for the six unknown downstream variables. The algebra is given in detail in Appendix 2. The equation for u_f (the final streaming velocity) is presented here for ease of reference:

$$4u_f^3 - u_f^2\left[1 + (5/2)\ (B_{zo}^2 + \beta_o B_o^2) + 8B_x^2\right]$$
$$+ u_f\left[B_x^2\left(B_o^2(4 + 5\beta_o) + 2\right) - B_{zo}^2/2\right]$$
$$- B_x^2 B_o^2\left[1 + (5/2)\ \beta_o B_x^2\right] = 0 \qquad (4.1)$$

The variable u_f is dimensionless and is normalized to u_o as are all velocities. Only the positive real roots of (4.1) are physically meaningful, and they are only meaningful if they lead to real values for the other five downstream variables. Since the coefficients of (4.1) are real, there will either be one real root or three real roots. At the transition from one to three real roots, two of the three roots are equal to each other. We want to find the lines in the B_x, B_{zo}-plane on which u_f equals one and the lines across which the number of real roots changes.

If u_f equals one, the downstream streaming velocity is the same as the upstream streaming velocity $(u_f = u_o)$. In analogy with neutral gas dynamics we refer to the lines on which the final and initial states are the same as Mach one lines. In a plasma there are three distinct shock transitions, and each one has a Mach one line associated with it. To find the Mach one lines, we set $u_f = 1$ in (4.1). The resulting cubic in B_x^2 can be factored and is found to be the same as (3.11) which defined the three $c = 0$ lines.

The equation for the boundaries between regions with a different number of positive real roots is not as easy to find. We can determine the boundaries' intersection with the B_x-axis by setting B_{zo} equal to zero in (4.1). The cubic then factors into

$$\left(u_f - B_x^2\right)^2 \left[4u_f - \left(1 + 5/2\ \beta_o B_x^2\right)\right] = 0 \qquad (4.2)$$

This equation shows that there are three real roots to (4.1) all along the B_x-axis. But u is only one of six variables which can undergo a transition. In Appendix 2 it is shown that if $u_f = B_x^2$, then the magnitude of the change in magnetic field, B_r, is given by

$$B_r^2 = \frac{2}{3B_x^2}\,(1 - B_x^2)\left[4B_x^2(1 - 5\beta_o/8) - 1\right] \qquad (4.3)$$

From (4.3) we can see that for B_r to be real

$$1 \geq B_x \geq \tfrac{1}{2}(1 - 5\beta_o/8)^{-\frac{1}{2}} \qquad (4.4)$$

The segment of the B_x-axis defined by (4.4) is the only part of the B_x-axis where there are three meaningful solutions to the Rankine-Hugoniot relations. If we assume that the neighborhood of the B_x, B_{zo}-plane near this segment also contains three real roots, we can predict that the boundary we seek will intersect the B_x-axis at the two extremes of (4.4). Note that if $\beta_o = 6/5$ both intersections occur at $B_x = 1$. Also notice that the lower intersection corresponds to the point in (4.2) where all three roots are equal.

The rest of the boundary was found from (4.1) with the aid of a digital computer and is shown along with the Mach one lines in Figure 4.2 (β_o is assumed to be 0.2 as usual). The three roots are labelled R_1, R_2, and R_3. Each Mach one line is labelled to indicate which root equals one on it. The magnitude of the various roots, relative to one, is also indicated in the regions which they appear. For example R_1 is less than one everywhere below the curved R_1 Mach one line and greater than one above it. To the right of the line labelled $R_1 = R_2$, R_1 becomes imaginary.

As we have already seen, not all the values of u_f are physically meaningful. For instance, there is a narrow band along the B_{zo}-axis with three real roots which is not shown in Figure 4.2 because two of the roots are negative and therefore not acceptable. Also, in Appendix 4 it is shown that for a final state to have a u_f greater than one, it is necessary to have a negative δ. This is clearly not possible since δ is an integral of positive quantities (see (2.47)). If we only consider laminar shocks*, we find an additional restriction on u_f. For the equations of motion to be valid, T/u^2 must be less than 3/5 at all stages of the wave including the final state. In summary, we require

$$1 > u_f > (5/3\ T_f)^{1/2} \qquad (4.5)$$

for laminar shock transitions.

---

* A laminar shock is defined to be a shock for which the two fluid equations we are using are valid throughout the whole shock transition.

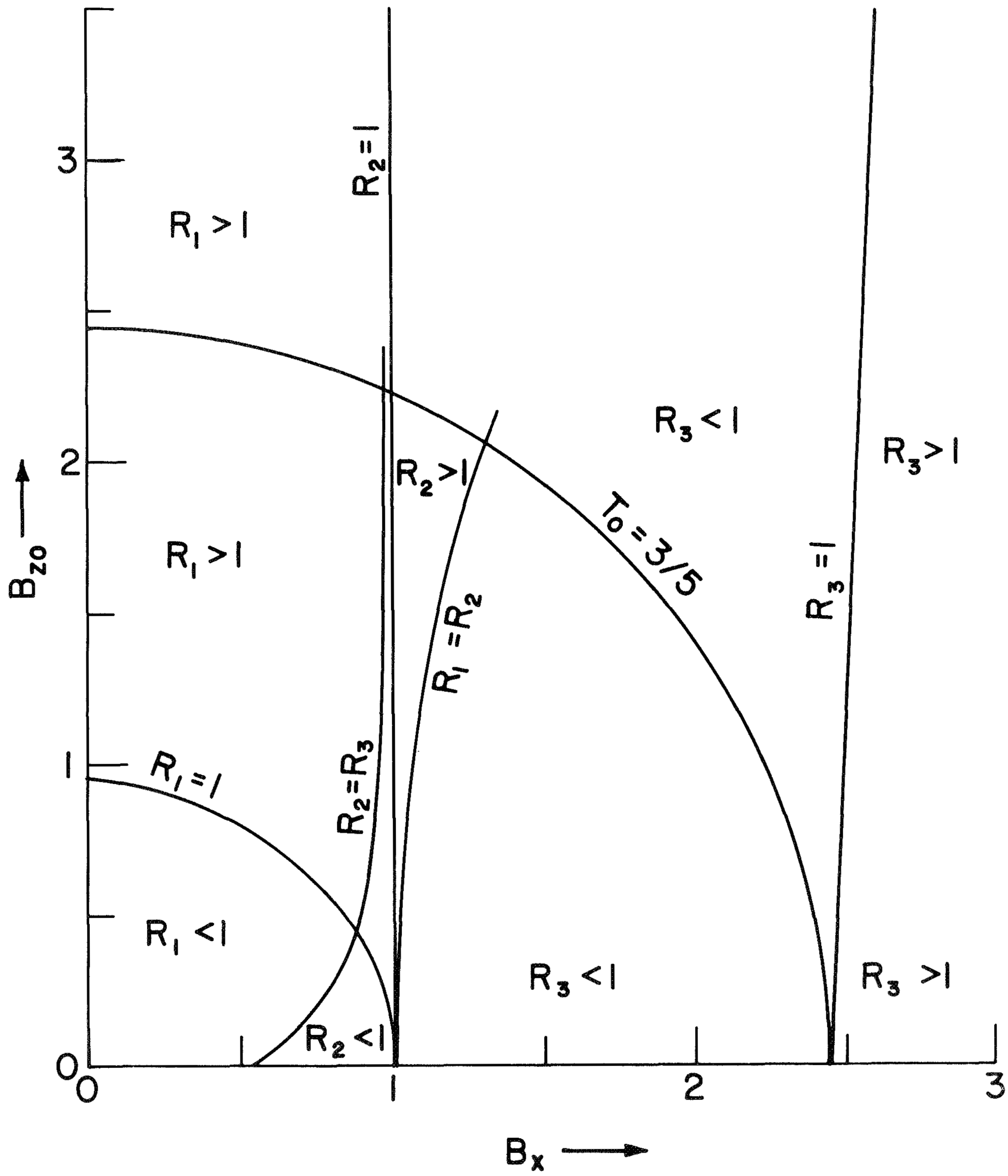

Figure 4.2 The location of the Mach one lines as calculated from the Rankine-Hugoniot relations with β_0=0.2.

By evaluating (4.1) in the region of the B_x , B_{zo}-plane bound by $B_x = 1$ and $T_o = 3/5$, we find there are three distinct regions with roots satisfying (4.5). They are shown in Figure 4.3 and are labelled 0, 1, or 2 depending upon the number of allowed roots in the region. The subscripts m or s indicate whether the equilibrium point is a minimum or a saddle point. Root R_1 is always a saddle point in the range allowed by (4.5), and R_2 is always a minimum. Inside the $T_o = 3/5$ line, R_3 is too small to be an acceptable root for laminar shock transitions. The dotted line in Figure 4.3 is the $R_2 = R_3$ boundary of Figure 4.2 and is included for ease of comparison. By using Figures 4.2 and 4.3, one can follow the evolution of the various roots throughout the region of the B_x , B_{zo}-plane being considered in the figures.

Let us for example see how R_2 varies. To the left of the $R_2 = R_3$ line, R_2 is imaginary. Just to the right of this line R_2 is real, but it is too small to satisfy (4.5). R_2 is on the lower surface of the potential well in this region and therefore is not an acceptable root for a laminar shock wave. On the line separating regions 0 and 1_s from 1_m and 2_{ms} , R_2 is equal to the lower limit of (4.5). It increases as we move to the right until, at $B_x = 1$, it equals one. Beyond this line R_2 lies above the $V = 0$ plane and is not an acceptable root. Beyond the $R_1 = R_2$ line, roots R_1 and R_2 are imaginary.

The Rankine-Hugoniot relations enable us to find the location of the various equilibrium points when they reach the $V = 0$ plane. In the next section we will find where they are located in the initial configuration of the potential well. By knowing where the equilibrium points start and finish we will be able to understand how the shape of the

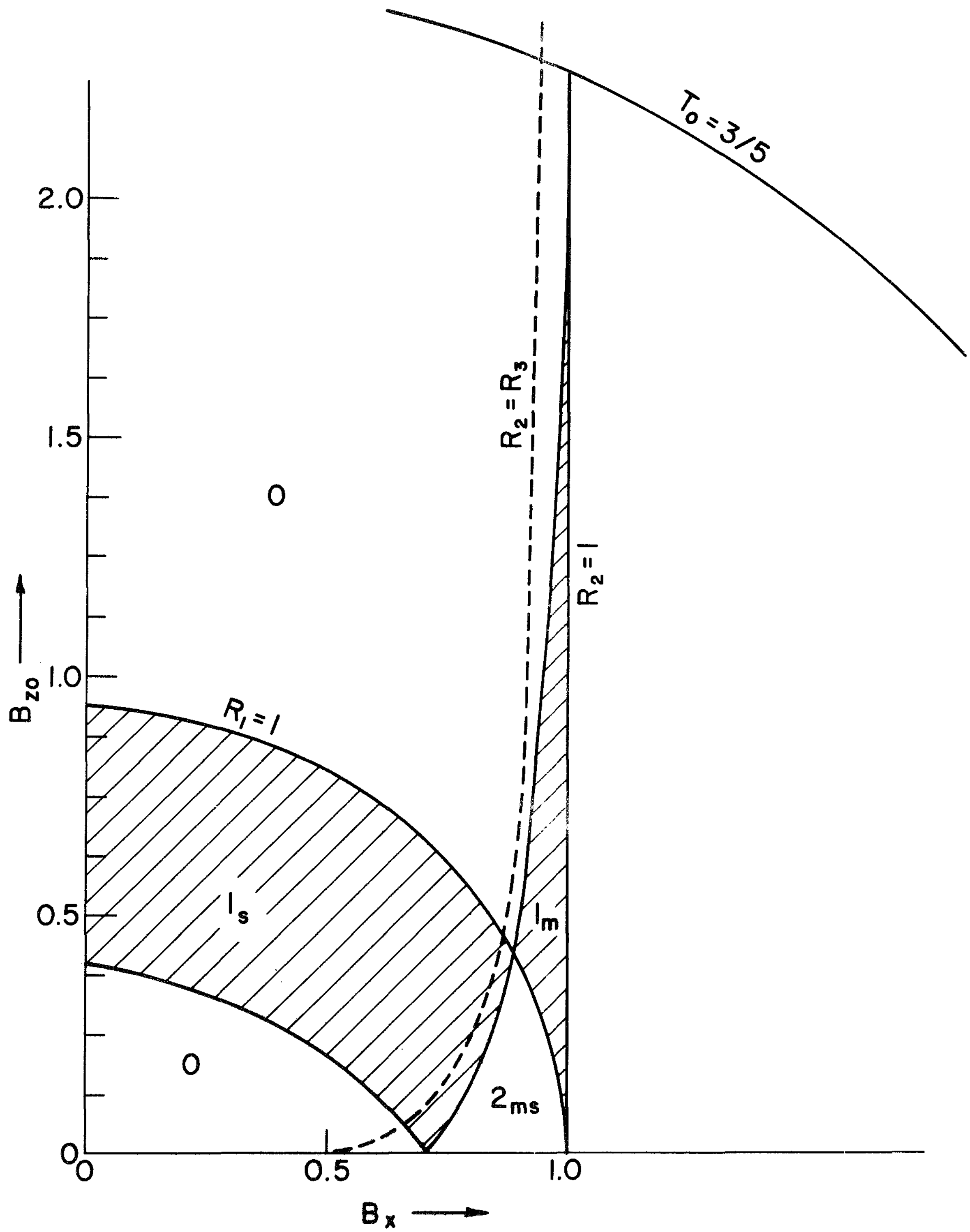

<u>Figure 4.3</u> The number of final states in each region is denoted by a 0,1, or 2. The subscripts indicate whether the equilibrium point is a minimum or a saddle point.

potential well evolves during the course of a shock wave.

B. The Initial Shape of the Potential Well

The equilibrium points in the potential well occur where the derivatives of the potential vanish. From (3.24) and (3.25) we see that this can only happen if

$$(B_z - B_{zo})\ (u - B_x^2) = B_{zo}(1 - u) \tag{4.6}$$

and

$$B_y(u - B_x^2) \ = \ 0 \tag{4.7}$$

If $u = B_x^2$ is to be an equilibrium point, then either $B_{zo} = 0$ or $B_x = 1$. We will discuss this somewhat special case below to show how the potential varies from region to region. In the meantime, we will examine the nature of the equilibrium points in the other parts of the B_x , B_{zo}-plane. If we assume that $u \neq B_x^2$ at the equilibrium points, then we must require

$$B_y = 0 \quad \text{and} \quad B_z = B_{zo}(1 - B_x^2)/(u - B_x^2) \tag{4.8}$$

The requirements of (4.8) must be met at all stages of the shock transition. The exact location of the equilibrium points along the B_z-axis changes as δ increases and changes the relationship between B_z and u. But at no stage of the wave does an equilibrium point move off the B_z-axis. This simplifies the analysis considerably. Now we only need to evaluate the potential along the B_z-axis to find all the equilibrium points.

By using (2.40) and (2.48) with $\delta = 0$, we can eliminate T and B_z from (2.55). The resulting equation for V, in terms of u and the initial conditions, was plotted with the aid of a computer. The equilibrium points were found from these curves and were categorized and plotted in the same format as we used with the Rankine-Hugoniot roots.

In Figure 4.4 the two results are compared. The cross hatched areas are regions that have an equilibrium point which is acceptable initially but not by the time it reaches $V = 0$ plane. In general, as friction heats the plasma the distance between the equilibrium points and the breaking line decreases. In the cross hatched areas one of the roots actually reaches the breaking line and moves out of the range acceptable for laminar shock transitions. There are no instances where an initially unacceptable root becomes acceptable. The important thing to note here is that in most areas the number and types of equilibrium points remain unchanged during the course of the wave. Even though the detailed shape of the potential well is altered by friction, the general topology remains unchanged in most areas.

Although there are five distinct regions where the number and types of equilibria vary, there are only three basic shapes the potential assumes in these regions. The profiles of these three shapes along the

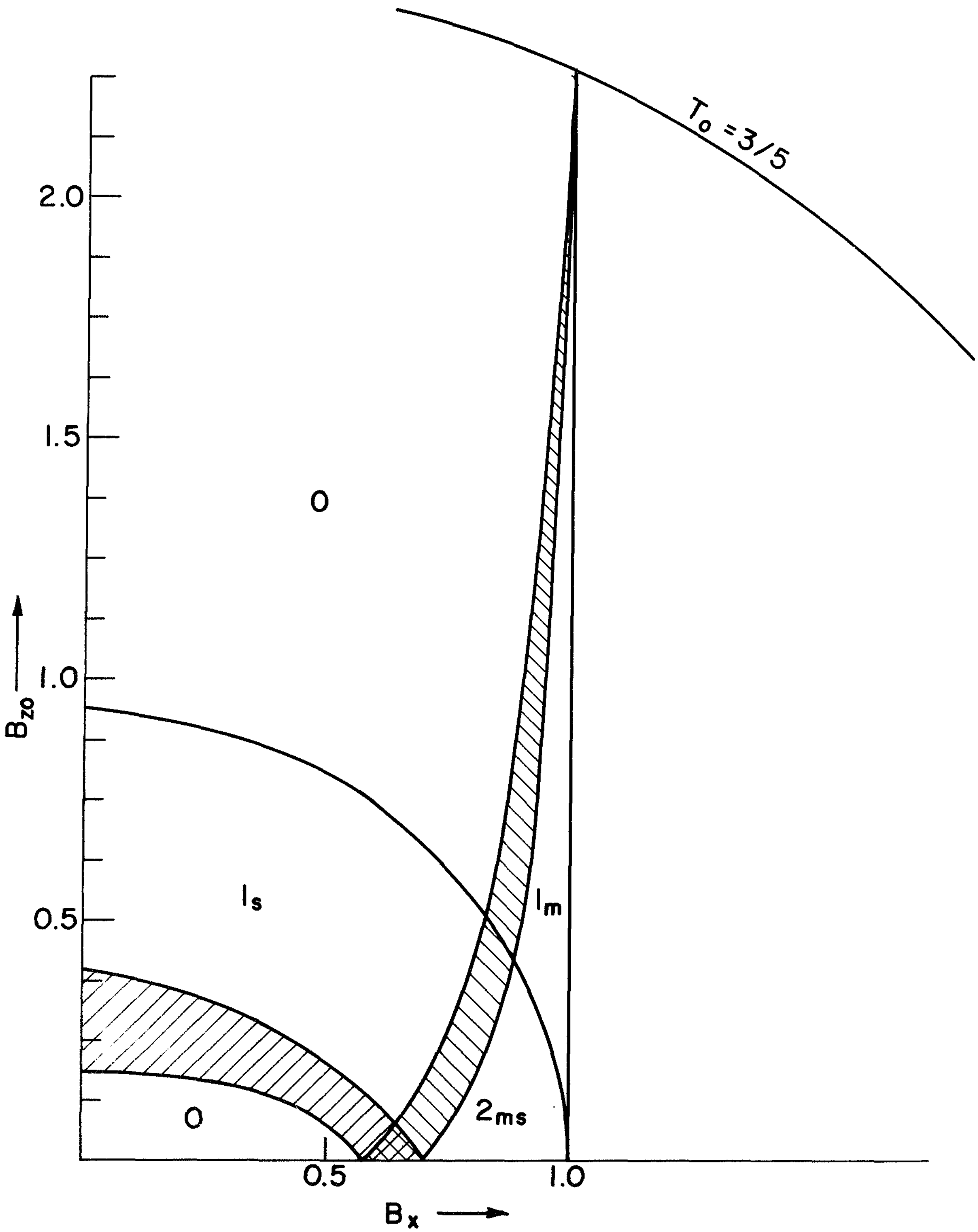

Figure 4.4 The cross hatched areas are regions where an initially acceptable root moves beyond the breaking line before it moves up to the V=0 plane.

B_z-axis are shown in Figure 4.5. The potential profile labelled (a) in Figure 4.5 has the general shape of the potential in 1_s and the upper of the two 0 regions. As indicated in the figure, the origin is located at the equilibrium point labelled as a maximum in region 1_s and the single acceptable root is at the saddle point. On the R_1 Mach one line the two equilibria overlap. Above the Mach one line, in the region labelled 0 , the origin is at the saddle point and the downstream equilibrium point predicted by the Rankine-Hugoniot relations is at the maximum. It is clear energetically that a particle starting out at the saddle point can not reach the other equilibrium point. All equilibrium points corresponding to final streaming velocities greater than one lie above the $V = 0$ plane initially. The only way the particle could ever reach one of these is if the coefficient of friction, ν , were negative. This would give δ a negative value and the potential well would drop instead of rising. Since ν is always positive we conclude that these equilibrium points are not acceptable for downstream states.

Figure 4.5(b) shows the general shape of the potential well in the 0 region below the 1_s region. Here the saddle point has moved beyond the breaking line and the only equilibrium point left is the origin itself.

The third profile is similar to the one in Figure 4.1 and corresponds to the type found in regions 1_m and 2_{ms} . In region 1_m , which is above the R_1 Mach one line, the origin is at the saddle point. The only allowed transition is to the equilibrium point labelled as a minimum. This point corresponds to R_2 in the Rankine-Hugoniot relations. In the 2_{ms} region the origin is at the maximum and there are two allowed roots.

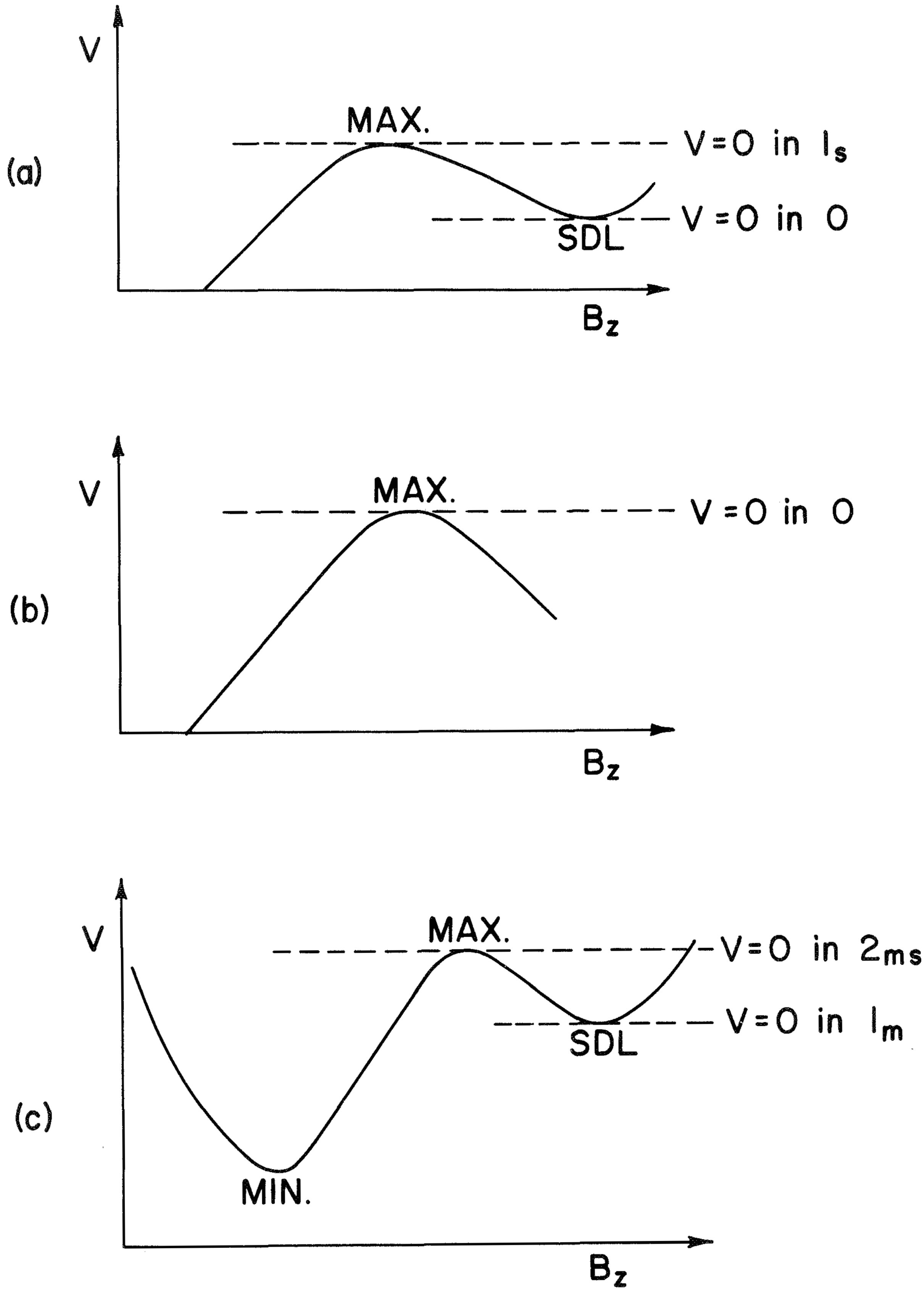

Figure 4.5 Three typical potential well profiles.

We are now in a position to examine the potential on the B_x-axis and on the $B_x = 1$ line. Along the part of the B_x-axis where there are two acceptable roots, R_1 equals R_2 and the potential well is similar to Figure 4.5(c). The main difference is that the equilibrium points corresponding to R_1 and R_2 are at the same potential and are equidistant from the origin. Since B_{zo} is zero, there is symmetry in all directions about the origin. Rotating the profile of the potential about the origin generates a two dimensional potential well shaped like a sombrero. The origin is at the peak of the sombrero and the equilibrium points form a circle around the rim. All points on this circle are equally acceptable as downstream states so it is possible for B_y to be non-zero downstream.

As we move above the B_x-axis, R_2 moves away from the origin and drops below R_1 which moves closer to the origin. The potential looks like Figure 4.5(c) or Figure 4.1. Since the rim is no longer level there are only two points on it which are equilibrium points. The upper one is a saddle point (R_1) and the lower one is a minimum (R_2).

The potential well is also shaped like a sombrero (a level one) along the $B_x = 1$ line. Only here the origin is on the rim of the sombrero rather than at the central peak. There are an infinite number of equilibrium points forming a circle around the rim. But they all lie in the $V = 0$ plane so the particle can not move to reach them. None of the potential is below the $V = 0$ plane and so no wave motion is possible.

Notice the difference in the behavior of the roots R_1 and R_2 as they move through their respective Mach one line. On the R_1 Mach one line, the equilibrium point corresponding to R_1 is at the origin and the jump in all six downstream variables goes to zero. Near the $B_x = 1$ line, which is the R_2 Mach one line, R_2 does not coincide with the origin. The jump in the magnetic field does not go to zero although the jump in the streaming velocity and temperature do. Such shocks are called Alfvén shocks by some authors[20]. The jump in the magnetic field approaches $-2B_{zo}$ as we approach the $B_x = 1$ line. This means that a magnetic field which initially had a perpendicular component of $+B_{zo}$ upstream ends up with a perpendicular component of $-B_{zo}$ downstream.

There is still one more characteristic of the potential well to be investigated. We want to find the initial location of the breaking line relative to the $V = 0$ plane. In particular we want to find the region of the B_x , B_{zo}-plane where the breaking line lies entirely above the $V = 0$ plane. We will call this region the S-region, the S standing for stable.

It is easily shown that when B_x is less than one, the point on the breaking line with the lowest potential occurs at the breaking line's intersection with the negative B_z-axis. To find the boundary of the S-region all we have to do is find out when this intersection occurs exactly at $V = 0$. The value of u at the breaking line, u_b , is

$$u_b = (5T_o/3)^{3/8} \tag{4.9}$$

Using this in (2.48) we find

$$(B_z - B_{zo})_b = - B_{zo} - (B_{zo}^2 + c_b)^{\frac{1}{2}} \tag{4.10}$$

where

$$c_b = 2(1 + T_o - 8u_b/5) \tag{4.11}$$

These two equations can be used in (2.55), the equation for V, to give an equation for the boundary of the S-region in terms of the initial conditions. The boundary was found with the aid of a digital computer and the results for $\beta_o = 0.2$ are shown in Figure 4.6.

If there is friction, the breaking line can move above the $V = 0$ plane even if initially some of it was below. The regions where this is possible are obviously regions 1_m and 2_{ms}. We saw an example in Chapter 2 where friction "stabilized" a magnetosonic wave. Now we know that it only stabilized it for motion in the B_z-direction, but the concept is the same in the two dimensional case we are considering here. Frictional waves in region 1_m and 2_{ms} are stable if the friction is large enough to keep them from reaching the breaking line before it moves out of their range of motion. The amount of the dissipation needed to stabilize the wave is smaller the closer the wave is to the S-region.

Now that we have a clear understanding of the various features of the potential well, we will find out what types of wave motion are possible in such potentials. We will consider waves both with and without friction.

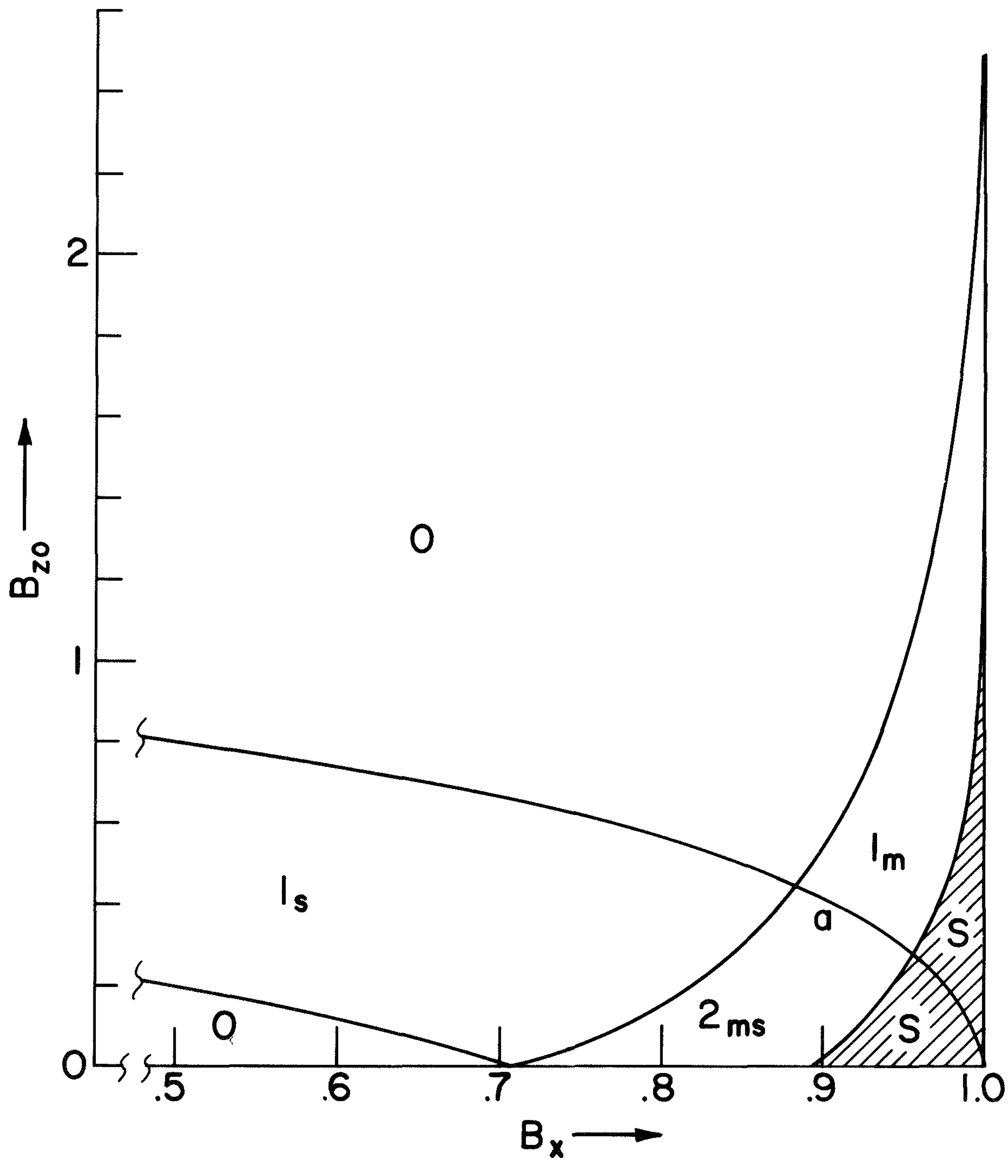

Figure 4.6 The location of the S-region.

C. Waves in the Absence of Friction

In the absence of friction the potential well analogy is exact. The potential does not move or change shape. If there were no perpendicular magnetic fields in our analogy (say $\gamma = 1$) , we could easily find the possible types of wave motion. Let us assume that there is no magnetic field acting on our analogous particle for the time being and see how it would move.

In the regions where all of the breaking line lies below the $V = 0$ plane, the waves would just grow monotonically until they broke. Where part of the breaking line is above the $V = 0$ plane the waves could make several oscillations before breaking. Just how many they would make would depend upon the initial perturbation. And if the waves were started in the S-region they would oscillate forever since the breaking line is out of their range of motion.

Since the origin is an equilibrium point, there is a fourth possibility, namely that the particle could return to the origin and come to rest there. It is clear that this will not happen unless the direction of the initial perturbation is carefully chosen. One obvious choice, in the region where the origin is a maximum and at least part of the potential along the positive B_z-axis lies above the $V = 0$ plane, would be to start the particle moving on the ridge line that runs along the plus B_z-axis. From (3.25) we see that the gradients in the y-direction are zero on the B_z-axis. Since the perpendicular potential gradients are zero and we are assuming, for the time being, that there is no magnetic field acting on our imaginary particle, it would continue moving on the ridge line until it reached the $V = 0$ plane. It would then return back to the origin and come to rest. These solitary waves would be like the magnetosonic ones we saw earlier and would also be unstable to any perturbations in the B_y-direction.

In the real case, where $\gamma \neq 1$ and there is a magnetic field in our particle analogy, these four types of motion are still found. The presence of the magnetic field greatly alters the regions where each type of motion exists however. Only the region of completely stable motion is unchanged since it still depends upon the breaking line being completely above the $V = 0$ plane. There is also a new type of wave motion made possible by the magnetic field. In region IV_i the magnetic field causes the particle to just orbit endlessly around the origin without ever growing into a nonlinear wave.

Recall that the strength of the magnetic field is on the order of B_x/γ. The smallness of γ means that the force exerted by the magnetic field will in general predominate over that due to the gradients in the potential. It is only when the velocity of the particle or B_x is on the order of γ that the two forces become comparable. When $B_x < \gamma$, as it is in region II_r, the potential gradients become the dominate force. Below the R_1 Mach one line the decreasing influence of the perpendicular magnetic field is clearly seen by the emergence of regions II_c and II_r as B_x approaches γ. In region I_r, which extends from $B_x = 0$ to $B_x = 1$, the transition is not so clearly defined but we expect that it too will occur when $B_x \approx \gamma$.

(a) Wave Trains in Region II_c

In the absence of friction, the waves in region IV_i do not grow into nonlinear waves and are therefore not of much interest. In region II_r the waves grow monotonically and break unless the initial perturbation is carefully chosen (i.e. magnetosonic waves), In between is region II_c . We expect that the waves in region II_c will have the characteristics of both regions IV_i and II_r .

Waves in region II_c are sensitive to both the strength of the magnetic field and the shape of the potential well. Since B_x is so small throughout region II_c , it has very little effect on the shape of the potential well. For angles up to 75 to 80 degrees from the B_x- axis, B_{zo} is also small and the potential is essentially independent of the initial conditions. As α approaches $\pi/2$, B_{zo} increases and the potential evolves from one resembling Figure 4.5(b) into one resembling 4.5(a). From (3.32) we can see that where $\cos\theta$ is positive the potential is increased by the B_{zo} term and where it is negative the potential is lower and therefore steeper.

In the regions of II_c where the potential is independent of the starting conditions, waves with the same value of B_x will have very similar behavior. In terms of Mach numbers, this means that the wave behavior will depend upon the Mach number times the cosine of α .

Figures 4.7 and 4.8 show examples of wave motion in region II_c . In the first figure α is 87° which means that B_{zo} is of

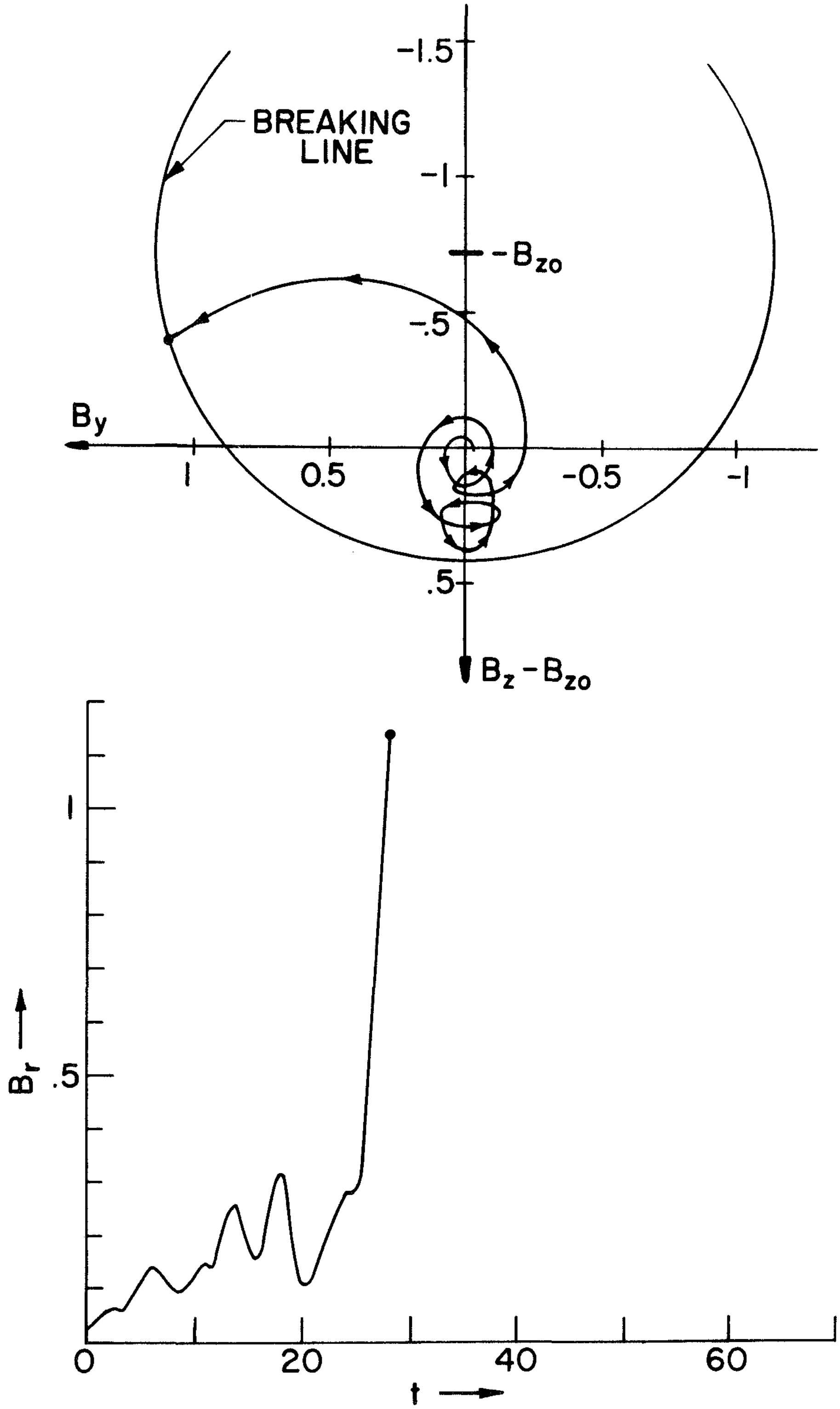

Figure 4.7 Breaking wave train in region II_c.

M_A=1.4, α=87°, B_x=0.037, B_{zo}=0.71, β_o=0.2.

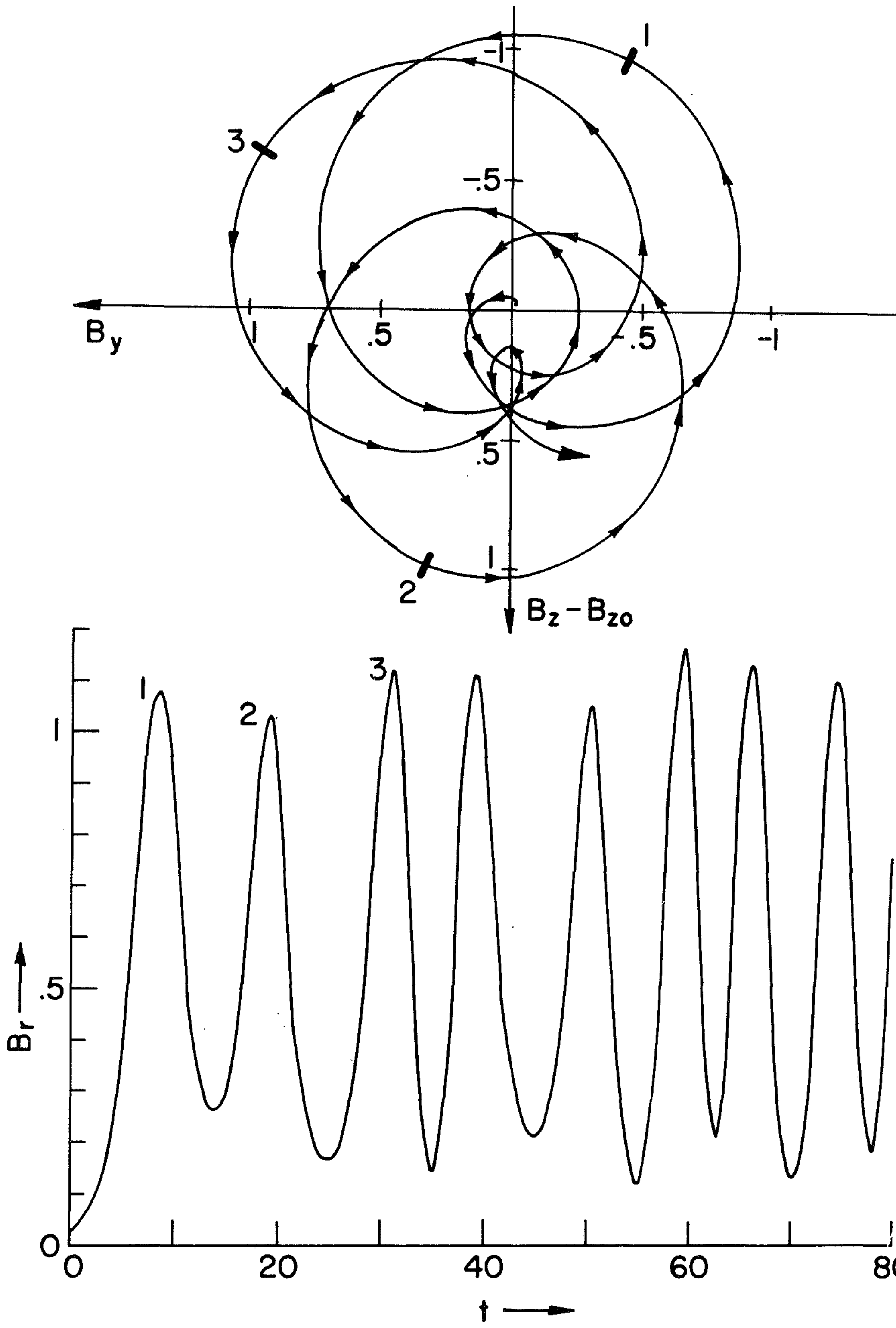

<u>Figure 4.8</u> A wave train in region II_c. M_A=18, α=45°, B_x=B_{zo}=0.039, β_o=0.2.

order one ($B_{zo} = 0.71$ to be precise) and the potential well resembles Figure 4.5(a). The wave is fairly stable as long as it stays where $\cos\theta$ is positive and the potential is shallow. The polar graph clearly shows the effect of the steeper gradients where $\cos\theta$ is negative.

In Figure 4.8, α is 45° and B_{zo} is small ($B_{zo} = B_x = .0393$). The polar graph follows the first three oscillations of the wave. The points on the polar graph corresponding to the three maximums are labelled with a number designating which peak they correspond to. Because of the symmetry of the potential well, the particle's motion is quite symmetric from one oscillation to the next. Eventually the wave will break, but for many practical applications the length of the wave train can be considered to be infinite.

(b) Solitary Waves in Regions II_r and II_c

While wave trains of various lengths are the most common form of wave motion in regions II_c and II_r, they are not the only kind. For certain special initial perturbations and for low enough Mach numbers, solitary waves are possible. A solitary wave is defined to be a wave which, after a finite number of oscillations, returns to its initial equilibrium state. For a solitary wave to occur the amplitude of the change in the magnetic field, B_r, must reach a maximum or a minimum just as the particle crosses the B_z axis. If this happens, the equations of motion are symmetric about this point, and the particle will return to the origin after repeating the previous oscillations in reverse order.

Figure 4.9 shows a simple solitary wave from region II_c. The symmetry of the motion is most apparent in the polar graph. Much more complicated solitary waves are possible. For example in Figure 4.8 the minimum after the third peak occurred very close to the B_z-axis (see the polar graph). The symmetry about this minimum is apparent in the next two or three oscillations of the wave train. If the particle had been exactly at the B_z-axis, the wave train would have died out after repeating the three previous oscillations.

For both magnetosonic and whistler waves, it is well known that there is an upper limit to the Mach number for which solitons exist. For the cold magnetosonic case the limit is $M_A = 2$. For the whistler case the limit is essentially independent of β_o and occurs at

$$M_A = (2\gamma^2)^{-\frac{1}{2}} \approx 30 \tag{4.12}$$

In Figure 4.10 we show the results of a computer calculation for the minimum values of B_x and B_{zo} for which solitary waves exist as a function of the angle of propagation. The minimum values for B_x and B_{zo} correspond to maximum values for the Mach number (see (2.23)). The B_x-axis is expanded by a factor of ten in Figure 4.10 to enlarge the II_c region. This also has the effect of compressing small values of α against the B_x-axis and enhancing the values of α near $\pi/2$.

As one would expect from our previous discussion, the soliton breaking line occurs at a constant B_x until α is about 80°. Within

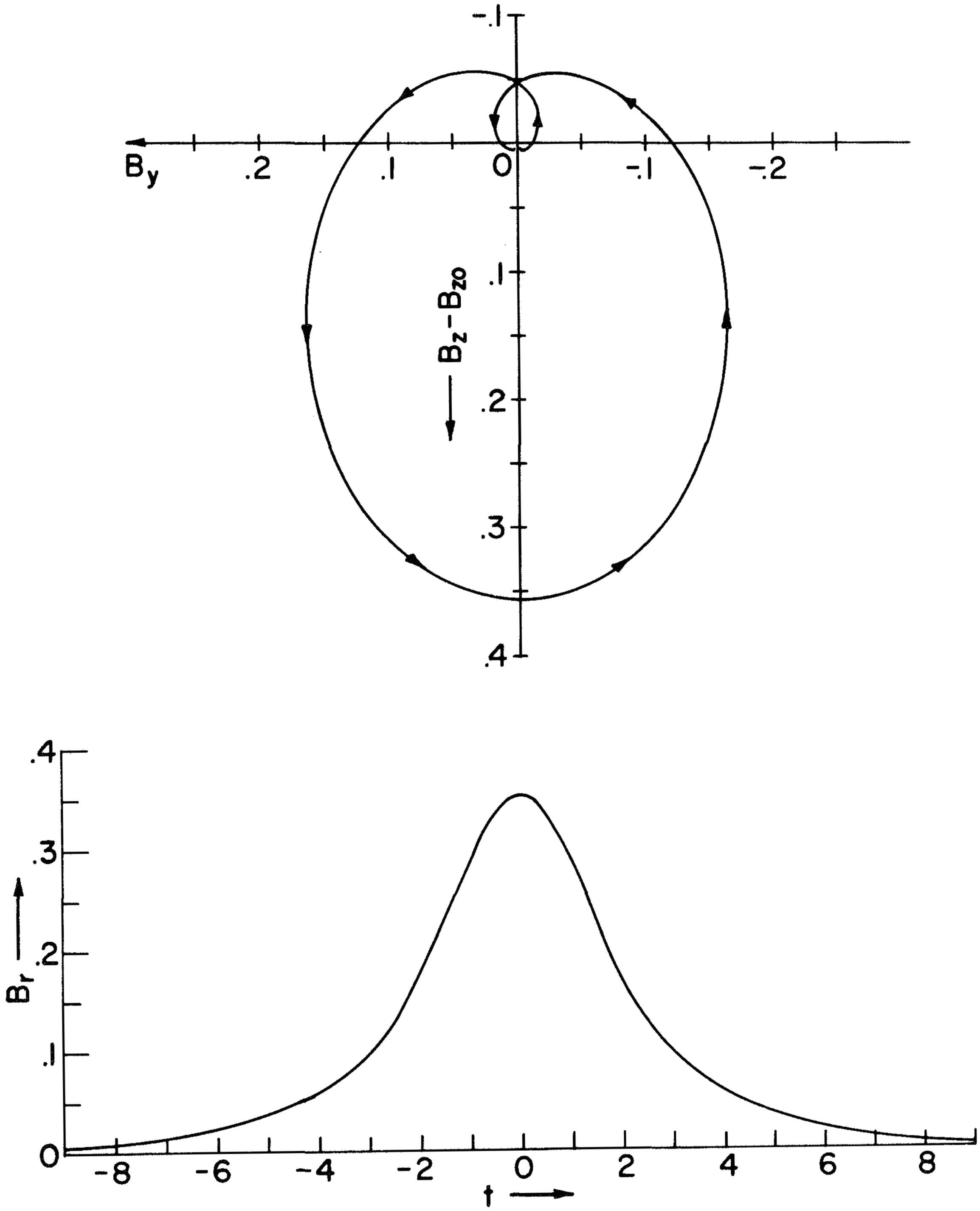

Figure 4.9 An oblique soliton. $M_A=1.54$, $\alpha=87^{\circ}$, $B_x=0.034$, $B_{zo}=0.65$, $\beta_o=0.2$.

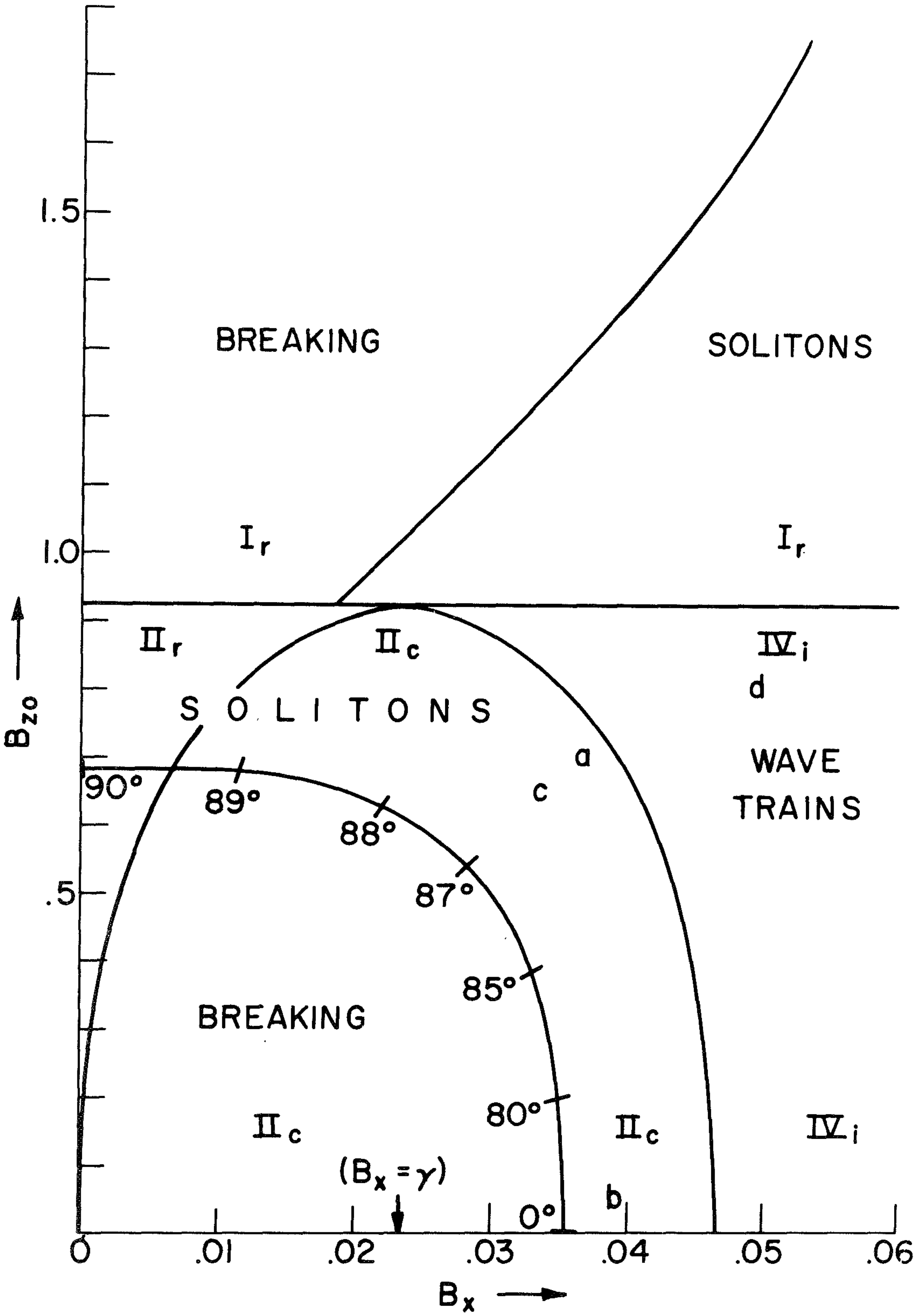

Figure 4.10 The breaking line for solitons. Note the expanded scale along the B_x-axis.

this range of angles the equation for the maximum Mach number for solitons is

$$(M_A)_{MAX} \approx (2\gamma^2)^{-1/2} \cos \alpha \tag{4.13}$$

As B_{zo} increases, the slope of the potential where $\cos \theta$ is positive decreases permitting solitons with smaller values of B_x. Finally at $\pi/2$ the breaking line at $\theta = 0$ reaches the $V = 0$ plane and solitons are possible with $B_x = 0$.

In region II_c of Figure 4.10 the locations of the waves in Figures 4.7, 4.8, and 4.9 are indicated by the letters a, b, and c. In region IV_i the location of the wave for 4.12 is indicated by a "d".

(c) Solitary Waves in Region I_r

The behavior of the waves in region I_r has been investigated by several authors (see references 12 and 13 for example). These waves are often referred to as submagnetic waves since they move, relative to the plasma at $x = -\infty$, at a speed less than the Alfvén speed. In a warm plasma, the relevant speed for a shock transition to R_1 is not simply the Alfvén speed. From (2.23) and (3.11) we find that the warm plasma Mach number is given by

$$M_{WARM} = M_A \left[\frac{M_A^2 - 5\beta_o/6}{M_A^2 - \left(5\beta_o \cos^2\alpha\right)/6} \right]^{-1/2} \tag{4.14}$$

The key to understanding the waves in region I_r is to notice that if the velocity of the particle stays small, so that

$$v B_x \approx \gamma \qquad , \tag{4.15}$$

a balance can be achieved between the potential forces and the magnetic forces. For B_x on the order of one, the velocity must be on the order of γ and the potential on the order of $-\gamma^2$. Since γ^2 is such a small number, the particle essentially moves along the intersection of the $V = 0$ plane with the potential surface. In the S-region (see Figure 4.6) the $V = 0$ lines from two closed curves passing through the origin. The inner one goes around the peak of the sombrero (recall that in region I_r the origin is at the saddle point on the rim of the sombrero) and the outer one is on the outer part of the rim. Outside of the S-region, the outer $V = 0$ line intersects the breaking line. Waves moving along the outer loop break unless the initial state of the plasma lies in the S-region.

The inner $V = 0$ curve never intersects the breaking line, but that does not mean that the inner wave solution always exists. As B_x gets smaller, the velocity of the particle must increase to keep the magnetic force comparable to the potential forces. This means that the particle must move further and further away from the $V = 0$ line. When B_x is in the order of γ the particle moves so far from the $V = 0$ line that the wave breaks. The breaking line for the inner waves of region I_r is shown in Figure 4.10. To the left of this line, B_x is too weak to prevent the wave from reaching the breaking line. To the right of it, we find that the waves are simple solitary waves. As B_{zo} increases, the potential gets steeper on the negative $(B_z - B_{zo})$-axis requiring a larger value of B_x. This is clearly shown in Figure 4.10.

Cordey[12] analyzed the waves in region I_r by expanding the equation of motion in terms of γ^2. He found that the waves oscillated with a very small amplitude about the $V = 0$ line and concluded that they were not exactly solitary waves because of these oscillations. Our computer analysis of these waves shows that while the oscillatory modes are a natural mode of the system, they are only excited if the particle is perturbed from the path where the potential and magnetic forces balance. Cordey in effect did this when he substituted the zero order orbit into the first order equations of motion. In the exact solution these oscillatory modes are not found.

Kellogg[13] did some computer calculations of waves in region I_r and also concluded that these waves are not quite solitary waves. He found that oscillations appeared as the waves returned to the origin and then the waves changed into outer wave type solitons which eventually broke. Our experience with computer calculations of solitary waves leads us to conclude that these oscillations and the subsequent emergence of the outer wave soliton were the result of computer generated "friction" rather than a real indication of the wave behavior. Because of the finite word size in a computer, single precision calculations are only accurate to about one part in a million. Small errors generated when the amplitude of the wave is large can add or subtract energy from the particle. These errors are greatly magnified when the particle nears the origin. If the particle has too much energy it will overshoot the origin and continue moving on the other side. In region I_r this leads to the appearance of an outer wave (see Figure 3.4(c) for the shape of the potential near the origin in region I_r).

In our study of region I_r many waves were generated on the computer with a wide variety of initial conditions and values of γ. In every case the maximum value of B_r occurred as the particle crossed the negative B_z- axis, (within the accuracy permitted by a finite integration step size). Also, there was no indication of oscillations even when the mass ratio was small enough that they should have easily been seen according to Cordey's results. This leads us to conclude that the waves in region I_r are simple solitary waves unless they break before reaching the negative B_z- axis. Like all solitary waves, they are unstable to even small perturbations which makes them difficult to analyze either analytically or numerically.

D. Laminar Shock Waves

If we introduce friction into the problem, the situation is complicated by the changing shape of the potential well. However, the change in shape is, in general, quite minor and doesn't alter the topology of the potential well. The primary effect of friction is to raise the potential well upwards as a whole. As it moves upwards, the equilibrium points that were initially below the $V = 0$ plane move up to the $V = 0$ plane and become possible final states of the plasma. If there is any dissipation the equilibrium point that is initially at the origin can not be the location of a final state because it immediately moves above the $V = 0$ plane.

The region of the potential surface where the particle can move is further reduced by the fact that the dissipation heats the plasma thereby increasing the minimum value that u can reach before the wave breaks (u_b). With friction present we must replace (4.9) with

$$u_b = [(5/3)\ (T_o + \delta)]^{1/2} \tag{4.16}$$

The maximum value for B_z is

$$(B_z)_b = [B_{zo}^2 + 2(1 + T_o - 8u_b/5)]^{1/2} \tag{4.17}$$

When B_{zo} and T_o are small, we find that initially

$$u_b \to 0\ ,\quad (B_z)_b \to (2)^{1/2} \tag{4.18}$$

As friction increases δ, u_b increases and $(B_z)_b$ decreases.

(a) Shock Waves in Regions 2_{ms} and 1_m

The possible types of laminar shocks are really quite similar to the types of frictionless waves. In region 1_m and 2_{ms} of Figure 4.3 the waves are generally quite stable. They are absolutely stable in the S-region part of 1_m and 2_{ms} (see Figure 4.6) and friction can stabilize the rest of 1_m and 2_{ms} by raising the breaking line above the $V = 0$ plane. But since it is possible for the particle to reach the breaking line before it moves out of the allowed range of motion, the waves in this region can break. Clearly, the farther the initial conditions are from the S-region and the closer they are to the left-hand boundary of the 1_m and 2_{ms} regions, the more likely the wave will be to break before it is stabilized. Whether the wave breaks or not will also depend upon the magnitude of the collision frequency and the direction of the initial displacement as we saw in our discussion at the end of Chapter II.

In Figure 4.11 we show an example of a laminar shock wave in region 2_{ms} . The location of the wave in the B_x , B_{zo}-plane is indicated in Figure 4.6 by the letter "a" . The transition is to the equilibrium point which is a minimum (R_2) . To generate this wave in a reasonable amount of time it was necessary to weaken the perpendicular magnetic field by assuming a γ of 0.2 which is about eight times larger than the real value. The effect of the perpendicular magnetic field was further reduced by using a high value for the collision frequency $(\nu = 10)$. This kept the particle's velocity small. Another effect of the large value for the collision frequency is the absence of oscillations about the equilibrium point as, for example, there were in Figure 2.4 where the collision frequency was only 0.1.

(b) Wave Trains in Regions 1_s and 0

In the two regions labelled 0 in Figure 4.3 there are no roots acceptable for laminar shock transitions and in region 1_s the

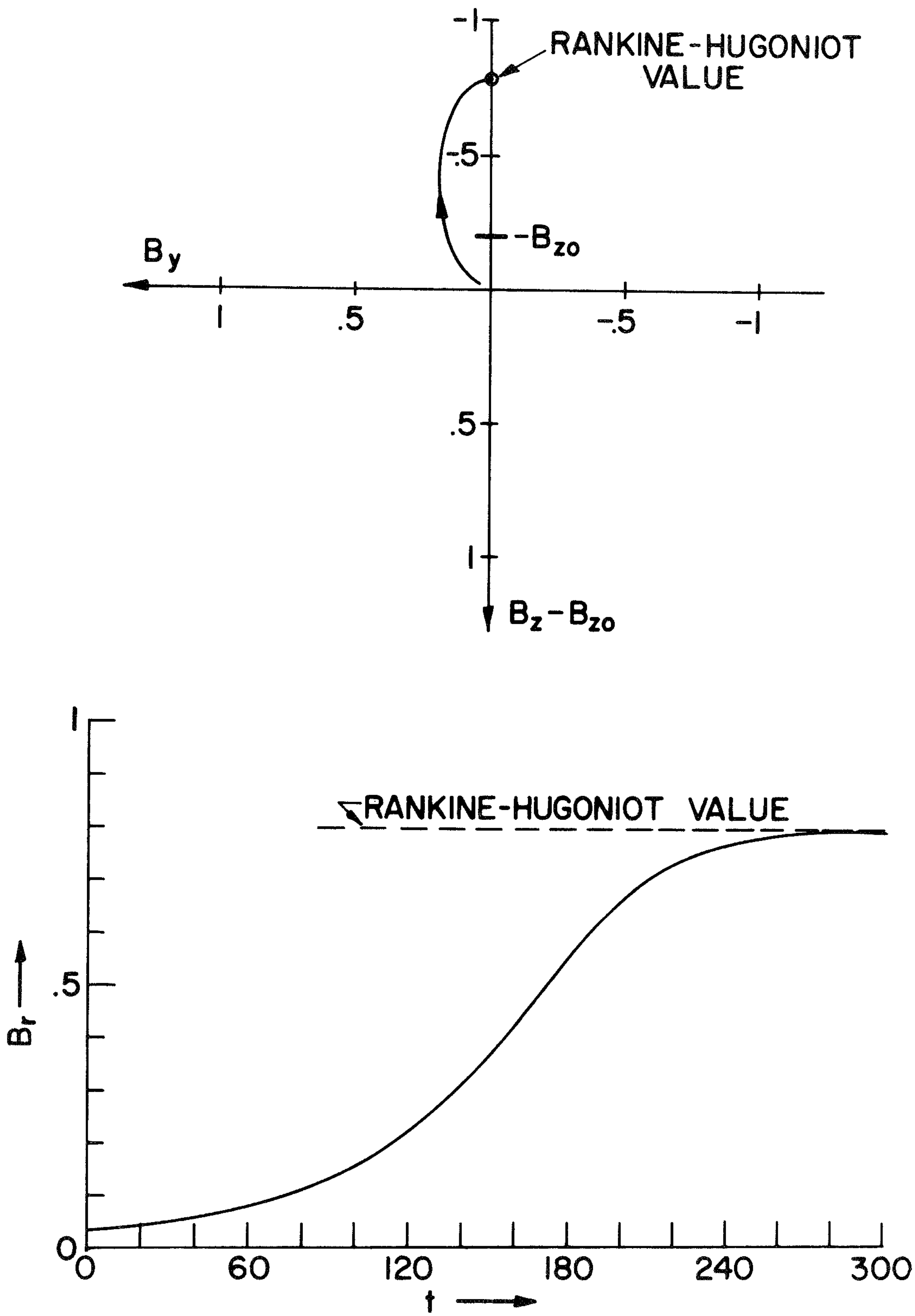

Figure 4.11 A shock wave to R_2 in region 2_{ms}. M_A=1.085, α=12.5°, B_x=0.9, B_{zo}=0.2, ν=10, γ^2=1/25, β_o=0.2.

only root is a saddle point. Waves started with an arbitrary initial perturbation in these regions must eventually break. How many oscillations they make before they break will depend upon the relative importance of the magnetic field and the potential gradients. Friction has very little effect on the potential gradients but it does reduce the stabilizing effect of the magnetic field by lowering the particle's velocity. It also heats the plasma and moves the breaking line closer to the origin. Even a very small amount of friction will eventually heat the plasma enough to cause a wave train to break. This can be done without appreciably altering the shape of the wave train.

The effect of adding a small amount of friction $(\nu = .005)$ to the wave shown in Figure 4.8 is shown in Figure 4.12. Instead of the long wave train we found in the frictionless case, we see that the wave breaks on the third oscillation. If the friction had been larger the wave would have broken even sooner. Notice that the shapes of the wave trains are almost identical. The wave breaks not because friction has cause the particle's distance from the origin to increase but because the breaking line moved into the particle's path.

(c) Shock Waves in Region 1_s

There is a frictional analogue to the soliton type solutions we found in the frictionless case. In regions 1_s and 2_{ms} one of the equilibrium points is a saddle point. While we don't expect the particle to come to rest at a saddle point in general, laminar shock transitions to these final states are possible. They are just as reasonable (or

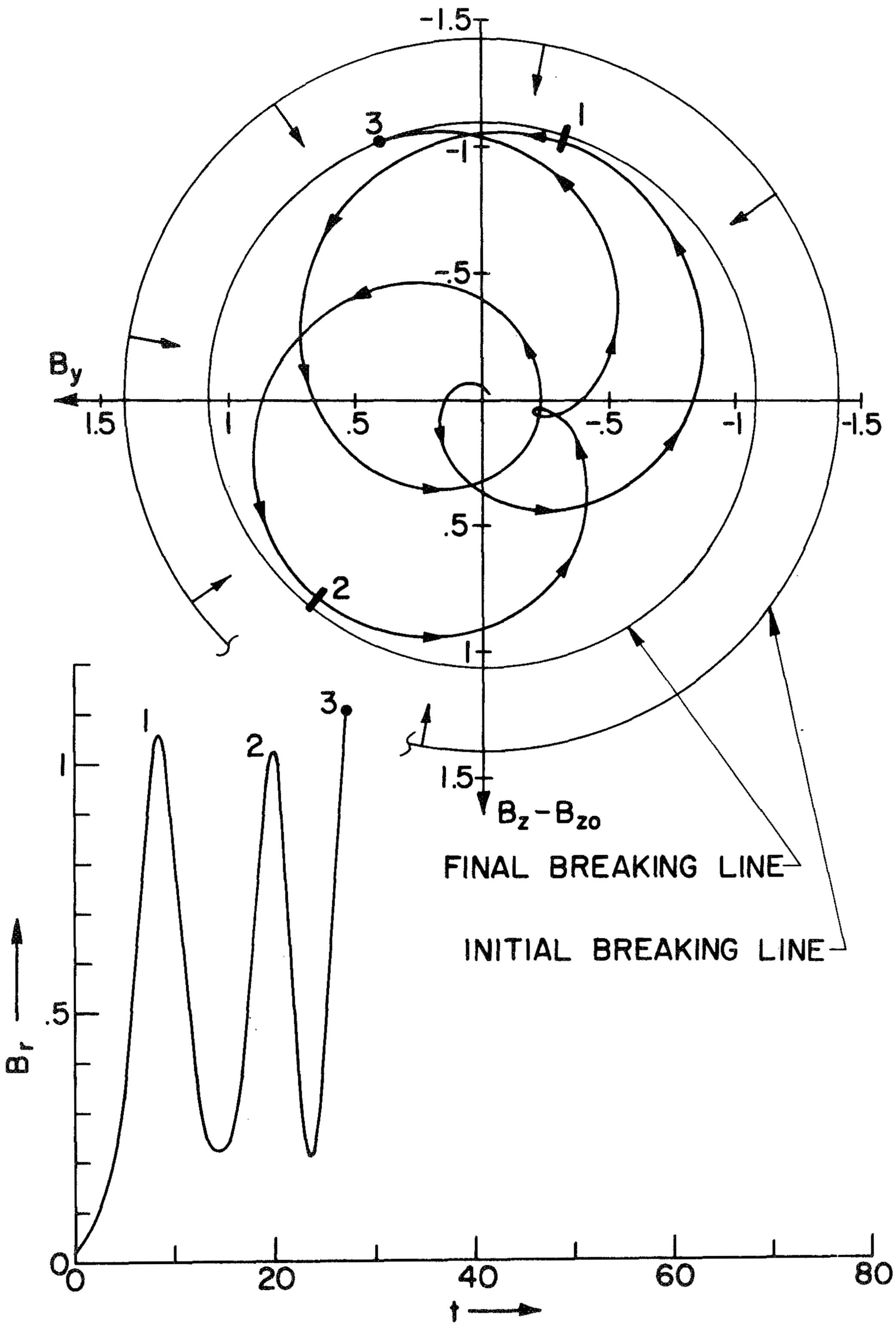

Figure 4.12 The effect of friction on the wave train shown in Figure 4.8. Notice how the breaking line moves into the path of the particle. ν=0.005.

unreasonable) as solitons are. In fact the fairly common example of a frictionally damped magnetosonic wave belongs to this class of transition. As in the case of solitary waves these transitions are only possible for certain initial perturbations. The particle must reach the saddle point just as it reaches the $V = 0$ plane. Of course there is a finite range of starting conditions that give waves which closely approximate these mathematically singular solutions. Any particle near a saddle point and the $V = 0$ plane will be moving slowly and may give the appearance of having made a laminar shock transition for a finite time.

In Figure 4.13 a laminar shock transition to a saddle point is shown. Its location in the B_x , B_{zo}-plane is indicated by the letter "d" in Figure 4.10. Many initial perturbations were tried before a satisfactory wave resulted. If we were to follow this wave for a long time it would continue on past the equilibrium point and eventually break since it is impossible to exactly reach the saddle point as it passes through the $V = 0$ plane. The dotted lines in Figure 4.12 show the motion of the particle after it leaves the region of the saddle point.

This concludes our discussion of purely laminar waves. In the next chapter we will expand our model to include the high Mach number shock waves which do not have solutions completely within the laminar framework we have developed thus far.

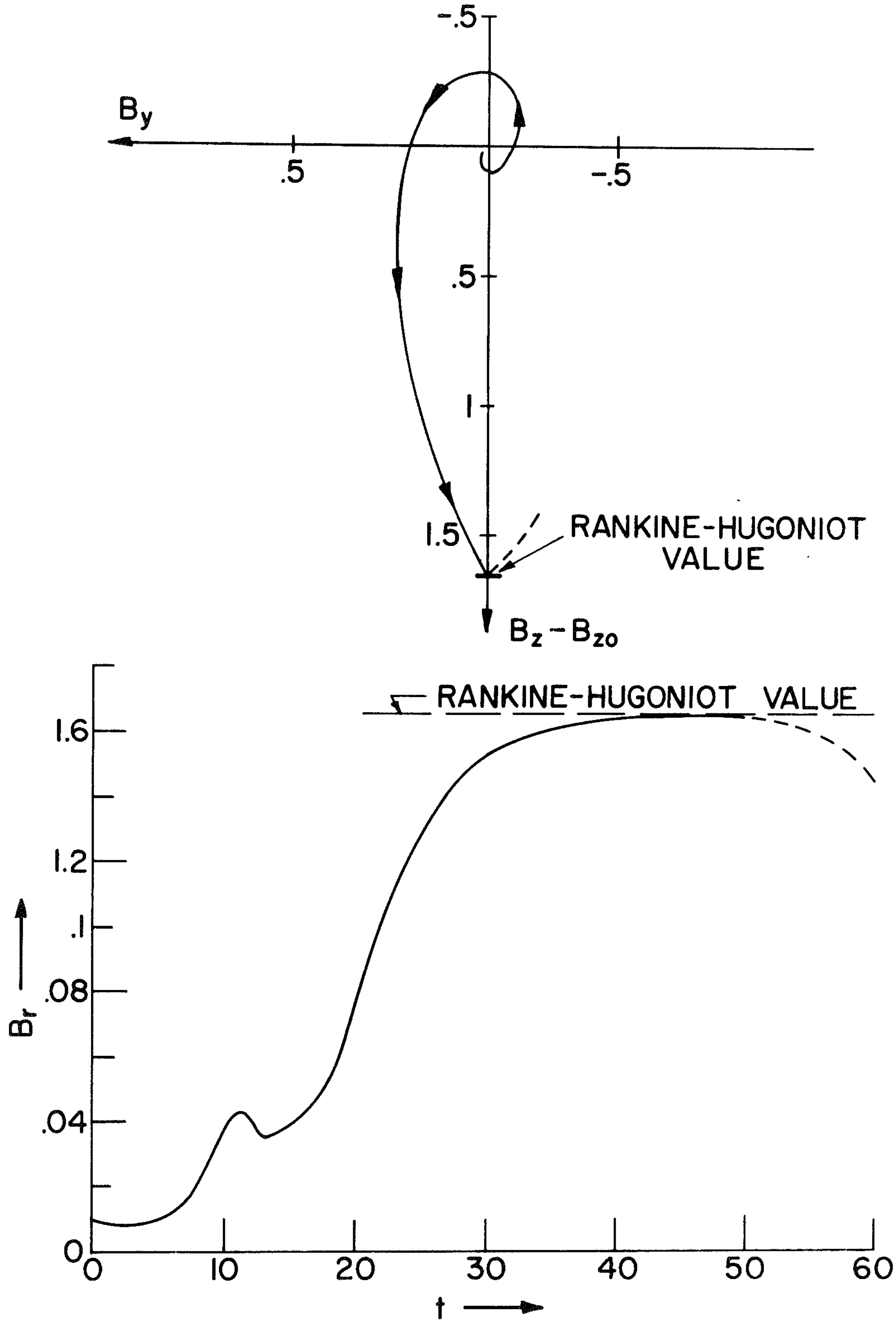

Figure 4.13 Shock wave to a saddle point in region 1_m. $M_A=1.225$, $\alpha=86.4^\circ$, $B_x=0.05$, $B_z=0.8$, $\nu=0.4785$.

CHAPTER V

DOUBLE SHOCK WAVES

By including a frictional dissipation term in the equations of motion we have been able to generate laminar shock waves for Mach numbers up to two or three. If we try to go to higher Mach numbers, our present model fails. We find that E_x becomes very large, violating the quasi-neutrality assumption. This can not be prevented by increasing the friction or changing the starting angle as we did in the lower Mach number regions of 1_s . This is because at high Mach numbers the only equilibrium point is located where T/u^2 is greater than 3/5 and there is no way to get there without E_x becoming very large. See Figure 5.1 for an example of a typical high Mach number potential well profile. We have included the lower branch, which we generally excluded in the previous chapters, to show the location of the equilibrium point predicted by the Rankine-Hugoniot relations. All points of the lower branch have T/u^2 greater than 3/5. Notice that there are no equilibrium points on the upper branch except for the origin itself. Since many interesting laboratory and astrophysical shock waves occur at these high Mach numbers, we will modify our theory to include high Mach number shock waves.

A. Model for High Mach Number Shock Waves

There are several possible ways, mathematically, to prevent E_x from becoming large. Most of these are of dubious physical validity

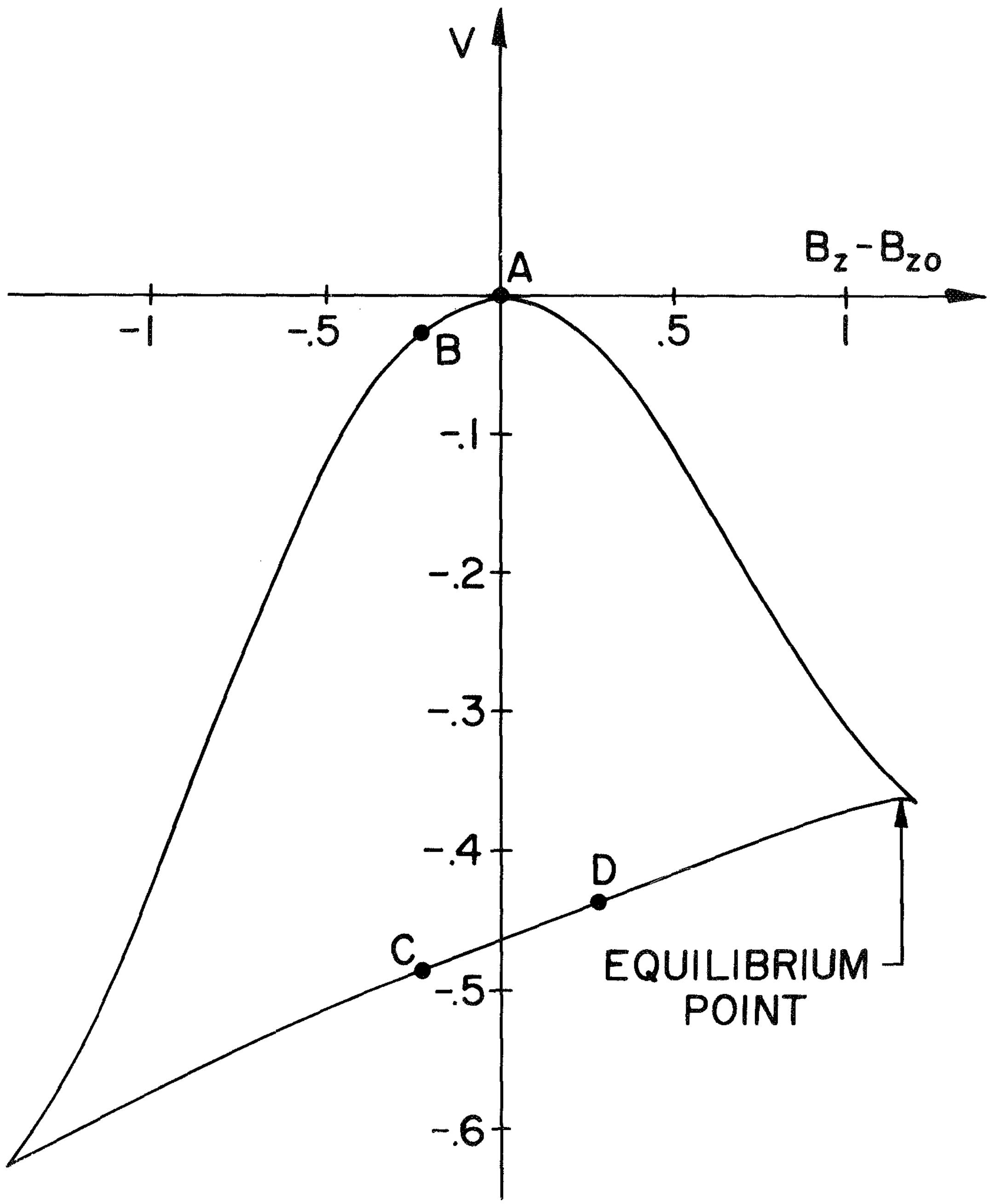

Figure 5.1 The initial shape of the potential well for a magnetosonic wave. M_A=10, β_o=0.2.

however. One of the most common techniques is to include a viscous force term in the ion's equation of motion of the form

$$\vec{F}_{viscosity} = \hat{i}\,\mu \frac{\partial^2 u}{\partial x^2} \tag{5.1}$$

Since the derivatives of u become large when E_x becomes large, the viscous force will be large near the breaking line. If μ is large enough, the viscous force can prevent wave breaking. The inclusion of such a force may be valid at moderate Mach numbers $(M_A \approx 5)$, but it is doubtful that it is valid at high Mach numbers. As the Mach number is increased, either E_x will get too large before the viscosity becomes effective enough or μ must be made very large. Since μ is related to some form of microscopic turbulence, a large value for μ implies a large amount of turbulence which casts doubt upon the validity of using a laminar description at all.

Rather than introducing another form of macroscopic dissipation, such as viscosity, we will adopt an approach suggested by Tidman[21] which takes a microscopic picture of the plasma. In the introduction to this thesis, we noted that there were two distinct length scales in our problem. We found that the length scale for magnetic waves was much greater than the length scale for electrostatic fluctuations. What Tidman has suggested is that in an otherwise laminar and slowly varying magnetic wave there could be embedded a highly turbulent and very thin electrostatic transition. The thickness of such a region might be only a few Debye lengths. An example of what a double shock structure might look like is shown in Figure 5.2.

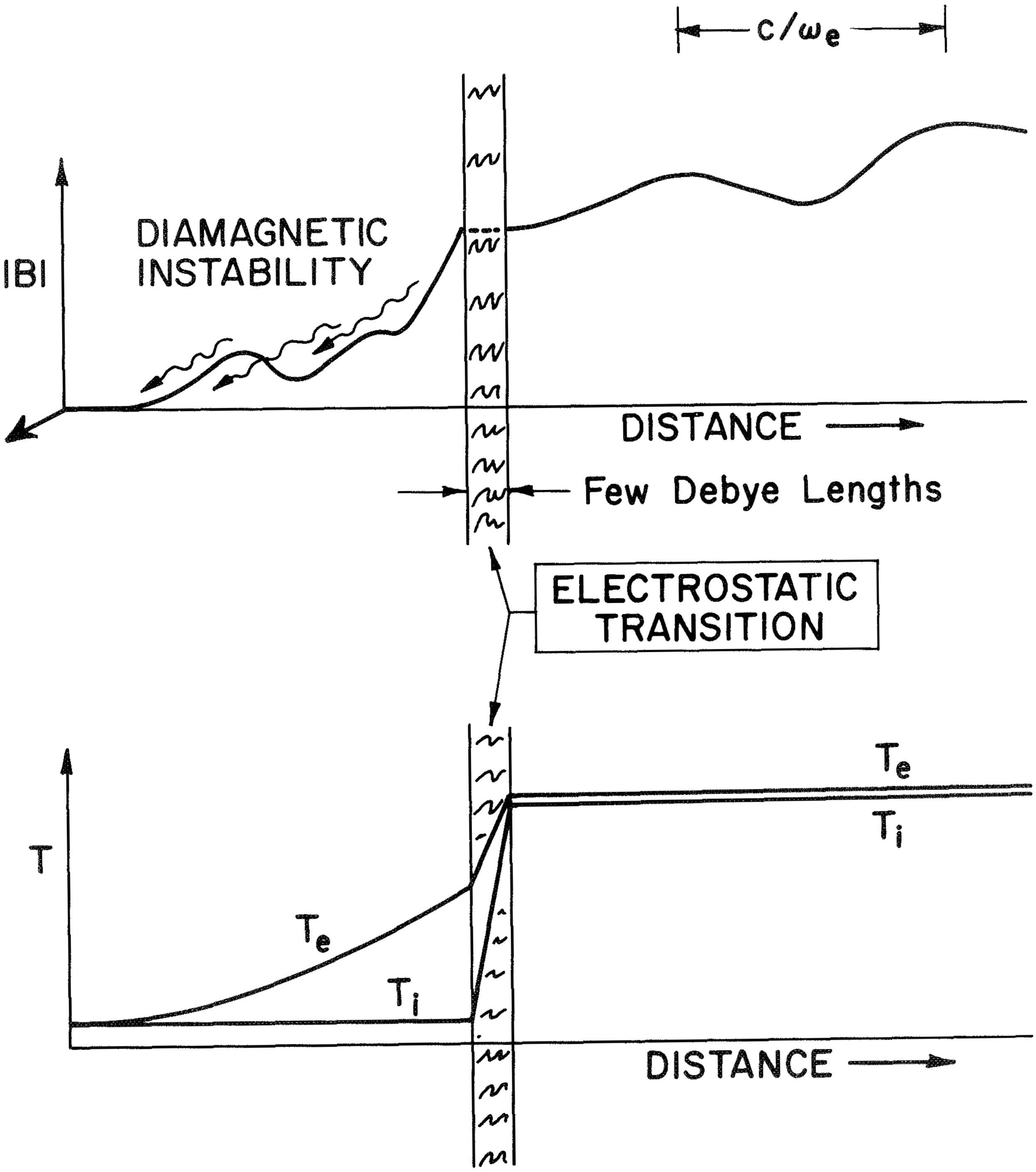

Figure 5.2 A typical double shock wave.

To create this electrostatic transition, we need a plasma instability which generates intense electrostatic turbulence. As usual in plasmas, there is no shortage of possible instability mechanisms. In fact, it seems reasonable to expect that more than one instability will be involved during the course of the transition and that some instabilities that predominate for a particular range of Mach numbers and angles of propagation will be insignificant under different starting conditions. We will briefly outline the characteristics of one likely instability mechanism for high Mach number shocks and then see how this double shock structure can be included in the theoretical framework developed in the previous chapters.

B. A Possible Instability Machanism

We can consider the shock wave to consist of three distinct regions whose general features are outlined in Table 2.

upstream region	interaction region	downstream region
Density = $n_o < n_f$	Density $\approx \frac{n_o + n_f}{2}$	Density = $n_f > n_o$
Beta < 1	Beta $\approx$ 1	Beta > 1
$T_e \gg T_i$	T_e & T_i increasing	$T_e \approx T_i$
$M_A \gg 1$	Mach Number $\approx$ 1	$M_A < 1$

<u>Table 2</u>

The upstream and downstream ion distributions are assumed to be simple Maxwellians. In the interaction region, the two Maxwellian ion distributions overlap as the upstream plasma mixes with the downstream plasma. Some of the plasma is in the upstream state and some in the downstream state forming an unstable, bimodal, ion distribution. The ion distribution in each of the three regions is shown in Figure 5.3. By assuming that $T_e >> T_i$, we allow the instabilities generated by the interacting ion beams to overcome the stabilizing effects of the smeared out electron distribution. The electron thermal velocity is assumed to be large enough, compared to the change in the streaming velocity, to prevent the electron distribution from becoming bimodal. The turbulence generated by the instability in the interaction region will be very resistive to both ion and electron streaming. As a result both species will be heated and the downstream temperature will exceed the upstream temperature.

If this instability is strong enough, the dissipation it produces can take place over a few Debye lengths producing a double shock structure. Referring to Figure 5.2 again, we see that in the leading edge of the shock there is a laminar wave growing in amplitude. As the wave grows, the weak instabilities generated by the diamagnetic currents heat the electrons. This is included in the model through the anomalous collision frequency. The friction in effect primes the plasma for the subsequent instability by making T_e larger than T_i. At some point, the mixing between the upstream and downstream plasmas results in a strong instability and the plasma makes an electrostatic transition to the downstream state which is once again laminar. When viewed on the scale of

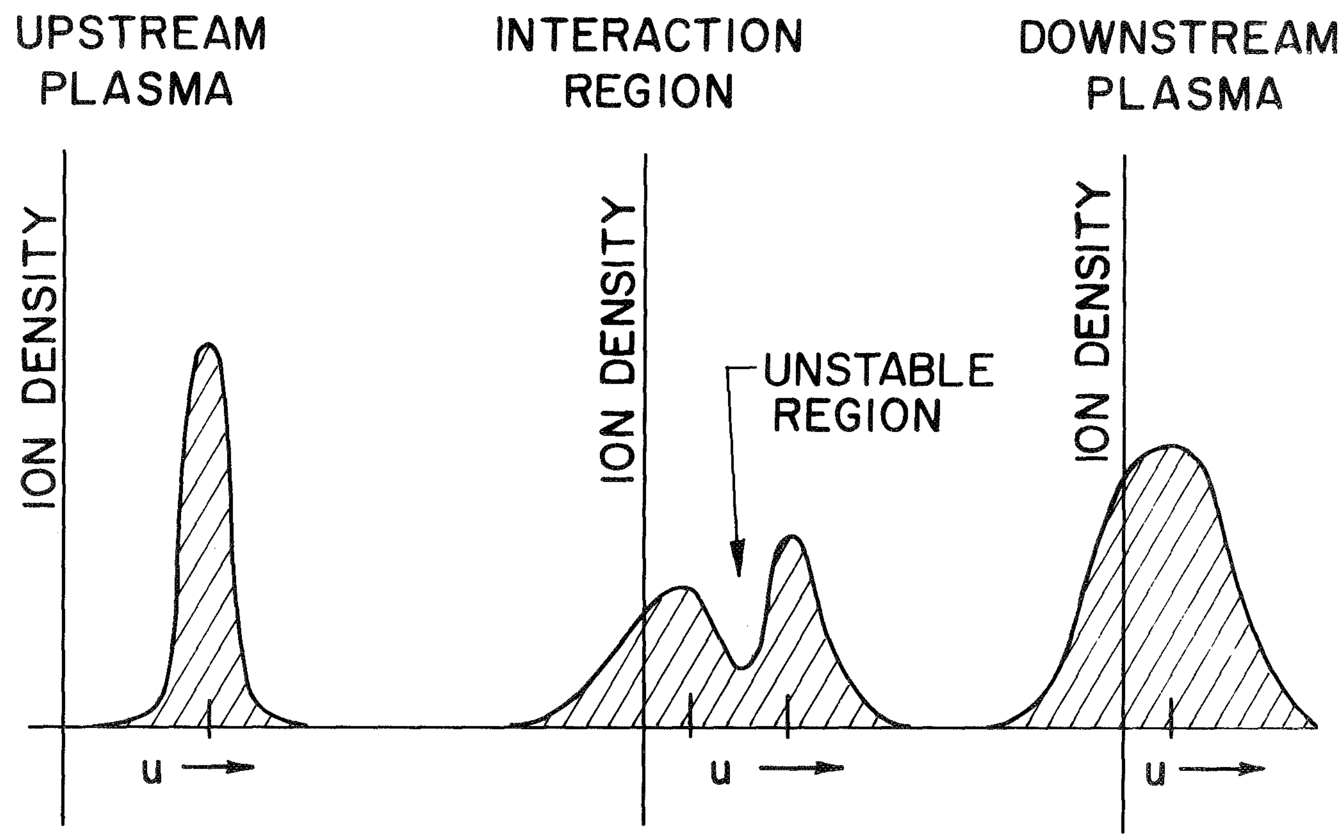

Figure 5.3 The evolution of the ion density distribution through the shock wave.

the magnetic waves, this turbulent electrostatic region is very thin.

C. Relationship Between Double Shock Waves and Two Fluid Theory

Since the two fluid equations are not valid in the thin electrostatic region, we can't use them to follow the detailed motion of the plasma there. But because the region is so thin and turbulent, we can make reasonable guesses as how to join on upstream and downstream laminar solutions to either side of the transition region. If we assume that the plasma emerges from the electrostatic transition with a Maxwellian distribution and an isotropic pressure, the same conservation relations that were valid upstream are valid downstream. Also we can assume that $\vec{B}$ will be constant across the transition region because it is so thin and turbulent that the integral of any currents through it will be negligible. These assumptions do not uniquely determine the downstream state however. There are still two free parameters which depend upon the details of the instability. They can be considered to be the amount of dissipation that takes place in the transition (i.e. the jump in δ or entropy) and the direction of the downstream current.

Another free "parameter" is the location of the electrostatic transition. The two fluid theory gives no criteria for determining where the plasma will become unstable. This can only be found from a microscopic theory. We will therefore assume that the instability mechanism described above is the relevant one for generating double shock waves in high Mach number plasmas and look at Table 2 to see what conditions characterize the interaction region.

From Table 2 we find that during the course of the electrostatic transition the local Mach number decreases below one and the local beta increases to over one. Also just prior to the transition region, the electron temperature is several times larger than the ion temperature. There is really no sharp boundary between the laminar regions and the turbulent regions but, since we can't follow the plasma into the turbulent region, we must draw such a boundary and decide which regions are laminar and which are turbulent. A convenient point for dividing the two regions is the value of $\vec{B}$ at which the dissipation has increased the electron to ion temperature ratio to ten. This is somewhat arbitrary but not unreasonable.

To see how all this fits into the potential well analogy, we consider a double shock wave for a high Mach number magnetosonic wave ($M_A = 10$) . Figure 5.1 shows the initial shape of the potential well profile and the position of the particle during the course of the shock wave. The changing shape of the well due to frictional heating is neglected in the figure. The changes in the various physical parameters during the course of the wave are shown in Figure 5.4. The particle starts out at A in Figure 5.1 and rolls to B . Friction and adiabatic compression heat the plasma as it changes from A to B . At B T_e is ten times greater than T_i , and we assume that an electrostatic transition takes place. The particle drops straight down to C on the lower branch of the potential well keeping B_z constant. Now we have to decide what values to give the two free parameters, δ and the direction of the current.

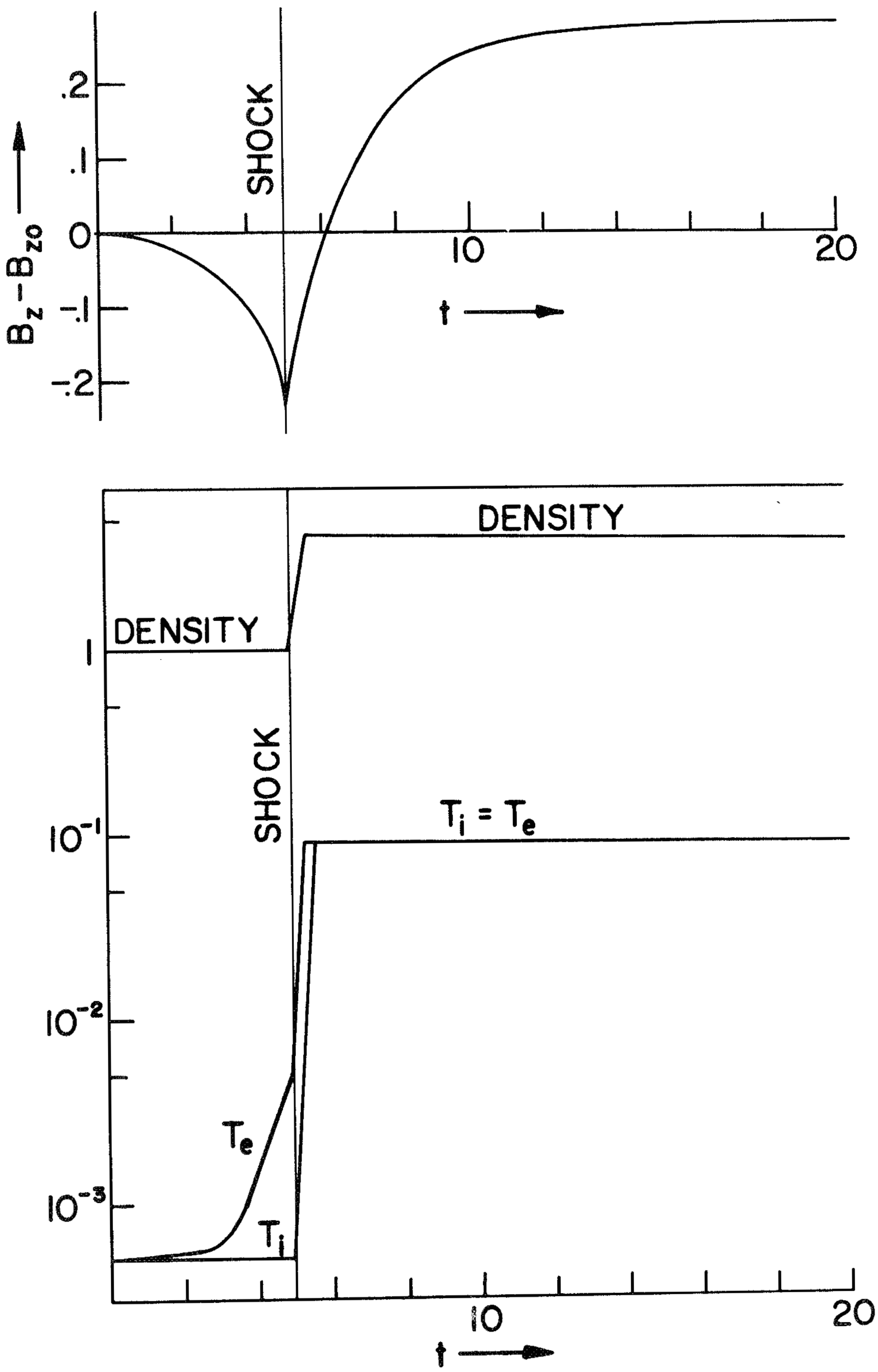

<u>Figure 5.4</u> Magnetosonic double shock wave. Electrostatic transition when T_e/T_i=10. M_A=10, β_o=0.2.

Specifying δ is equivalent to specifying the level of the potential surface relative to the $V = 0$ plane. To keep the example as simple as possible, we assume that there will be no friction after the transition. To get a laminar wave downstream, we must choose δ such that the final equilibrium point lies on the $V = 0$ plane. This is accomplished by assuming that δ jumps to δ_f, where δ_f is the final value of δ as determined by the Rankine-Hugoniot relations.

In the magnetosonic case it is easy to determine what direction the current must be in. We clearly do not want to introduce y-components of velocity, and if the particle moves to the left, toward the breaking line, the wave will eventually break. So we require that the direction of the current be such as to move the particle towards its equilibrium position. Thus the particle moves from C and comes to rest at D, which is the final location of the equilibrium point.

Although the magnetosonic case is easy to analyze mathematically, it seems highly implausible that such behavior could be found in nature. The whole process is very unstable to any perturbations in the y-direction and depends critically upon the jump in δ and the direction of the downstream current. For this model to be useful, there must be a fairly wide range of acceptable values for δ and the direction of the downstream current. In the previous chapters we also found that the magnetosonic case was unstable but that the stability improved quickly as the magnetic field became more closely aligned with the direction of the incident streaming velocity. To see how effective B_x is we briefly examine the shape of the lower surface of the potential well.

From Figure 5.1 we can see that the gradients on the lower surface are generally smaller than on the upper surface. From (3.24) and (3.25) we find that when B_x and B_{zo} are small (Mach number high) the increase in the steepness of the potential well with increasing B_r is proportional to u. On the lower surface u is only about one fourth of its value at a corresponding point on the upper surface. (See (A2.18) which shows that for high Mach numbers $u_f \rightarrow 0.25$.) This means that the lower surface will be roughly one fourth as steep as the upper surface and as a consequence a smaller magnetic force will stabilize the waves.

Another factor to be considered in determining the stability of waves on the lower surface is the particle's velocity. The velocity of the particle is proportional to the square root of the distance it is below the $V = 0$ plane. We will generally assume that δ increases to δ_f in the electrostatic transition so that the downstream equilibrium point is at the $V = 0$ plane. Since the gradients are roughly one fourth as steep on the lower surface, the particle's velocity will be approximately one half what it would be on the upper surface. This reduces the effectiveness of the magnetic field by a factor of two which, because of the smaller gradients, leaves a net gain of a factor of two in the strength of the magnetic forces over the potential gradients.

The advantage of having a shallower potential well is offset by the fact that the breaking line is much closer to the origin when the particle is on the lower surface. This is because of the heating that takes place in the electrostatic transition. To find the initial location of the breaking line we note that for high Mach numbers c_b in (4.11) approaches two. Using this in (4.10), with the assumption that B_{zo} is small, we find that the magnitude of $\vec{B}$ at the breaking line is approximately equal to $\sqrt{2}$. It is easy to show, with the help of Appendix 2, that after the electrostatic transition the magnitude of $\vec{B}$ at the breaking line is approximately 0.7 or roughly one half of its initial value. This sharp reduction in the range of the particle's motion negates most of the advantages gained by having a shallower potential well.

An example of an oblique double shock wave is shown in Figures 5.5 and 5.6. This is a fairly low Mach number example ($M_A = 10$, $\alpha = \pi/4$) chosen to correspond to typical solar wind conditions. The initial conditions are slightly inside region IV_i . Friction causes the wave to spiral down the potential peak and grow in amplitude. When T_e/T_i equals 10, we assume that the particle drops to the lower surface and that δ increases to δ_f . There is no friction on the lower surface since the thermalization of the electrons and ions in the electrostatic transitions removed the conditions which made the plasma unstable upstream of the transition.

In Figure 5.5 the dominant effect of the perpendicular magnetic field is clearly seen in the spiral motion of the particle as it drifts about the peak in the lower potential surface located on the positive $(B_z - B_{zo})$-axis at 0.21. In Figure 5.6 we see that, although the fields are continuous across the shock, the density jumps from one to four and the temperature jumps sharply to 3/16 ($T_e = T_i = T/2 = 3/32$) .

At this low of a Mach number the downstream wave is quite stable

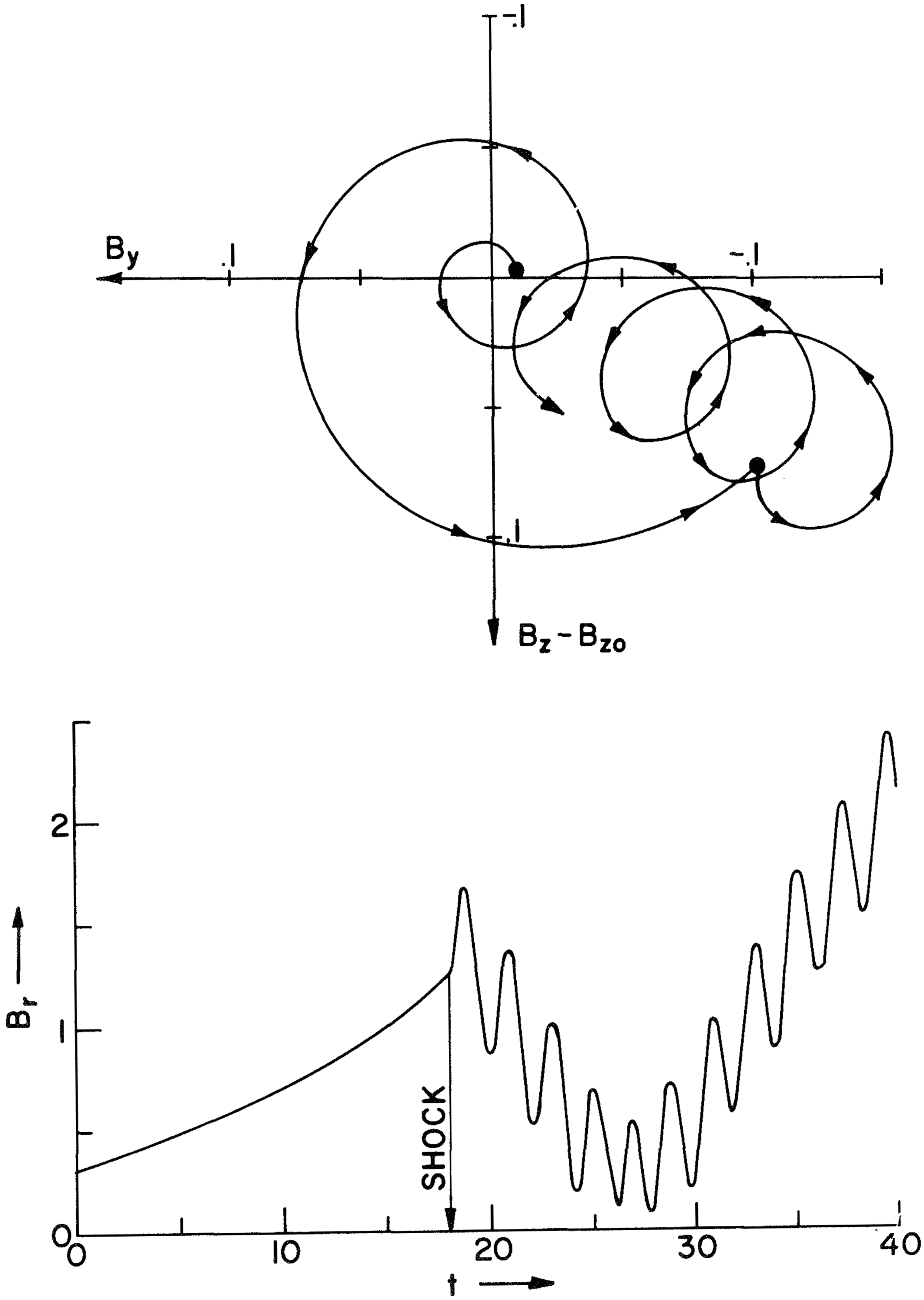

Figure 5.5 An oblique double shock wave. $M_A=10$, $\alpha=45°$, $B_x=B_{zo}=0.707$, $\beta_0=0.2$. Before the jump $\nu=0.5$.

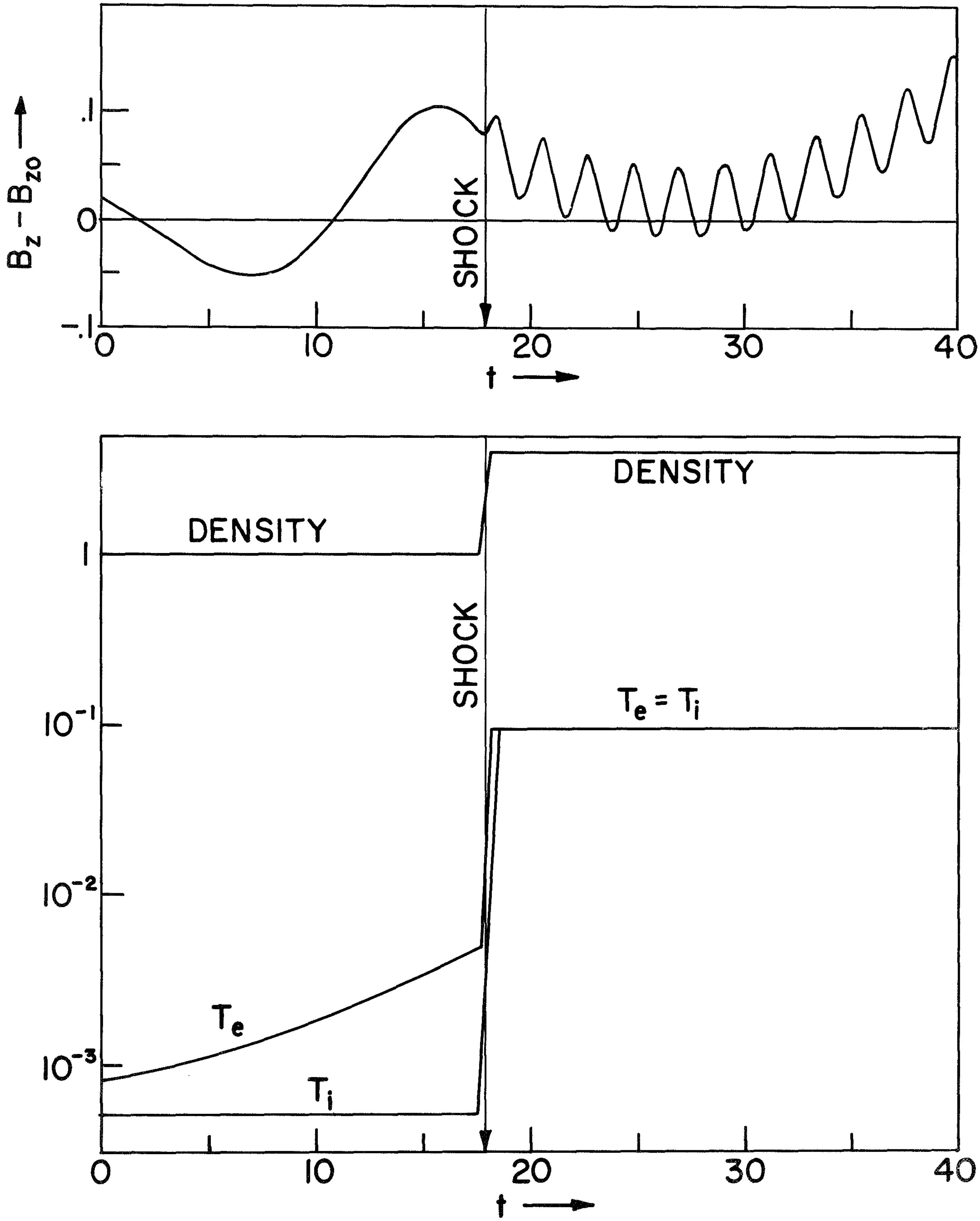

Figure 5.6 The variations of B_z, density, and temperature through a double shock wave. The jump occurs when $T_e/T_i=10$.

and we are free to choose any direction for the downstream current. At higher Mach numbers ($B_x \approx \gamma/2$) we find that some choices for the direction of the downstream current lead to waves which quickly break while others give fairly long wave trains. At very high Mach numbers ($B_x < \gamma$) the problem becomes more and more like the magnetosonic example we considered above and only a very narrow band of starting directions will result in a non-breaking downstream wave. Formal solutions can be found for any Mach number no matter how high but as B_x decreases, the stability of the waves decreases also.

The validity of this theory will depend upon experimental verification. The shocks described by it are characterized by a laminar precursor with most of the heating going into the electrons, a thin region of intense electrostatic noise and rapid heating of the ions, and then a laminar region of random magnetic field variations. The fluid theory can predict neither the location of the transition, the amount of dissipation in the transition, nor the direction of the current after the transition. These all depend upon the details of the instability and have to be determined either experimentally or by a kinetic theory.

CHAPTER VI

CONCLUDING REMARKS

To our knowledge this work presents the most complete two fluid theory of laminar shock waves to date. Many previous results are generalized or clarified and several new results are presented.

The theory of waves in the absence of friction we developed generally agrees with the results of previous authors. Our disagreemnet with their results[12,13] in region I_r is noted in Chapter IV. By choosing an energy conservation relationship as an equation of state, rather than a seemingly simpler relationship between the pressure and density as other authors[12,17] have done, we are able to easily apply the potential well analogy to warm plasmas that Saffman[11] found so useful in explaining the behavior of cold plasmas. We have used a digital computer to generate examples of a wide variety of waves and to confirm our analytical conclusions. Among the new results we have obtained numerically is the location of the soliton breaking line at arbitrary angles of propagation shown in Figure 4.10.

The theory of nonlinear waves with frictional dissipation had been considerably less developed than the frictionless case. Most authors have neglected the heating effects of the friction[8,18] for simplicity. We saw an example in Figure 4.12 of how important the heating of the plasma can be in determining the wave behavior. Again it is our choice of an equation of state that permits a thorough analytic treatment of laminar shock waves. The tendency has been to relate the work done by friction to an increase in temperature through a differential equation. By using an algebraic energy conservation relationship, we avoid introducing another differential equation into an already complicated set of equations. It also permits us to expand the potential well analogy, in a slightly modified form, to the case where friction is heating the plasma. The problem is complicated by the changing shape of the potential well, but by using the Rankine-Hugoniot relations we are able to calculate the final shapes of the potential well. The numerical results confirm the analytic conclusions we reached.

We have adapted the theory of double shock waves[21] to the two fluid model and shown how it fits naturally into the potential well analogy. This has permitted an increase in the range of validity of the two fluid model into a region of considerable interest (i.e. high Mach number shock waves).

With better kinetic theories and experimental results the quantitative results of the theory can be improved by dropping the obviously incorrect assumptions of an isotropic pressure and a constant collision frequency. However, we are confident that the qualitative behavior of the waves will not be affected by improving on these assumptions. For example, the quasi-neutrality assumption will still lose its validity when the plasma streaming velocity decreases to near the local sound speed regardless of the exact relationship between the plasma parameters and the sound speed.

APPENDIX 1

In this appendix an expression for E_x is derived to show that $|E_x| \to \infty$ as $T/u^2 \to 3/5$. The starting point for the derivation is (2.5) which must first be made dimensionless. Then (2.38) and (2.39) are used to eliminate $\dot{u}$ and $\dot{T}$. Finally, (2.29) and (2.30) are used to eliminate v and w . The procedure for making (2.5) dimensionless is shown in detail to demonstrate how the other equations in Chapter II were made dimensionless.

We recopy (2.5) here for ease of reference,

$$\frac{d}{dx}\,(mnu^2 + nT_e) = -\,ne\left[E_x + (v_e B_z - w_e B_y)/c\right] \tag{A1.1}$$

Since nu is equal to a constant, j , (A1.1) can be rewritten as

$$mu\,\frac{d}{dx}\left(u + T_e/mu\right) = -\,e\left[E_x + (v_e B_z - w_e B_y)/c\right] \quad . \tag{A1.2}$$

To make (A1.2) dimensionless we use the equations in section II.B where the dimensionless variables are defined. For example, (2.19) is used to replace B_z in (A1.2),

$$B_z \to B_z\ (4\pi m_t n u_o^2)^{1/2} \tag{A1.3}$$

The B_z on the left hand side of (A1.3) is dimensioned, the B_z on the right hand side is dimensionless. Making similar substitutions for the othe quantities we find

$$\left[\frac{4\pi m_t n e^2}{c^2\ Mm}\right]^{1/2} m u_o u \frac{d}{dx}\left[u_o u + \frac{m_t u_o^2\ T_e}{m u_o u}\right] =$$

$$- \frac{e}{c}\ (4\pi m_t n u_o^2)^{1/2}\ u_o\left[c\ E_x + v_e B_z - w_e B_y\right] \tag{A1.4}$$

Cancelling common factors and using (2.28) gives the dimensionless form of (2.5),

$$\frac{d}{dt}\left(u + \frac{m_t}{m}\ \frac{T_e}{u}\right) = - \left[c\ E_x + v_e B_z - w_e B_y\right]\Big/\gamma \tag{A1.5}$$

Note that c , like all velocities, is given in units of u_o . Also recall that $\gamma^2 = m/M$ and $m_t = m + M$.

Assuming that $\dot{T}_e$ can in general be written in the form

$$\dot{T}_e = Xu\dot{u} + Yu \quad , \tag{A1.6}$$

we can write the left-hand side (LHS) of (A1.5) as

$$\text{LHS} = \dot{u}\left[1 - (m_t/m)(T_e/u^2 + X)\right] + (m_t/m)Y \tag{A1.7}$$

Using (2.38) to eliminate $\dot{u}$ gives

$$\text{LHS} = - \frac{\left[\dot{B}_z B_z + \dot{B}_y B_y + 2\nu(\dot{B}_z^2 + B_y^2)/3u\right]\left[1 - (m_t/m)(T_e/u^2 + X)\right]}{\left[1 - (5/3)\ T/u^2\right]}$$

$$+ \left(m_t/m\right)Y \tag{A1.8}$$

The right hand side (RHS) of (A1.5) can be simplified by using (2.29) and (2.30) to eliminate v and w ,

$$\mathrm{RHS} = -\left[c\,E_x + (B_z\dot{B}_z + B_y\dot{B}_y)/\gamma + B_xB_yB_{zo}\right]/\gamma \tag{A1.9}$$

Combining (A1.8) and (A1.9) and solving for E_x gives

$$c\,E_x = -B_xB_yB_{zo} - \frac{(\dot{B}_zB_z + \dot{B}_yB_y)}{\gamma}\left[1 - \frac{\gamma^2 - (1+\gamma^2)(T_e/u^2 + X)}{1 - (5/3)\,T/u^2}\right]$$

$$+ \frac{2\nu(\dot{B}_z^2 + \dot{B}_y^2)}{3\gamma u\left(1 - (5/3)T/u^2\right)}\left[\gamma^2 - (1+\gamma^2)(T_e/u^2 + X)\right] - Y(1+\gamma^2)/\gamma\ . \tag{A1.10}$$

We can not go any further without finding explicit expressions for X and Y as defined in (A1.6). If we assume that T_i = constant then

$$\dot{T}_e = \dot{T} = -\frac{2}{3}\left[(T/u)\ \dot{u} - \nu(\dot{B}_z^2 + \dot{B}_y^2)\right] \tag{A1.11}$$

from (2.39). Thus

$$X = -\,2(T_e + T_i)/3u^2$$

and

$$Y = 2\nu(\dot{B}_z^2 + \dot{B}_y^2)/3u \tag{A1.12}$$

Substituting (A1.12) in (A1.10) and simplifying gives

$$E_x = -\frac{B_x B_y B_{zo}}{c} - \frac{1}{c\,\gamma[1 - (5/3)\,T/u^2]} \times$$

$$\left\{ (\dot{B}_z B_z + \dot{B}_y B_y) \left[1 - \gamma^2 + \frac{5\gamma^2\, T_e - T_i(3 - 2\gamma^2)}{3u^2} \right] \right.$$

$$\left. + \frac{2\nu(\dot{B}_z^2 + \dot{B}_y^2)}{3u} \left[1 - T_i(1 + \gamma^2)/u^2 \right] \right\} \qquad \text{(A1.13)}$$

Since B_x , B_y , and B_{zo} are finite, $|E_x|$ must approach infinity when T/u^2 approaches 3/5.

APPENDIX 2

If the plasma is in a state of equilibrium at $x = -\infty$, it is possible to relate the downstream state of the plasma to the upstream state. The equations giving the downstream state of the plasma in terms of the upstream state are called the Rankine-Hugoniot relations. They are found by assuming the validity of the equations of motion at infinity and by setting all the derivatives equal to zero.

Thus we find,

$$v_f = B_x B_{yf} \tag{A2.1}$$

$$w_f = B_x(B_{zf} - B_{zo}) \tag{A2.2}$$

$$w_f B_x = u_f B_{zf} - B_{zo} \tag{A2.3}$$

$$v_f B_x = u_f B_{yf} \tag{A2.4}$$

Eliminating v_f and w_f gives

$$(B_x^2 - u_f) B_{yf} = 0 \tag{A2.5}$$

and

$$(B_x^2 - u_f) B_{zf} + B_{zo}(1 - B_x^2) = 0 \tag{A2.6}$$

These two equations can be satisfied in three ways:

(a) $B_x^2 \neq u_f$,

$$B_{yf} = 0 \quad \text{and} \quad B_{zf} = B_{zo}(1 - B_x^2)/(u_f - B_x^2) \tag{A2.7}$$

(b) $B_x^2 = u_f \neq 1$, $B_{zo} = 0$ (A2.8)

(c) $B_x^2 = u_f = 1$ (A2.9)

We consider each case separately.

Case (a)

Substituting the values of (A2.7) in (2.33) and (2.35) gives

$$u_f + T_f/u_f = 1 + T_o + \tfrac{1}{2} B_{zo}^2 \left[1 - (1 - B_x^2)^2/(u_f - B_x^2)^2\right] \tag{A2.10}$$

and

$$1 = u_f^2 - 5(T_o - T_f) + B_{zo}^2 \left[B_x^2 \frac{(1 - u_f)^2}{(u_f - B_x^2)^2} + \frac{2(1 - u_f)}{(u_f - B_x^2)}\right] . \tag{A2.11}$$

Solving each of these for $5T_f$ we find

$$5T_f = 5u_f(1 - u_f)\left[1 - \frac{B_{zo}^2(1 + u_f - 2B_x^2)}{2(u_f - B_x^2)^2}\right] + 5u_f \, T_o \tag{A2.12}$$

and

$$5T_f = (1-u_f)\left[1 + u_f - \frac{B_{zo}^2(2u_f - B_x^2 u_f - B_x^2)}{(u - B_x^2)^2}\right] + 5T_o \qquad \text{(A2.13)}$$

Equating (A2.12) and (A2.13) and factoring out $(1 - u_f)$ gives

$$(1 - u_f)\left[1 + 5T_o - 4u_f + \frac{B_{zo}^2}{(u_f - B_x^2)^2}\left[(5/2)u_f^2 + u_f(\tfrac{1}{2} - 4B_x^2) + B_x^2\right]\right]$$

$$= 0 \qquad \text{(A2.14)}$$

If $u_f = 1$, (A2.7) shows that the upstream and downstream magnetic fields are equal. In fact it is easily seen that all the variables are equal to their upstream values if u_f equals one. We will drop this trivial root which simply notes that the upstream state is in equilibrium.

Multiplying (A2.14) through by $(u_f - B_x^2)$ and collecting terms with equal powers of u_f gives

$$4u_f^3 - u_f^2\left[1 + 5T_o + 8B_x^2 + 5/2\ B_{zo}^2\right]$$

$$+ \quad u_f\left[B_x^2(4B_x^2 + 4B_{zo}^2 + 10\ T_o + 2) - B_{zo}^2/2\right]$$

$$- \quad B_x^2\left[B_{zo}^2 + B_x^2 + 5T_o\ B_x^2\right] = 0 \qquad \text{(A2.15)}$$

Using $$T_o = \beta_o\ B_o^2/2 \quad , \qquad \text{(A2.16)}$$

and $$B_o^2 = B_x^2 + B_{zo}^2 \quad , \tag{A2.17}$$

we can write (A2.15) in terms of β_o rather than T_o ,

$$4\,u_f^3 - u_f^2\left[1 + 5/2\;(B_{zo}^2 + \beta_o B_o^2) + 8B_x^2\right]$$

$$+ \quad u_f\left[B_x^2\left(B_o^2(4 + 5\beta_o) + 2\right) - B_{zo}^2/2\right]$$

$$- \quad B_x^2\,B_o^2(1 + 5/2\;\beta_o\;B_x^2) \;=\; 0 \tag{A2.18}$$

If $B_x = 0$ then (A2.18) simplifies to a quadratic in u_f :

$$8u_f^2 - 2u_f\left[1 + 5/2\;B_{zo}^2\;(1 + \beta_o)\right] - B_{zo}^2 \;=\; 0 \tag{A2.19}$$

If $B_{zo} = 0$, (A2.18) can be factored into

$$\left[4u_f - (1 + 5/2\;\beta_o B_x^2)\right]\left[u_f - B_x^2\right]^2 \;=\; 0 \tag{A2.20}$$

We have already assumed $u_f \neq B_x^2$ in deriving (A2.20) so the root we are interested in gives, for the case $B_{zo} = 0$,

$$u_f \;=\; \frac{(1 + 5/2\;\beta_o B_x^2)}{4} \tag{A2.21}$$

Case (b)

Substituting (A2.8) into (2.33) and (2.35) gives

$$B_x + T_f/B_x^2 + \tfrac{1}{2}(B_{zf}^2 + B_{yf}^2) = 1 + T_o \tag{A2.22}$$

and

$$1 - B_x^4 + 5(T_o - T_f) - B_x^2(B_{zf}^2 + B_{yf}^2) = 0 \tag{A2.23}$$

Eliminating T_f we get

$$5B_x^2\left[1 + T_o - B_x^2 - \tfrac{1}{2}(B_{zf}^2 + B_{yf}^2)\right] = 1 - B_x^4 + 5T_o$$

$$- B_x^2(B_{zf}^2 + B_{yf}^2) \tag{A2.24}$$

Solving for $(B_{zf}^2 + B_{yf}^2)$ we find

$$(B_{zf}^2 + B_{yf}^2) = \frac{2}{3B_x^2}\left[1 - B_x^2\right]\left[4B_x^2 - (1 + 5T_o)\right] \quad . \tag{A2.25}$$

This equation has two interesting features. First it only determines the magnitude of the magnetic field and leaves its direction arbitrary and second it is only physically valid for a certain range of B_x^2 namely

$$\frac{(1 + 5T_o)}{4} < B_x^2 < 1 \tag{A2.26}$$

See the discussion following Figure 4.5 for more insight into the significance of these roots.

Case (c)

The third case requires that $B_x^2 = u = 1$. Substituting this into (2.33) and (2.35) gives

$$T_f = T_o + \tfrac{1}{2}\left[B_{zo}^2 - (B_{zf}^2 + B_{yf}^2)\right] \tag{A2.27}$$

and

$$5T_f = 5T_o - \left[(B_{zf} - B_{zo})^2 + B_{yf}^2\right] - 2B_{zo}(B_{zf} - B_{zo}) \quad . \tag{A2.28}$$

Combining these two equations to eliminate T_f gives

$$5\left[B_{zo}^2 - (B_{zf}^2 + B_{yf}^2)\right] = -2\left[(B_{zf}^2 + B_{yf}^2) - B_{zo}^2\right] \tag{A2.29}$$

or

$$(B_{zf}^2 + B_{yf}^2) = B_{zo}^2 \tag{A2.30}$$

Substituting this into (A2.28) we find

$$T_f = T_o \tag{A2.31}$$

In this case there is no change in the streaming velocity or temperature. There is also no change in the magnitude of the magnetic field. But according to (A2.30) the direction of the field is arbitrary. In the discussion after Figure 4.5 the significance of this root is made clear. The important point made there is that the plasma can not change from its upstream state so the existence of different downstream equilibrium points is irrelevant.

APPENDIX 3

In this appendix we linearize the equation of motion in a slightly more generalized form than we used in Chapter III. We assume that there is friction rather than assuming that ν is initially zero as we did in Chapter III. The reason for doing this is to see how the pure imaginary roots of region IV_i behave if a small amount of friction is added.

Assuming that the variables in the equations of motion deviate from their equilibrium values like

$$A = A_o + A_1 e^{\lambda t} \qquad , \tag{A3.1}$$

we find for (2.29) to (2.32)

$$\lambda B_{z1} = \gamma(v_1 - B_x B_{y1}) \tag{A3.2}$$

$$\lambda B_{y1} = -\gamma(w_1 - B_x B_{z1}) \tag{A3.3}$$

$$\gamma\lambda v_1 = \left[B_{z1}(1 - \lambda\nu - B_{zo} \tau) - w_1 B_x\right] \tag{A3.4}$$

$$\gamma\lambda w_1 = v_1 B_x - (1 - \lambda\nu) B_{y1} \tag{A3.5}$$

where we have used (3.6) to eliminate u and

$$\tau = (1 + 5T_o/3)^{-1} \tag{A3.6}$$

Notice that (A3.4) and (A3.5) differ from (3.4) and (3.5) by the inclusion of a term proportional to ν . To solve (A3.2) to (A3.5) we must set the determinant of the coefficients equal to zero:

$$\begin{vmatrix} \lambda & \gamma B_x & -\gamma & 0 \\ -\gamma B_x & \lambda & 0 & \gamma \\ (\lambda\nu - 1 + B_{zo}\,\tau) & 0 & \gamma\lambda & B_x \\ 0 & (1 - \lambda\nu) & -B_x & \gamma\lambda \end{vmatrix} = 0 \tag{A3.7}$$

Expanding the determinant gives

$$\lambda^4 + \lambda^2\left[B_x^2(1/\gamma^2 + \gamma^2) + B_{zo}\,\tau - 2\right]$$
$$+ (1 - B_x^2)(1 - B_{zo}\,\tau - B_x^2) + \nu\lambda\left[2\lambda^2 + 2B_x^2 - 2 + B_{zo}\,\tau\right] = 0 \ . \tag{A3.8}$$

Using the notation of (3.9) we can write (A3.8) as

$$\lambda^4 + \lambda^2 b + c + \nu\lambda\left[2\lambda^2 + 2(B_x^2 - 1) + B_{zo}\tau\right] = 0 \tag{A3.9}$$

If we write

$$\lambda = i\lambda_i + \lambda_r \tag{A3.10}$$

and assume

$$\lambda_i >> \lambda_r \approx \nu \tag{A3.11}$$

Then

$$\lambda^4 \cong \lambda_i^4 - 4i\lambda_i^3 \lambda_r \tag{A3.12}$$

$$\lambda^2 \cong - \lambda_i^2 + 2i\lambda_i \lambda_r \tag{A3.13}$$

Substituting this into (A3.9) we get

$$\lambda_r = - \nu \frac{(2\lambda_i^2 + 2(1 - B_x^2) - B_{zo} \tau)}{2(2\lambda_i^2 - b)} \tag{A3.14}$$

where

$$2\lambda_i = b \pm \sqrt{b^2 - 4c} \tag{A3.15}$$

The plus sign gives the high frequency solution and the negative sign gives the low frequency solution. Using (A3.15) in (A3.14) gives

$$\lambda_r = - \nu \frac{\left(2\lambda_i^2 + (1 - B_x^2) + (1 - B_x^2 - B_{zo}^2 \tau)\right)}{\pm 2(b^2 - 4c)^{\frac{1}{2}}} \tag{A3.16}$$

From Table 1 in Chapter III we see that c is positive in region IV_i. If $B_x < 1$, both $(1 - B_x^2)$ and $(1 - B_x^2 - B_{zo}^2 \tau)$ must be positive to have c positive.

Therefore:

$\lambda_r < 0$ for the high frequency root

$\lambda_r > 0$ for the low frequency root

when $B_x < 1$. Thus we find that the high frequency mode decays and the low frequency mode grows when we add a small amount of friction and $B_x < 1$.

If $B_x^2 > 1$ we can write $c = x \cdot y$ where

$$x = B_x^2 - 1 > 0 \tag{A3.17}$$

and

$$y = (B_x^2 + B_{zo}^2 \tau - 1) > 0 \tag{A3.18}$$

We can also write

$$b = B_x^2 \left(\frac{1}{\gamma} - \gamma\right)^2 + x + y \quad . \tag{A3.19}$$

Using these in (A3.16) we find

$$\lambda_r = -\nu \quad \frac{\left[B_x^2\left(\frac{1}{\gamma} - \gamma\right)^2 \pm \sqrt{b^2 - 4c}\,\right]}{\pm 2 \sqrt{b^2 - 4c}} \tag{A3.20}$$

In the high frequency mode (positive root) the numerator is clearly positive so $\lambda_r < 0$ and this mode will decay.

To find the behavior of the low frequency mode we must examine the numerator more closely. We would like to show

$$B_x^2\left(\frac{1}{\gamma} - \gamma\right)^2 < \sqrt{b^2 - 4c} \tag{A3.21}$$

Squaring both sides and using (A3.19) gives

$$B_x^4\left(\frac{1}{\gamma} - \gamma\right)^4 < B_x^4\left(\frac{1}{\gamma} - \gamma\right)^4 + 2B_x^2 + 2B_x^2\left(\frac{1}{\gamma} - \gamma\right)^2 (x + y)$$

$$- 2xy + x^2 + y^2 \qquad , \tag{A3.22}$$

or

$$2B_x^2\left(\frac{1}{\gamma} - \gamma\right)^2 (x + y) + (x - y)^2 > 0 \tag{A3.23}$$

Thus we see that when $B_x^2 > 1$, the numerator of (A3.20) is negative for the low frequency mode so that λ_r is negative and the low frequency mode decays.

In summary:

high frequency mode decays for all B_x

low frequency mode decays for $B_x > 1$

low frequency mode grows for $B_x < 1$

APPENDIX 4

In Chapter IV we state that roots to the Rankine-Hugoniot relations with u_f greater than one are not acceptable as final states since they require a negative value for δ. See (2.47) for the definition of δ. In the region of the B_x, B_{zo}-plane which we are considering, only the root labelled R_1 is greater than one. It is greater than one in all of region I_r. To prove that shock transitions to R_1 in region I_r are not physically possible we first show that the initial location of the equilibrium point corresponding to R_1 is above the $V = 0$ plane. Next we prove that every point on the potential surface rises as δ is increased. Finally we argue that since R_1 is initially above the $V = 0$ plane, it must remain above the $V = 0$ plane for δ positive, even though its position along the B_z-axis varies with δ.

We showed in Chapter III that in region I_r the origin ($B_z = B_{zo}$) is a saddle point which is a minimum for motion in the B_z-direction. Since the origin is on the $V = 0$ plane, all points on the B_z-axis in the neighborhood of the origin lie above the $V = 0$ plane. Since the derivative of the potential in the B_y-direction is zero all along the B_z-axis, there will be an equilibrium point on the B_z-axis anywhere the derivative in the B_z-direction is also zero. We will now prove that there is a point between B_z equals zero and B_z equals B_{zo} where the derivative in the B_z-direction is zero.

If u equals one and B_y and δ are zero, (2.48) shows that

$$B_z = \pm B_{zo} \tag{A4.1}$$

Using this result in (2.55) we find that the potential at $B_z = - B_{zo}$ is initially negative if B_x is less than one, which we assume it is. Somewhere between $B_z = B_{zo}$ (the origin) and $B_z = - B_{zo}$ the potential along the B_z-axis must be zero since we know that it is greater than zero for B_z slightly less than B_{zo} and negative for $B_z = - B_{zo}$. From elementary calculus we know that if $f(a) = f(b)$, $\dot{f}$ is zero at at least one point between a and b. At least one of these possible equilibrium points must lie above the $V = 0$ plane since part of the potential surface in the interval is above the $V = 0$ plane.

We can narrow the location of the equilibrium point down even further by using (4.8). This equation shows that if u is greater than one, which is initially in the interval $-B_{zo} > B_z > + B_{zo}$, the equilibrium point must be in the interval $0 > B_z > + B_{zo}$. Again this assumes that B_x is greater than one.

Now that we have established that there is an equilibrium point on the B_z-axis which lies above the $V = 0$ plane, we want to see what effect increasing or decreasing δ has on the level of the potential surface relative to the $V = 0$ plane. We rewrite (2.55) here for ease of reference:

$$V = - \tfrac{1}{2}\Big\{1 - u^2 + 5T_o - 5(T_o + \delta)u^{-2/3} - B_x^2\left[(B_z - B_{zo})^2 + B_y^2\right] - 2B_{zo}(B_z - B_{zo})\Big\} \tag{A4.2}$$

The explicit dependence on T has been eliminated by using (2.46). Differentiating with respect to δ gives:

$$\frac{dV}{d\delta} = \left[u - (5/3)T/u^2\right] \frac{\partial u}{\partial \delta} + \frac{5}{2} u^{-2/3} \tag{A4.3}$$

From (2.48) we find

$$\frac{\partial \delta}{\partial u} = \frac{5}{3} \frac{(\delta + T_o)}{u} - u^{5/3} \tag{A4.4}$$

or

$$\frac{\partial u}{\partial \delta} = - u^{-2/3} \left[u - (5/3)\ T/u\right]^{-1} . \tag{A4.5}$$

Using this in (A4.3) gives

$$\frac{dV}{d\delta} = \frac{3}{2} u^{-2/3} \tag{A4.6}$$

This shows that all points on the potential surface rise or fall as δ increases or decreases. The rate is higher the smaller u is.

Since R_1 is a local maximum and we have proved that all the points on the potential surface are increasing in potential as δ increases, it is clear that the potential of R_1 is going to increase too. The location of the equilibrium point will move towards larger B_z since u is smaller in that direction and therefore the potential is rising faster. However the equilibrium point will always remain above the $V = 0$ plane for δ positive. The only way R_1 can reach the $V = 0$ plane in I_r is for δ to decrease. This would require a negative collision frequency which is physically meaningless.

REFERENCES

1. T. Gold, in Gas Dynamics in Cosmic Clouds, Ed. by H.C. Van de Hulst and J.M. Burgers (North-Holland Publishing Company, Amsterdam, 1955), p. 103.
2. W.N. Axford, J. Geophys. Res. 67, 3791 (1962).
3. P.J. Kellogg, J. Geophys. Res. 67, 3805 (1962).
4. N.F. Ness, C.S. Scearce, and J.B. Seek, J. Geophys. Res. 69, 3531 (1964).
5. J.H. Wolfe, R.W. Silva, and M.A. Meyers, J. Geophys. Res. 71, 1319 (1966).
6. M. Martone, Phys. Letters 22, 73 (1966).
7. A.E. Robson, and J. Sheffield, Univ. of Texas, Tech. Note CN-24/A-6 (1968).
8. R.Z. Sagdeev, in Reviews of Plasma Physics, Vol. IV, Ed. by M.S. Leontovics, (translated from the Russian by Consultants Bureau, New York, 1966), p. 23.
9. J.H. Adlam, and J.E. Allen, Phil. Mag. 3, 448 (1958).
10. P.G. Saffman, J. Fluid Mech. 11, 16 (1961).
11. P.G. Saffman, J. Fluid Mech. 11, 552 (1961).
12. J.G. Cordey, Some Aspects of Finite Amplitude Hydrodynamic Waves in a Plasma, Ph.D. Thesis, University of London, King's College (1964).
13. P.J. Kellogg, Phys. Fluids 7, 1555 (1964).
14. A. Banos, and R. Vernon, Nouvo Cimento 15, 269 (1960).
15. J.G. Cordey, Phys. Fluids 7, 778 (1964).
16. K. Hain, R. Lüst, and A. Schlüter, Rev. Mod. Phys. 32, 967 (1960).
17. T. Kakutani, T. Kawahara, and T. Tanuiti, J. Phys. Soc. Japan 23, 1138 (1967).
18. A. Cavaliere, and F. Engelmann, Nucl. Fusion 7, 137 (1967).
19. K.W. Morton, Phys. Fluids 7, 1800 (1964).

20. J.E. Anderson, Magnetohydrodynamic Shock Waves, (MIT Press, Cambridge, 1963).

21. D.A. Tidman, University of Maryland, Tech. Note BN-585 (1968)